white areas on the slides. Occasionally, sponges were dislodged from the brains during removal of the skull, as fibrous tissue filled in the bony defect in the skull and formed a slight attachment between the skull and the tops of the sponges (Figure 3.1d). Specimens were carefully detached from the skull and replaced in the defect cavity, but on soaking in OCT and freezing for sectioning it is evident from their floating position relative to the rest of the brain tissue that they had moved. When evaluating the defect size, the walls of the cavity were measured. When evaluating the areas within the scaffold, a visually verified approximation of the defect surrounding the scaffold was used.

Immunostaining

MHC-II positive cells were present within both polymers to different degrees. The difference was statistically significant for material (P = 0.021) but not over time (P = 0.116). MHC-II positive areas were greater in PLGA than PCL (1.2% compared to 0.5%) at the 1 week acute phase of inflammation and did not change over time in PLGA. An increase in the mean MHC-II expression levels found in PCL (from 0.5% to 0.8%) over time was not statistically significant and did not surpass the mean level in PLGA at either time point.

The cellular area in both materials measured from H&E images increased significantly over time (P = 0.000), roughly doubling from about 12% to about 25%, with a trend of PCL having 5-10% higher cellular ingrowth than PLGA (P = 0.069), while the Combined Cellular and Material Area decreased over time by about a third (P = 0.021) from around 45% to around 30% with no significant difference in material (P = 0.967). This difference reflects the degradation of materials at a higher rate than ingrowth and accounts for the overall decrease in non-void space within the implant.

In analyzing inflammation peripheral to the defect cavity OX-42 and GFAP in-

tensities were measured in L1 and L2 regions (Figure 3.1c). For Ox-42 (activated microglia) time was the only significant factor. P values from 3-way ANOVA and interactions were as follows: group = 0.7253, time = 0, region = 0.0603, group+time = 0.5159, group+region = 0.9649, time+region = 0.2228 (Figure 3.3b). Astrocytic activation was measured by GFAP intensities in regions L1 and L2, showing both group and region to be significant factors. P values from 3-way ANOVA and interactions were as follows: group = 0.0001, time = 0.0889, region = 0.0469, group+time = 0.0003, group+region = 0.6454, time+region = 0.2149 (Figure 3.3c). Significant multiple comparison tests shown with starred groups reveal that time was a significant factor but in contrasting ways between groups. There was increasing intensity over time for controls, decreasing for PLGA, and constant for PCL (Figure 3.3).

OX-42 positive activated microglia were observed in control defects at 1week (Figure 3.3b) and declined by 4 weeks, reflecting a decrease in microglial activation. There was also a concomitant increase over time of GFAP positive cells consistent with other brain injury models (Aihara et al., 1995; Chen et al., 2003; Holmin and Mathiesen, 1995). In contrast to the control, polymer sponge groups showed a decreasing trend over time from 1 to 4 weeks for GFAP positive activated astrocytes and 3-way ANOVA showed the three material groups (including control) had significant differences, indicating that there was a decrease in GFAP from region L1 to L2. The two polymer groups had similar microglial activation (OX-42) compared to the controls, though the decrease in the PLGA group over time was not significant. Representative images of microglial morphology adjacent to the defect site in region L1 and further away in region L2 are shown in Figure 3.4. Highly activated microglial cells appear to have large bright cell bodies and short fibers while unactivated microglia have more diffuse fibrous labeling and no large cell bodies.

GFAP expression around both polymers was less than the control after 4 weeks and did not differ from each other at that late time point. However, in contrast to microglial activation, PLGA groups had significantly higher levels of GFAP than PCL at one week and the PCL groups were not significantly changed over time (Figure 3.3c, and Figure 3.5). Astrocytes are activated by cytokines from the activated microglia (Bianco et al., 2005) leading to increased production of GFAP. GFAP levels reflect their activation level, the highest of which can indicate glial scar formation. GFAP labeled astrocytes with long thin fibers activated next to the polymer implanted defects contrast the control regions at 4 weeks, which had higher activation based on GFAP intensities (Figure 3.3c) and show astrocytes close to the defect border aligning and densely entangling their fibers (Figure 3.5).

Ingrowth of GFAP positive astrocytes into the sponges was seen in both polymers to occur from the bottom and edges up toward the middle, whereas MHC-II positive cells were seen distributed throughout the sponges. This suggests astrocyte migration into the scaffolds from host tissue and MHC-II infiltrating cells from peripheral blood residing in all areas of the sponge from the initial absorption. In the bottom corners of the sponges close to their contact with the lateral ventricles, nestin positive and Tuj-1 positive cells were found in close contact with the materials after four weeks (Figure 3.6).

3.5 Discussion

In brief summary, porous PCL and PLGA implants were able to decrease cell death and support neural cell growth *in vivo*, an improvement over controls where no biomaterial implants were used. Neither polymer caused any severe inflammatory reaction, actually modifying the response such that the environment was more

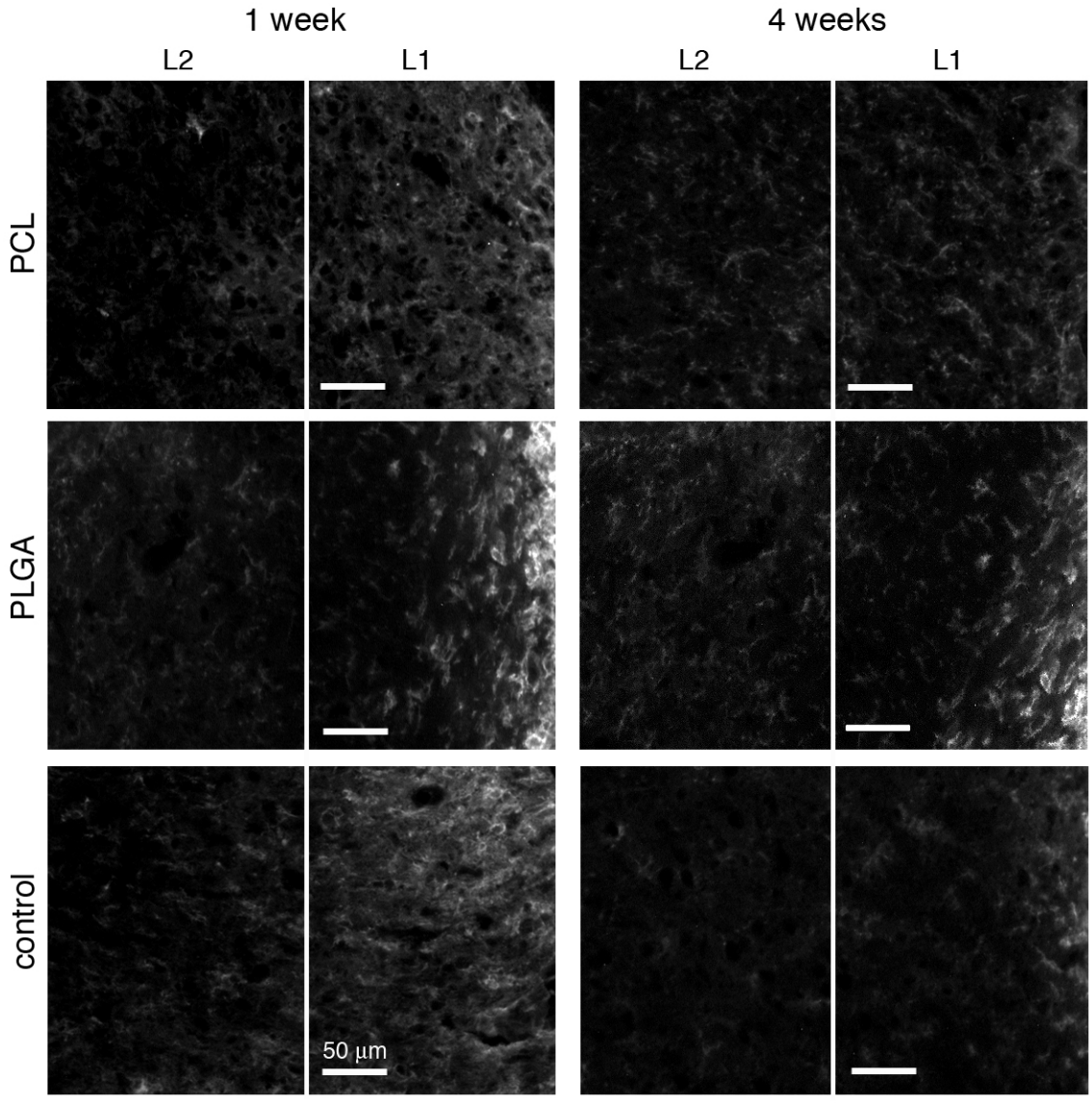

Figure 3.4: OX-42 immunohistochemistry for control, PCL, and PLGA. Images of immediately adjacent regions L2 and L1 with defects located on the right. 10x mag. scale bars 50 μm.

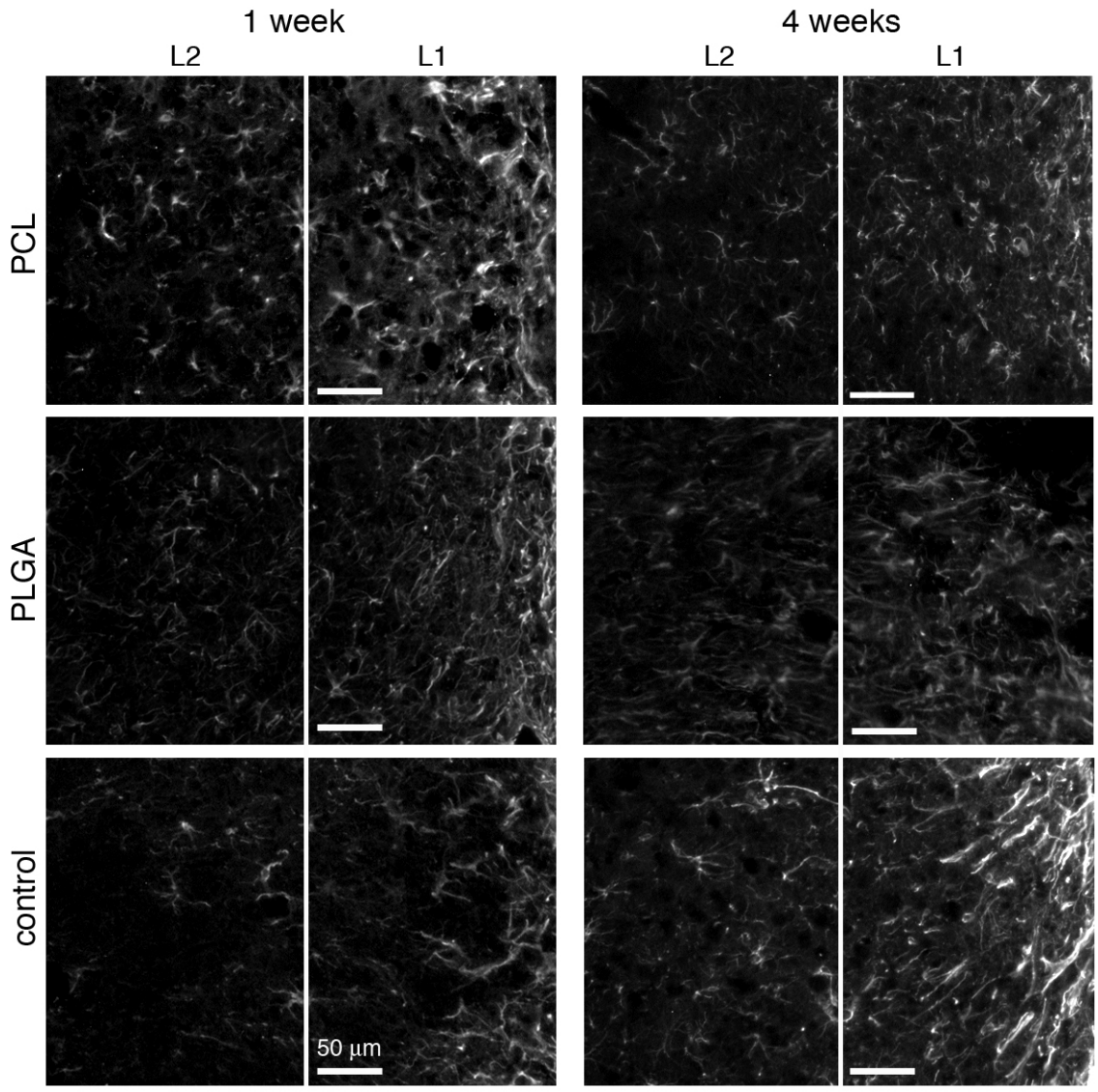

Figure 3.5: GFAP immunohistochemistry for control, PCL, and PLGA. Images of immediately adjacent regions L2 and L1 with defects located on the right. 10x mag, scale bars 50 μm.

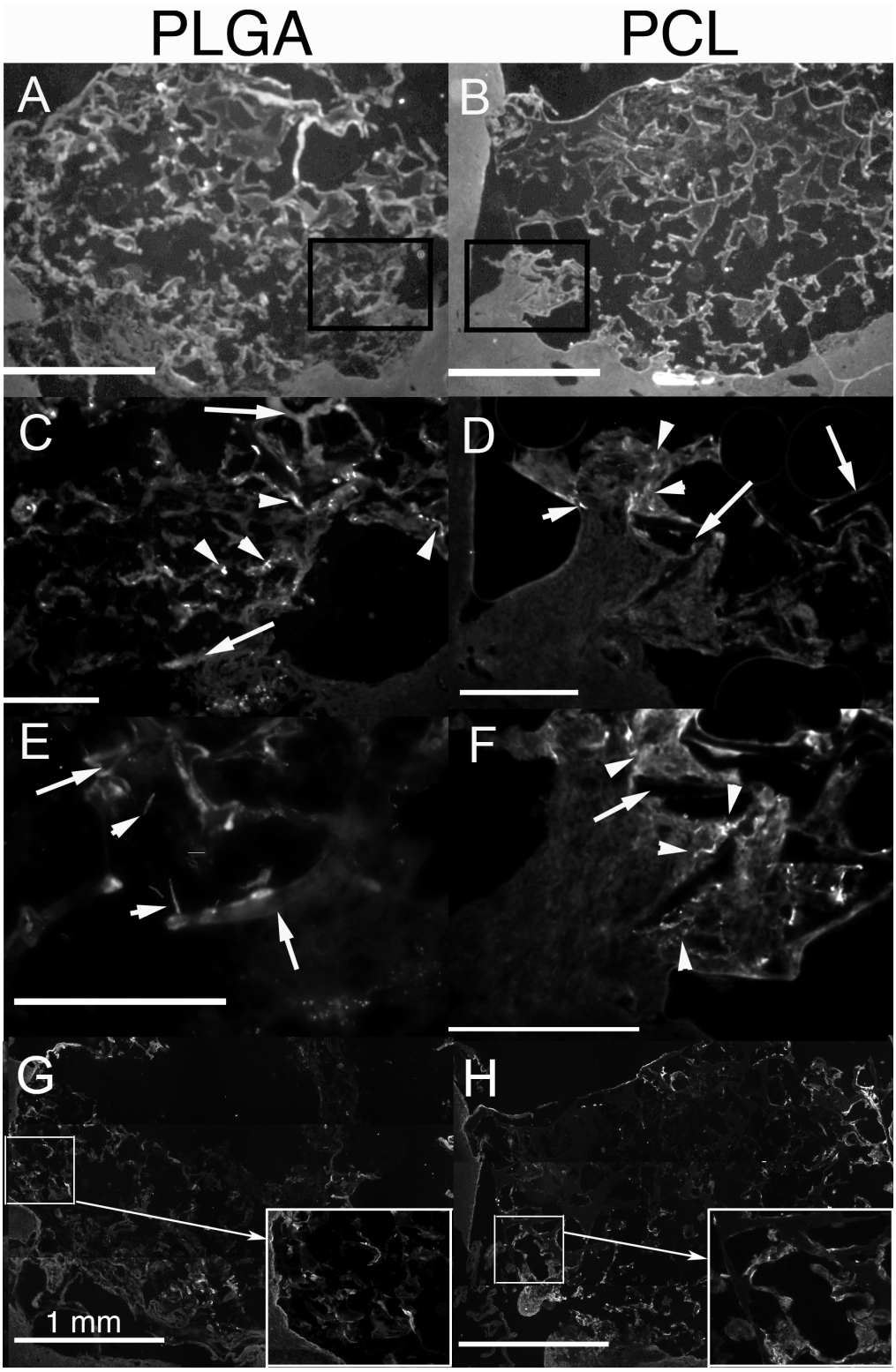

Figure 3.6: Representative immunofluorescent images identifying neural cells in PCL and PLGA. Top two images are provided for perspective in (A) PLGA and (B) PCL sponges at 4 weeks, no specific labeling. Boxes indicate corresponding regions for C,D,E, and F. Nestin labeled cells (arrowheads) in (C) PLGA and (D) PCL in close proximity to polymer materials (long arrows). Tuj-1 labeled cells (arrowheads) in (E) PLGA and (F) PCL interact with polymers (long arrows). GFAP labeled astrocytes in (G) PLGA and (H) PCL distributed within the sponges have highly fibrous lagelling (insets to G and H).

amenable to regeneration. Both polymers are suitable for use as a delivery vehicle of treatments, but PCL may provide advantages over PLGA depending on the treatment strategy.

The defect width of the control group over time compared to the polymer groups was smaller at 1 week and grew to be larger at 4 weeks. Since all the defects (control and implant) were first created in the exact same way, the surgical preparation was not a factor. The only difference would be the fact that the polymer was placed inside the cavity. It is possible that due to swelling, the control defects might become smaller as there was no polymer to hold the walls of the defect from caving in, which we consider more likely than caving out while still contained *in vivo*. With regard to analytical preparation, all brains were fixed by perfusion prior to any physical manipulation of the tissue. Upon dissection from the skull, it was apparent on visual inspection that the sizes of defects had grown in the control. Brains were frozen for sectioning in large pieces, with plenty of tissue surrounding the defect site to hold the walls in their original shape. In addition, most often it was the deeper regions of the defect, not the top edges, which showed the greatest increase in width (Figure 3.1b). It is clear from the histology in the remaining tissue that cell death, and not a simple physical expansion during preparation of the section for histology, is the major cause of differences in defect width. Delayed enlargement of defects due to secondary cell death is also a known common result of traumatic brain injury under several injury models. The mechanism of the attenuation of this cell death by the polymers in this study is unknown. Poly-ethylene glycol (PEG) has been shown to offer neuroprotective effects, though the mechanism is also unknown (Kerwin et al., 2002; Luo et al., 2004). Speculation on PEG interactions with proteins and mitochondria due to its ability to enter the cytosol could possibly provide some of

the reasons PCL and PLGA offered some benefit over no polymer implant, or why there was a small benefit from PCL over PLGA as these polymers differ slightly in pH and structure. Their phagocytosis by macrophages is a pathway into the cell which may be similar to the pathway that nanoparticles of PEG take (Kerwin et al., 2002; Luo et al., 2004). These possibilities remain to be investigated.

It was observed during the surgeries that implantation of the sponges decreased bleeding, similar to the effect from applying gauze or cotton during the surgeries to stop the initial bleeding, but the implants were never removed, as cotton was from the control groups, prior to closing. Macrophages ($CD8^+$) and microglia have been shown to be a mostly blood derived subset of MHC-II or ED1 reactive macrophages and microglia that reside mostly in the border of pannecrosis in contusion injury. These cells may play a strong role in lesion progression (Zhang et al., 2006). It is likely that the MHC-II^+ cells in the scaffolds of this study, which are mostly blood derived, contain a $CD8^+$ cell population, but the presence of a biomaterial scaffold may have played a role in decreasing tissue damage by either leading those cells away from the border of the defect or preventing them from reaching the parenchyma from the circulation by acting as a barrier and trap for infiltrating cells. It is possible that this passive prevention by the biomaterials was able to save some of the parenchyma from delayed death and to reduce the need for the parenchyma to form a glia limitans.

Both polymers allowed ingrowth of cells, though PCL showed a slightly higher rate than PLGA. Many of these cells inside the scaffolds were macrophages. As PCL and PLGA hydrolytically degrade, smaller molecular weight segments of the polymers are phagocytosed(Sun et al., 2006) by macrophages. The slower rate of hydrolytic degradation in PCL may have led to the lower level of macrophages (MHC-II labeling) compared to PLGA in the material scaffold for clean-up of degradation

products. The higher total cellular ingrowth in PCL compared to PLGA has also been seen subcutaneously for these materials, supposedly due to the difference in intial pH of the polymers and from their degradation rates, but the mechanism has not been fully elucidated (Sung et al., 2004).

Some of the infiltrating cells of the scaffolds aside from macrophages were likely fibroblasts and astrocytes, and possibly microglia from the cerebral cortex, although the microglia cannot be separately identified from circulating macrophages and neutrophils. However, astrocytes and microglia found in the parenchyma can be used to gauge levels of internal inflammation in the brain. Data at the early time point reflected lower microglial activation (OX-42) in PLGA groups than the PCL and control, but a lower astrocytic activation (GFAP) in PCL than the PLGA and controls. The contrasts in astrocytic and microglial activation between polymers may be due to a time course difference in the first few weeks, converging by the fourth week. However, microglia have been shown to play neuroprotective roles (Streit, 2002) which might explain why a higher microglial activation in the PCL group led to lower astrocytic activation than the PLGA group. Microglial activation may mediate astrocytic activation and the astrocytes propensity to form a glial scar. Regardless, the difference was short-lived and both polymers had similar astrocytic activation by 4 weeks, which was lower than the control group. Their earlier differences may manifest in a difference in neuronal damage in other areas of the brain, but this effect was not investigated and the overall differences in pathology were small. These lower levels of GFAP suggest that polymer sponges not only impede the growth of the defect size, but could also attenuate the amount of scarring which could occur in surrounding brain tissue while the increase over time in the control group suggests the standard formation of a glia limitans. The decrease in astrocytic

activity in polymer groups compared to control may be linked to the ability of cells to migrate into the polymers, as there is less of a cellular barrier.

Since the degradation rates of the polymers are based primarily on a constant factor, hydrophobicity, one can assume that longer time points would still compare inflammatory responses to the same difference in release rate of both polymers molecules from the bulk forms. The time point in this study of 4 weeks is not long enough to track the entire response over a majority of the degradation for both polymers. However, the time points chosen here reflect important points for comparison. The general time course of acute inflammation is within the first week, after which chronic inflammation sets in and remains relatively constant. Macrophages infiltrate a brain injury within the first week. Interventions to prevent secondary cell death are needed during the acute phase. Thus if there are differences in the tissue response elicited by the polymers, the most pivotal would have occurred in the first week, and be evident by four weeks, such as secondary cell death and cellular migration. Longer time points would likely either amplify the differences or dampen them. It is, however, possible that a sudden change in the release of polymer products could occur towards the end when the last portion of polymer might reach the small molecular weight needed to be phagocytosed all at once. If this is the case, it is likely that PCL, degrading more slowly yet being taken in by macrophages in the same way as PLGA, would probably cause less drastic a change. It is unlikely that longer time points would change the overall working conclusion of this study, that both PCL and PLGA can be used for implantation in the brain.

Though there was not extensive infiltration of the polymer scaffolds by nestin and Tuj-1 positive cell types at 4 weeks, it is not unexpected since these implants contained no bioactive treatment or cells. The neighboring subependymal zone could

be a source of progenitor cells entering the defect site and contacting or entering the scaffolds based on the location of the few cells that were observed and evidence in literature of nestin positive cells from the subependymal layer migrating toward lesions(Chen et al., 2003; Holmin et al., 1997). Though there can be no comparison of relative permissiveness of the two polymers to progenitor and neuronal ingrowth from the data, they can both be deemed permissive. Other cell types in the scaffold surrounding the few nestin and Tuj-1 positive cells are likely astrocytes and could play a supportive role in allowing those nestin and Tuj-1 postive cells to interact with the sponges (Figure 3.6). Longer time points would be helpful in future studies to determine any differences in support of neural cell ingrowth between the polymers. It is plausible that additional experimental biological factors such as stem cells or growth factors may play a much larger role than any differences between the polymer material for this type of interaction.

3.6 Conclusions

Lesions in the brain benefit from the presence of polymeric scaffolds and will likely be more effectively treated with drug, growth factor, or stem cell delivery in the scaffolds. PCL and PLGA should be considered both biocompatible and beneficial for traumatic brain injury in sponge scaffold form. From the data on ingrowth and infiltrating inflammatory cells, combined with its longer residence time, PCL may have an advantage over PLGA for future studies, and is a suitable material for use in studying the macro-architectural influences on CNS regeneration.

Acknowledgments

The authors would like to thank Dr. K. Holmberg for advice on techniques and helpful discussions, Steve Gross for his help with the preliminary surgeries for this

work, and Jason Kutch for help writing Matlab code.

CHAPTER IV

Interconnected channels and aligned microgrooves promote cerebral cortex regeneration

4.1 Overview

The purpose of this study was to compare designed scaffolds to a random-pored sponge scaffold to determine what role scaffold architecture plays in a cortical injury model. Cylindrical scaffolds (3mm x 3mm) were made of poly(ϵ-caprolactone) polymer with two different molds from a 3-D Printer to have 1) unidirectional channels and microgrooves oriented longitudinally within the cylinder or 2) orthogonally intersecting channels and microgrooves axial within the cylinder. Additional randomized porosity was imparted by a salt-leaching method. A control scaffold with no channels or microgrooves but containing random pores was also made. Scaffolds were implanted in a cylindrical defect created in rat cerebral cortex 3mm posterior to the bregma for 1, 4, and 8 weeks. Control animals had tissue removed but received no implant. Brains were coronally cryosectioned and stained. Antibodies for nestin, GFAP, and Tuj-1 were used to identify neural progenitors, activated astrocytes, and neuronal axons. Tissue ingrowth (H&E), astrocytic infiltration (GFAP), parenchymal inflammation (GFAP), and defect width (H&E) were quantified from images. Defect widths grew and parenchymal inflammation decreased over time with no statistical difference between groups. Total tissue ingrowth and astrocytic infil-

tration increased over time and was greatest in the orthogonal group. Specific cell ingrowth was qualitatively assessed from nestin and Tuj-1 labeling, which were observed aligned with microgrooves interiorly in the orthogonal and exteriorly on the longitudinal channel group.

Scaffold architecture can benefit brain tissue regeneration by integrating the following design principles: 1) Large (100s of μm) pores or channels oriented toward the parenchyma for increased astrocytic infiltration, 2) microgrooves oriented in the desired direction of cellular migration and neuronal alignment, 3) fully interconnecting channels for cellular migration and tissue integration.

4.2 Introduction

After severe traumatic brain injury (TBI), brain tissue undergoes a healing process which often includes necrosis and/or apoptosis in regions originally undamaged (Raghupathi, 2004; Williams et al., 2006). Several factors are used in determining treatment options for TBI patients. Clinical evidence suggests that surgical treatment such as craniotomy, debridement, or evacuation of hematoma may improve outcomes in severe TBI that consist of parenchymal mass lesions and neurological dysfunction, particularly when defect volume is greater than 50 cm^3, or 20 cm^3 if accompanied by a midline shift of at least 5 mm and/or cisternal compression on CT scan (Bullock et al., 2006). With or without surgical treatment, secondary cell death after the first few days continues to be a problem. Many investigations in the treatment of traumatic brain injury aim to prevent this secondary cell death, but regeneration of lesions of this size is still unattainable. Cell replacement or mediation therapies for regeneration have low survival rates if injected into defects without a supportive matrix (Lu et al., 2002; Molcanyi et al., 2007;

Schouten et al., 2004). For those large mass lesions which would require operative treatment, tissue engineering scaffolds could potentially be useful. A material vehicle or scaffold to maintain treatments would be beneficial (Tate et al., 2002). Additionally, polymer scaffolds alone in brain defects have beneficial effects on the size progression of the defect in a rat model (Wong et al., 2007). Because of the complex neural organization in the brain, and the heterogeneity of pathophysiologies and variability in locations, sizes, and shapes of injuries, there is no obvious organization for scaffolds for overall brain regeneration or surgical and implant treatment of TBI in general. However, architectural characteristics like pore size and permeability may influence neural tissue growth, although this has not been investigated for brain tissue engineering scaffolds.

Grooved features ranging from nanometers (nanogrooves) to 10-50 μm (microgrooves) are known to provide cues for sprouting, extension and alignment of neurites by neurons and organization of extracellular matrix by meningeal cells *in vitro* (Goldner et al., 2006; Manwaring et al., 2004; Tsuruma et al., 2006), and may be beneficial to neural tissue growth *in vivo*, though this has not been investigated. Neural cells from the cerebral cortex of rats sprout more neurons when the surface is microgrooved than flat, and extend mostly parallel to the grooves, though perpendicular extensions are increasingly seen with the increase in width of the top plateau surface of step-wise grooves (Goldner et al., 2006). Meningeal cells on surfaces with nanogrooves on the order of 300 nm also with micron scale roughness produce organized extracellular matrix *in vitro* (Tsuruma et al., 2006) which might help the alignment of regenerating axons. Topography could also help mediate foreign body responses. Increased nanoscale roughness on poly-(ϵ-caprolactone) (PCL) decreases the adhesion of fibroblasts *in vitro*, indicating that *in vivo* fibrosis would be less likely on these surfaces (Vance

et al., 2004).

In addition to designed nano-and micro-scale topography, macro-scale physical barriers to cell migration can be minimized while maintaining overall shape and volume through architectural design and 3-D fabrication techniques (Hollister, 2005). Interconnected macro-pores on the scale of 100s of μm are projected to provide better cell migration pathways and diffusion with decreased tortuosity in a number tissues such as bone and cartilage (Li et al., 2007; Malda et al., 2005; Otsuki et al., 2006). Though there is no known optimal pore size for brain tissue regeneration, a reasonable starting point based on cell size can be assumed.

Topographical and architectural characteristics such as these have been overlooked in the *in vivo* studies of brain injury in deference to biological factors such as substrate coating, growth factors, or stem cells (Park et al., 2002; Tian et al., 2005b). Random fiber meshes or sponges, or solid hydrogels have been used to deliver other biologic factors but have not, themselves, been systematically varied for investigation. It is important to develop an understanding of how the brain interacts physically with different architectures so that when biological factors are combined, their effects can be maximized. Several studies have shown the low survival rate of injected cells (Lu et al., 2002; Molcanyi et al., 2007; Schouten et al., 2004) and the low residence time of injected proteins and drugs is being addressed by the field of controlled release. In certain cases an implantable delivery vehicle can be indispensable and its specifications just as important as those of the biological agent. With the advance of the molecular understanding of the central nervous system, these physical facets need to be considered. To our knowledge there have been no specific designed architectures for scaffolds studied in the brain. The goal of this present study was to investigate differences in brain tissue regeneration with varying interconnected channels given a

backdrop of a combination of nano-and micro-scale features. In the cerebral cortex, neurons are organized into six generally transverse layers, parallel to the surface of the cortex. Their axons project vertically, perpendicular to the surface, in columns connecting the cortex with deeper regions of the brain. Information is therefore relayed between neurons in this vertical, columnar organization in groups spanning 300-600 μ wide (Kandel et al., 2000; Mountcastle, 1997). Macro-architectures were therefore selected for study which incorporated these organizational directions and layers into the guidance channels.

This study compared different designed poly(ϵ-caprolactone) (PCL) scaffold architectures to a random-pored PCL sponge scaffold to determine scaffold architecture effects on regeneration in a cortical injury model. Random nano-scale roughness of this material was imparted due to the casting solvent used, which might decrease the likelihood of fibrosis (Vance et al., 2004). Aligned microgrooves were created by the mold casting process to investigate the effects on neural alignment and migration and organization of supportive matrix. The grooves in this study were V-shaped, thus minimizing groove plateau and maximizing the potential parallel alignment of neural fibers along the grooves (Goldner et al., 2006; Clark et al., 1990; Curtis and Wilkinson, 1997). Finally, different interconnected channel designs were used to investigate the affects of pore connectivity on cell migration in cerebral cortex regeneration.

4.3 Methods

Porous scaffold design and fabrication

Porous implants were made of PCL (50,000 kDa MW, Solvay Chemicals, Houston, TX) dissolved in acetone, (13% wt.). 180-250 μm sieved salt crystals were used for porogen leaching in all designs to create a sponge architecture outside all

macro-channels. The general shape and size of the implants was a 3 mm by 3 mm cylindrical plug. Three designs were used: Cylinder (cylinder, no macro channels, only sponge), Channel (5 macro-channels, longitudinal only, with longitudinal microgrooves along the axis of the cylinder, vertical in the brain), and Orthogonal (orthogonal macro-channels, 5 longitudinal, 6 perpendicular, with microgrooves perpendicular to the cylinder axis, transverse in the brain) (Figure 4.1a, b, and c). Wax molds for the channeled scaffolds were designed in Rhinoceros software as a stereolithography (STL) file. This 3-D surface file was then converted to a series of files comprising each 2-dimenional cross-sectional layer of the mold. These layers were printed on a Solidscape 3D printing machine (Solidscape Inc. Merrimack, NH) using a waxy medium to form the mold layer-by-layer (Figure 4.1d, e, and f). There are two types of wax used, one that becomes the object and another that serves as a supporting material during the building and cutting process. Between the printing of each layer the newest layer is trimmed with a cutting tool so that the layer thicknesses are uniform. The final product from the machine is a solid two-phase wax. Dissolution of the supportive phase leaves behind the object originally designed. Microgrooves are an artifact of the 3D printing machine (Figure 4.1e). Grooves are formed between each layer of material as the mold is being built. To impart longitudinal microgrooves Channel molds were built with the cylinder on its side (Figure 4.1e and h) . To impart axial grooves, Orthogonal molds were built with the cylinder up-right (Figure 4.1f and i). After casting the polymer in each mold, the molds were dissolved with a proprietary solvent called BioAct to reveal the actual scaffold. BioAct and salt porogen were removed from the scaffold with several washes of 70% ethanol. Plain cylinder scaffolds were made in a re-usable cylindrical teflon mold and did not have microgrooves (Figure 4.1 g).

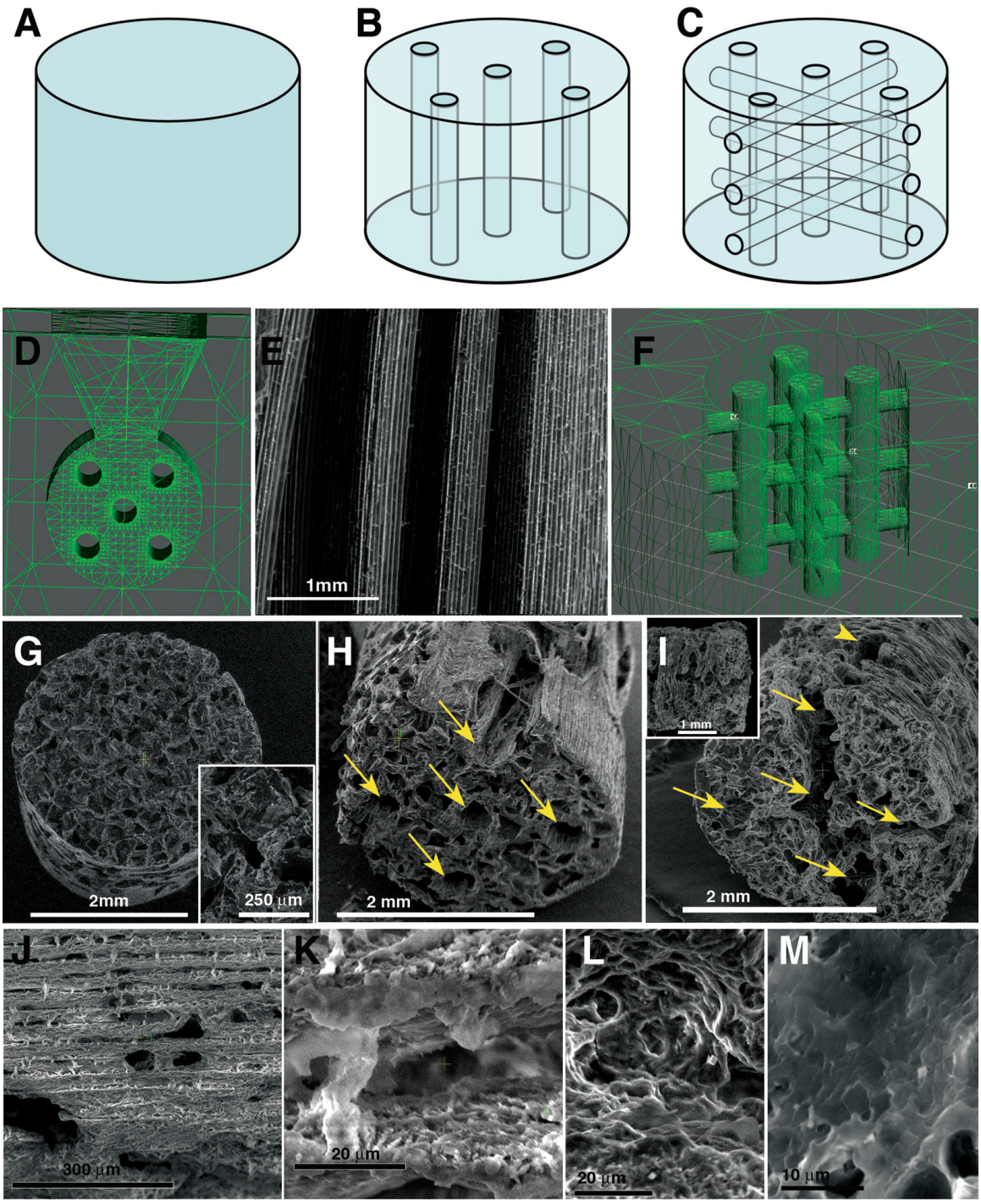

Figure 4.1: Schematic drawings and fabrication details of (a) Cylinder, (b) Channel, and (c) Orthogonal design scaffolds. Wire-frame renderings of the mold designs for casting (d) Channel and (f) Orthogonal scaffolds show the two orientations, (d) on-side, and (f) up-right in order to achieve microgrooves in the correct orientation. Microgrooves are oriented longitudinally along the walls and struts of the (e) wax mold forming the Channel design. SEM micrographs of the completed (g) Cylinder, (h) Channel, and (i) Orthogonal scaffolds show (g inset) salt generated pores, (arrows) channel openings at the ends and on the (arrowhead) side of the channel and orthogonal scaffolds. Microgroove directionality is also visible in (h)Channel and (I inset)Orthogonal scaffolds. Higher magnification of the exterior wall of a Channel scaffold (j,k,l,m) shows micro-porosity and roughness of the polymer after the casting process. All scale bars are individually labeled with lengths.

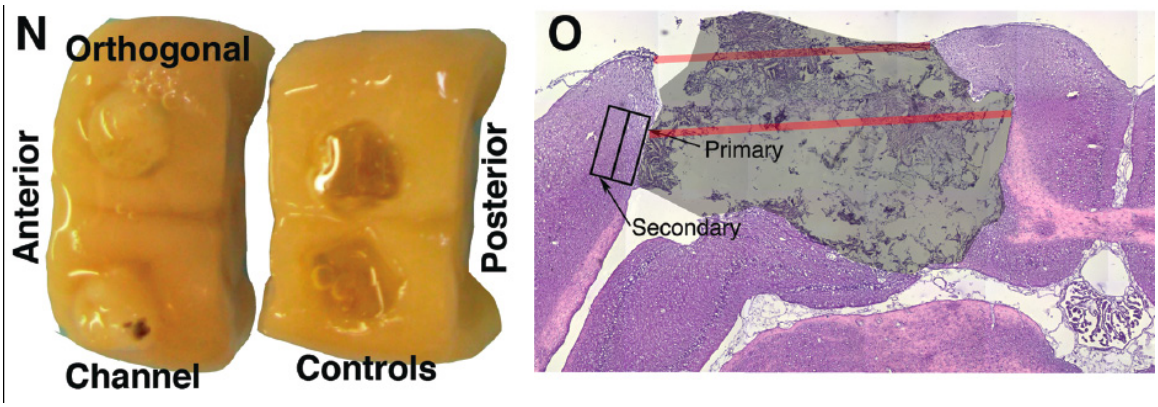

Figure 4.2: Gross images of implant groups and diagramed quantitative methods. (n) Gross images of samples removed from two rats after 4 weeks shows two designed scaffolds implanted in one and two control voids in the other brain segment. (o) A H&E stained section of a sample illustrates the (boxes) primary and secondary regions adjacent to the defect from which GFAP intensities were measured to gauge inflammation of the parenchyma, (red lines) method of measuring defect widths, and (gray outlined area) the mask drawn individually to demarcate the total area from which ingrowth was calculated. All scale bars are individually labeled with lengths.

Surgical implantation

Female Sprague Dawley rats (250-300 g) were anesthetized and skulls exposed on a stereotaxic frame. A 3 mm outer diameter treffine was used to drill 2 holes in the skull above the cerebral cortex (3 mm posterior of the bregma, 3 mm left and right). A plug of cortical tissue the same size as the implant was removed using the same treffine and forceps. Control groups received no implant but had tissue removed, leaving a void (Figure 4.2n).

Rats were sacrificed at 1, 4, and 8 weeks by transcardial perfusion. There were 5 rats for each time point; one rat for control with two defects (one in each hemisphere), two rats for channeled scaffolds with two defects each (Orthogonal in the right hemisphere, Channel in the left hemisphere), and two rats for plain cylinder (one Cylinder in each rat in the right hemisphere, left containing another design group not included in this study). All surgery, post-surgical recovery and euthanasia were performed according to a protocol approved by the University of Michigan Committee on the Use and Care of Animals.

Immunofluorescence, staining, and microscopy

Brains were cryosectioned coronally (14 μm thickness) onto gelatin coated slides. Stains and antibodies used were hematoxylin and alcoholic eosin (H&E), rabbit anti-GFAP (G9269 Sigma), mouse anti-Tuj-1 (MMS-435P Covance, Berkeley, CA), and mouse anti-nestin (Rat-401 Hybridoma Bank, University of Iowa) with a Vectastain ABC kit (Vector Labs, Burlingame, CA) and biotinylated Alexa-488 (Invitrogen/Molecular Probes, Carlsbad, CA). A mixture of 5% donkey serum (Jackson ImmunoResearch Laboratories Inc., Westgrove,PA) and 3% BSA was used for blocking non-specific binding.

Images were taken using a Spot camera and Spot Advanced software (Diagnostic Instruments, Sterling Heights, MI). All images for a montage were taken in the same sitting with the same exposure and processing settings. All images of sections with the same type of labeling were taken on the same day (when possible) or two to three consecutive days in batches. Specificities of primary antibodies were verified on stock sections of undamaged brain. Harris hematoxylin and alcoholic eosin stains were used for assessing a general overview of inflammation and morphology.

Quantification and statistics

Areas of ingrowth were calculated using a program (section 6.3) written in Matlab (Mathworks, Natick, MA) to apply a threshold based on greyscale values for both total and GFAP ingrowth based on a path (drawn in Adobe Photoshop) demarcating the defect area for normalization of the areas (Figure 4.2o). Auto-fluorescent dust and debris were removed from the images prior to quantification. A separate Matlab program (section 6.3) was used to calculate GFAP intensity on a grey scale of regions selected on each side of the defects. Two rectangular regions 200 μm wide were

selected extending to 400 μm from the edge, denoted as a primary and secondary edge region (Figure 4.2o). Lengths of these regions varied and were selected to exclude edge effect fluorescence, dust and debris, air bubbles and folds, and the hippocampus. Background intensity was calculated and subtracted for each image from regions of the cerebral cortex in the same section but distant from the defect site and visibly unaffected. All intensity data presented was corrected for background fluorescence.

Defect sizes were measured in Adobe Photoshop. Serial sections were measured until the middle of the defect was identified and that measurement was used. Distances were measured across the top and across the middle of defects from coronal sections as parallel lines perpendicular to the apparent angle of entry for the axis of the cylinder sponges (Figure 4.2o). Edges were defined where tissue looked like normal parenchyma continuous with further regions in the section. Scaffold dimensions were measured from SEM images after fabrication using the measuring tool in Adobe Photoshop and standard deviations calculated.

Standard error of the mean is shown in all graphs. Data was analyzed by 2-way ANOVA with group and time point as independent variables. If significance levels were below $p = 0.05$ individual comparisons were made with Tukeys Least Significant Difference post-hoc analysis. Statistics were calculated using Matlab software.

4.4 Results

Scaffold fabrication

The programmed layer thickness, from which the grooves are an artifact, was set to 38.1 μm when built using the Solidscape ModelMaker II. Microgrooves after the casting process were measured from SEM images to be 32 ± 4 μm on all wall areas that were designed straight relative to the z-axis (Figure 4.1). Curvature from the

z-axis created grooves on the tops and bottoms of channels which measured 119 ± 2 μm. Because of the orientation of the Channel group during the building of the molds, the top and bottom edges of all its channels as well as the exterior surfaces had wider grooves. Only the perpendicular channels in the Orthogonal design had increasing microgroove widths. All longitudinal channel diameters in both channel and orthogonal designs were designed to be 500 μm and measured 421 ± 27 μm after the casting process. Perpendicular channels in the orthogonal design were designed to be 300 μm and measured 280 ± 37 μm. Both the grooves and the channels had a shrinkage ranging from 6 to 16% after all the manufacturing steps, including drying of the scaffolds for SEM viewing. It is likely that the scaffolds expanded slightly when wet, reducing the shrinkage under working conditions.

Histology

One, four, and eight weeks after cortical implantation, brains were sectioned and examined histologically. Morphologically, tissue was observed in intimate contact with microgrooves in the Orthogonal design after 4 weeks (Figure 4.3) and 8 weeks (Figure 4.4). The interior of the Channel design contained mainly macrophages and monocytes as determined morphologically from H&E, and tissue formed a capsule around the outside by 8 weeks, typical of a foreign body response. This type of encapsulation was not seen in the other groups. Control groups remained voids.

Nestin-labeled filamentous structures were found within the Cylinder and Orthogonal groups by 4 and 8 weeks (Figure 4.5d, j, k, and l). There was also nestin labeling observed in small pockets of the fibrous capsule surrounding the Channel group (Figure 4.5f and g), though no staining was found within that scaffold group. There were more regions of nestin labeling in the Orthogonal group than the Cylinder group, and Orthogonal groups had some cells aligned with the grooves within channels (Figure

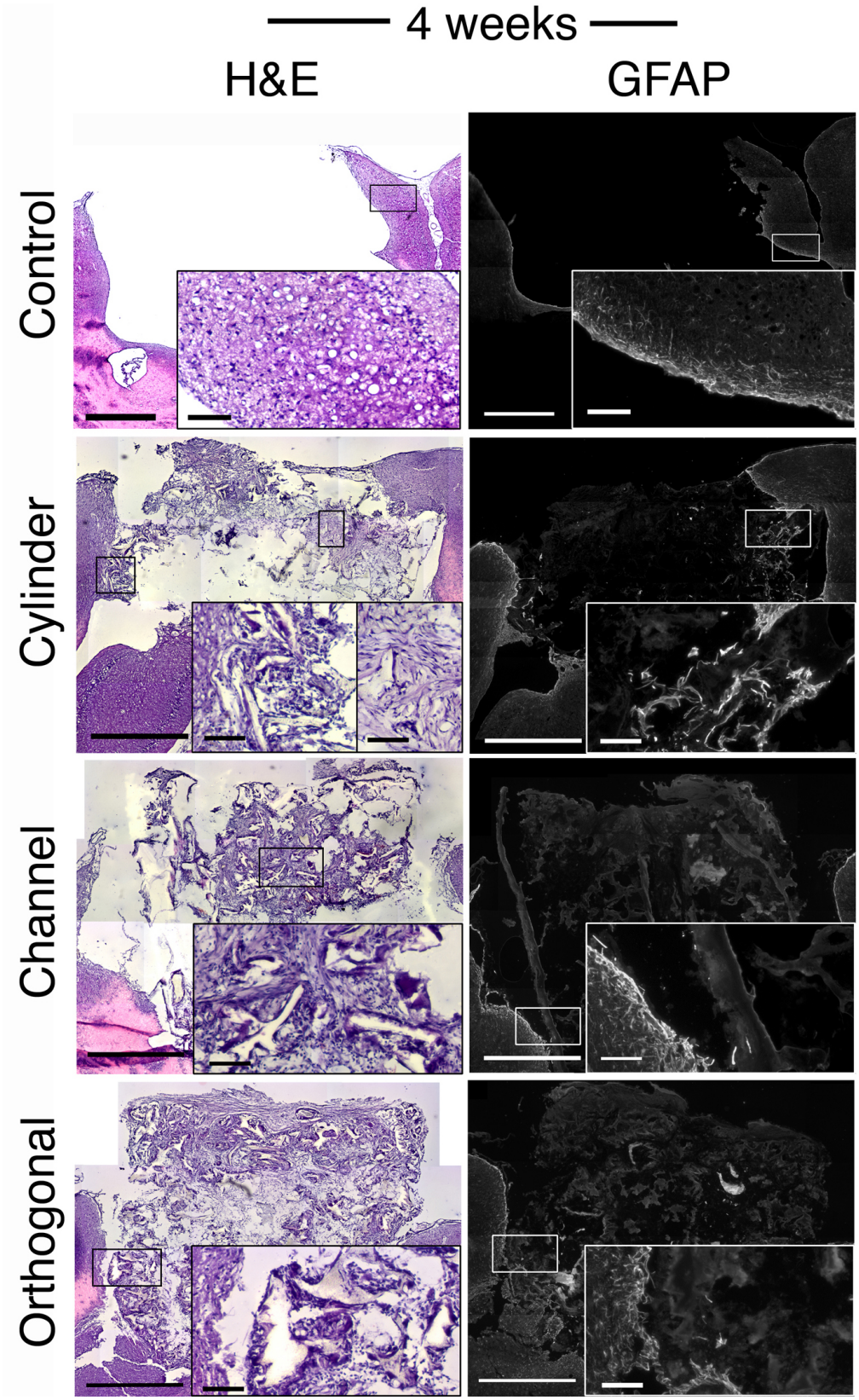

Figure 4.3: Representative and corresponding sections for cylinder, channel, and orthogonal scaffolds H&E stained and labeled for GFAP for 4 weeks implantation. Each larger overview image (scale bars 1mm) has a higher magnification inset indicated by the small boxes to show cellular details (scale bars 100 μm).

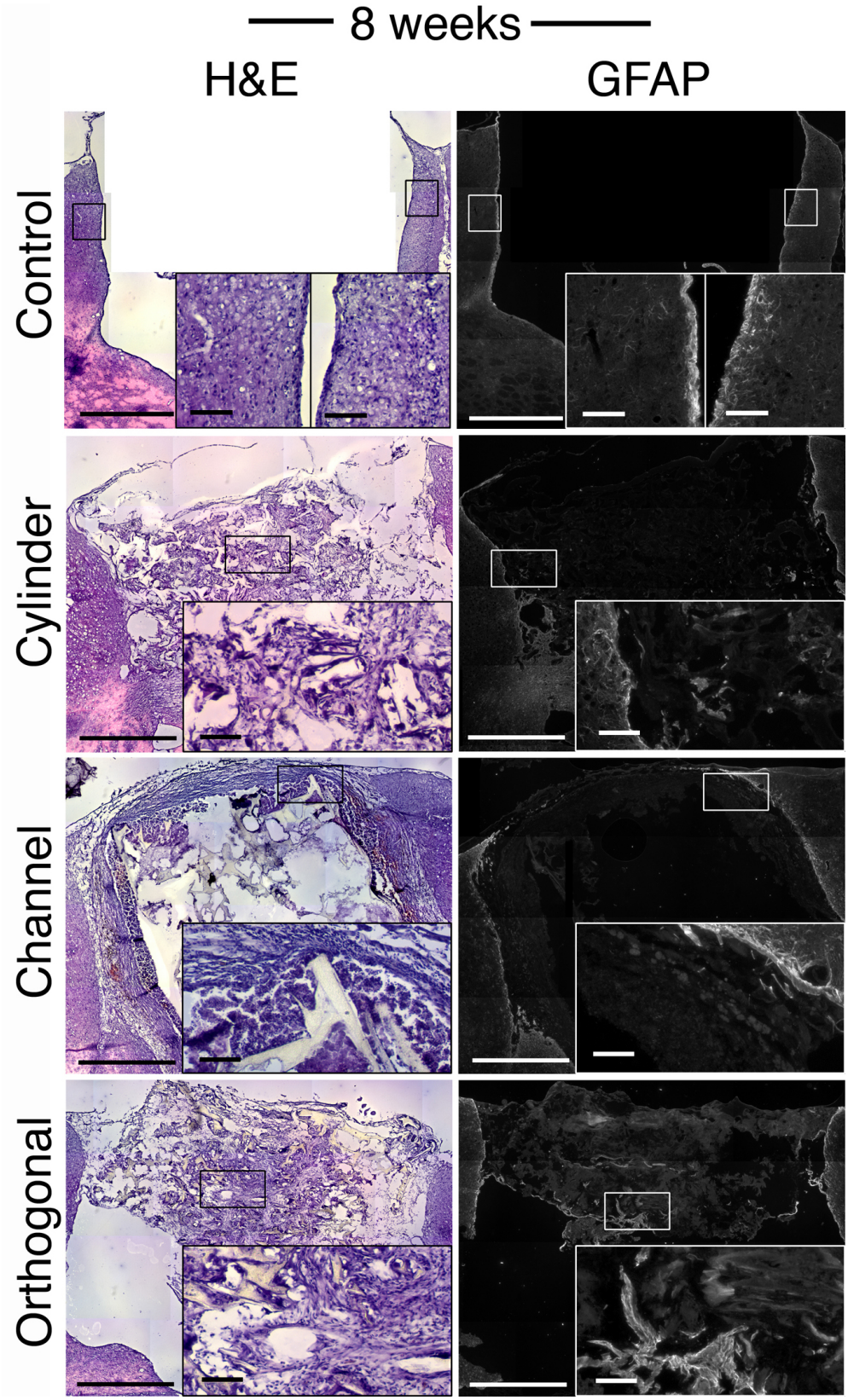

Figure 4.4: Representative and corresponding sections for cylinder, channel, and orthogonal scaffolds H&E stained and labeled for GFAP for 8 weeks implantation. Each larger overview image (scale bars 1mm) has a higher magnification inset indicated by the small boxes to show cellular details (scale bars 100 μm).

4.5k) and along the perimeter (Figure 4.5j and l). Tuj-1 positive axonal processes were seen within grooves inside the Orthogonal designs from an out of plane view (Figure 4.5m and n), and extended along grooves along the exterior of the Channel design from an in-plane view (Figure 4.5h and i) at 8 weeks. Though not found as extensively as the nestin filaments, Tuj-1 labeling was found in areas corresponding to some of the nestin labeled areas. Tuj-1 labeling was not obvious in the Cylinder group, and not organized (Figure 4.5e).

There was no statistical difference in the diameters of the defects over time or between groups, though the control group had an increasing trend over time and also had the highest mean value after 8 weeks (Figure 4.6a). Significance levels were calculated to be P(group) = 0.31, P(time) = 0.18. Previous literature also indicates that secondary cell death following brain injury is a common occurance, and damaged regions often expand weeks after the initial insult (Raghupathi, 2004; Williams et al., 2006). Total tissue ingrowth per area of scaffold, measured from H&E staining, was statistically higher in the Orthogonal group at 8 weeks compared to the other groups, (not including the control group which was empty inside the defect) and the Channel scaffold had the lowest total ingrowth in the first week (Figure 4.6b). These significance levels were P(group) = 0.03, P(time) = 0.005. Also, at 8 weeks the fibrous capsule surrounding the Channel design was included in total tissue ingrowth to the defect site. Though it was not within the scaffold itself, it was new tissue growth within the defect site. Astrocytic infilration, as measured by GFAP labeled areas within the scaffold, increased over time in all groups except the Channel group. Cylinder and Orthogonal groups had no significant differences from each other but had 5 times more GFAP than the Channel group at 8 weeks (Figure 4.6c), P(group) = 0.09, P(time) = 0.01. Inflammation in the primary and secondary regions was

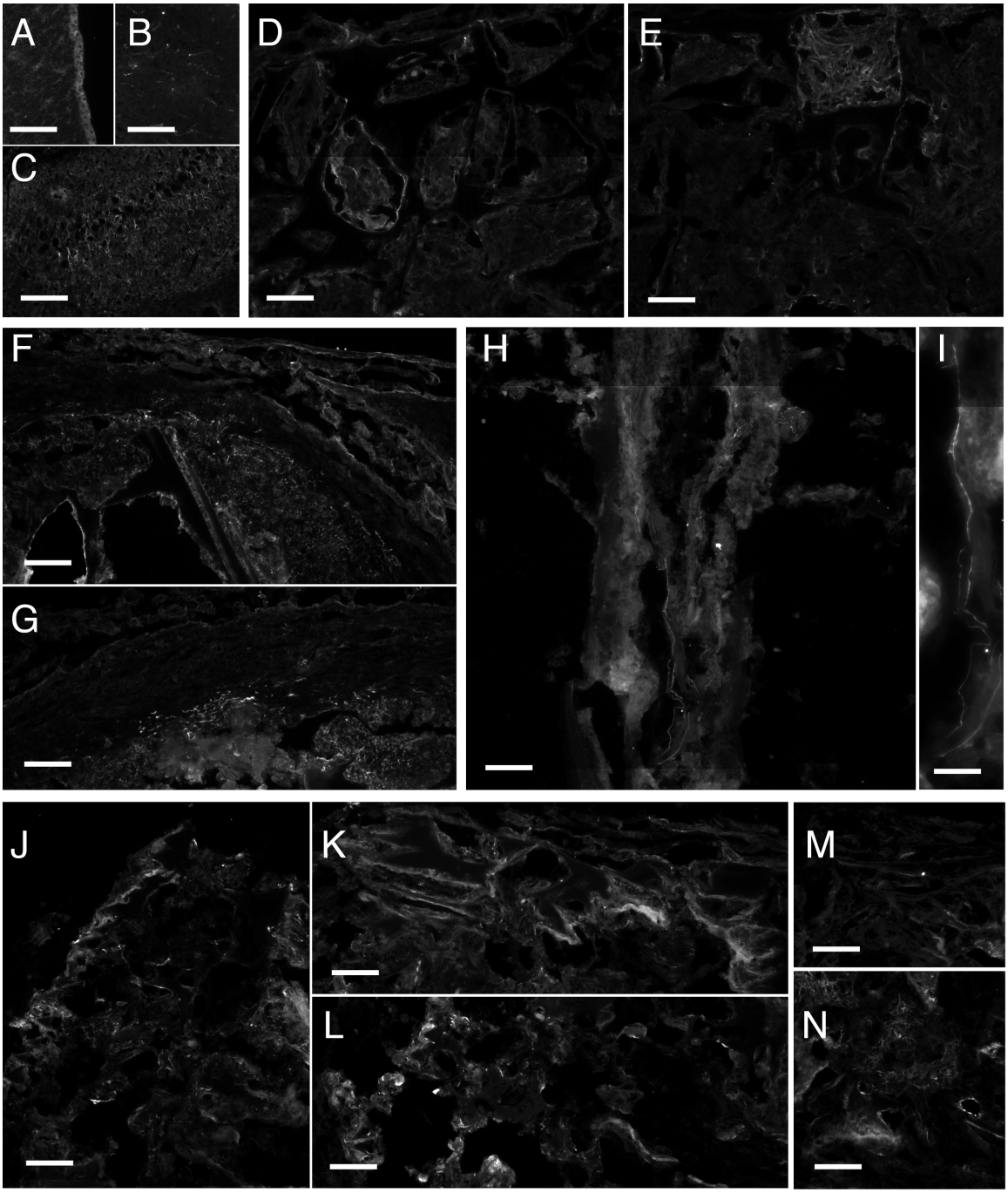

Figure 4.5: Nestin and Tuj-1 labeled sections of cylinder, channel, and orthogonal scaffolds from 8 week time points. All scale bars 100 μm except in (i) which is 50 μm. (a)Ependymal cells and some astrocytes as well as (b) microvasculature are labeled with nestin in a control brain. (c)neurons and axons are labeled with Tuj-1 in the neuropil of the CA1 region of the hippocampus. Cylinder implants have a small region near the top of the implant labeled with (d) nestin and (e) Tuj-1. Channel implants were labeled only at the exterior perimeters of the scaffolds with (f, g) nestin, and (h) Tuj-1, a higher magnification of the fiber in (h) is shown in (i). Orthogonal implants were labeled in areas deep within and also on the perimeter where microgrooves are shown in cross-section with (j,k,l) nestin and (m,n) Tuj-1. Fibers are seen aligned with some grooves in (k) and (m).

measured by GFAP labeling intensity. Not surprisingly, the primary edge regions had higher GFAP intensity than secondary regions, in all groups at all time points. There was a general decrease over time, most noticeable in the secondary regions (Figure 4.6d), and no significant difference between groups. Significance levels for this intensity data were P(group) = 0.84, P(time) = 0.0002.

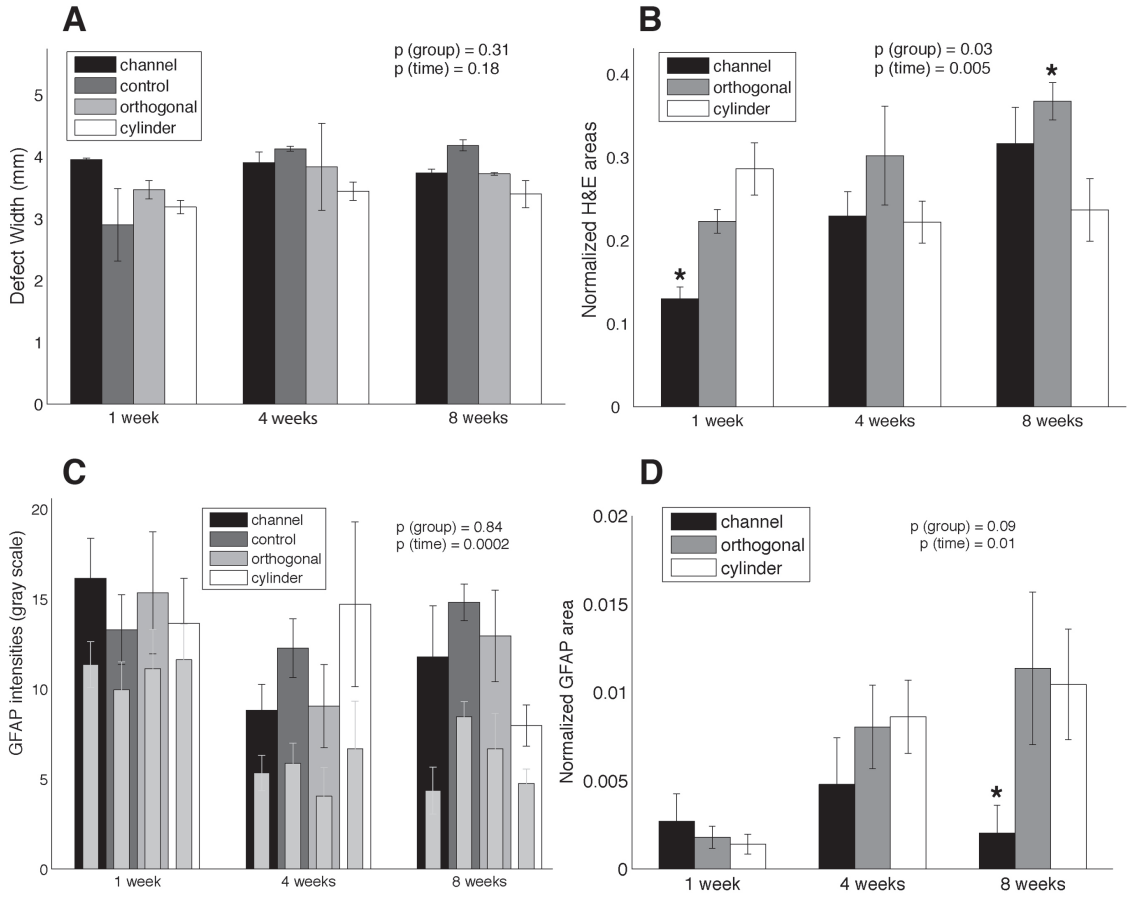

Figure 4.6: Quantification of defect widths, total cellular ingrowth, parenchymal inflammation, and astrocytic infiltration of cylinder, channel, and orthogonal scaffolds. (a) Defect widths over time show the control group increases the most, though not statistically significant. (b) Total cellular ingrowth from H&E staining shows inward migration in all implant groups over time, with starred groups significantly different from others at the same time point. (c) Intensity of GFAP labeling in primary and secondary (thin light gray bars in front) regions of adjacent parenchyma decrease over time and are not significantly different between groups. (d) Astrocytic infiltration of implant groups increases over time in cylinder and orthogonal groups. The starred channel group is significantly lower than the other two groups at 8 weeks.

4.5 Discussion

Orthogonal design scaffolds were more conducive to inward migration of cells than the other designs, and microgrooves on both channel designs were able to support alignment of neural fibers *in vivo*. The random pored cylinder scaffold was porous enough to allow inward migration, but did not support any alignment of fibers, while the channel design allowed alignment on its exterior microgrooves, but cells were unable to migrate into it.

The differences in the designs may have influenced the types of cells that were able to populate the scaffolds. Because the Channel design was open mostly to infiltration from the top and bottom, with no interconnecting channels entering from the sides, it is possible that fibroblasts and hematopoaetic cells entered quickly from the damaged dura and infiltrating peripheral blood, while lateral parenchymal cells were not able to migrate in as easily. Although the Channel design was not completely closed, and in fact contained several porous areas on the exterior (Figure 4.1h, j, and k), it was the only one that led to a fibrous capsule formation.

In the casting process, salt crystals in contact with the walls of the mold leave a pore in that wall of the scaffold. Since microgrooves cannot be perfectly filled with salt crystals of a larger size, extremities of grooves get filled with polymer, while contact with salt on the inside edges of the grooves can result in pores. Thus the lateral walls of the Cylinder design can have larger pores than the Channel design, as whole sides of salt crystals can be in contact with mold walls. Aside from pores resulting from salt leached crystals, PCL cast using acetone as the solvent results in a rough, often single digit micron scale porosity (Figure 4.1l and m). This means that the Cylinder design had a much smaller porosity along its lateral walls than the

other two designs.

Orthogonal designs have large lateral pores by virtue of the six orthogonal channels while the rest of the walls were similar to the Channel design, but with axially oriented microgrooves. The oriented grooves along the exterior of the Channel design did allow the fibrous tissue capsule to assume the longitudinal orientation and some neuronal processes to grow in that same longitudinal direction, but only exteriorly. The Orthogonal design showed nestin and Tuj-1 labeling in microgrooves as well, but this labeling was located inside the scaffold. It has been shown that nestin, an intermediate filament expressed in neural progenitors during development, is expressed in mature brains after injury in the microvasculature, the ependymal cells of the lateral ventricles and in some activated GFAP positive astrocytes after and may indicate the reversion of these glia to a more plastic state (Douen et al., 2004; Li and Chopp, 1999; Sahin Kaya et al., 1999). The data presented here showed astrocytic migration into the perimeters of scaffolds as well as nestin labeling within the scaffolds in similar and farther reaching areas. Also tuj-1 positive neuronal processes were found in areas corresponding to some of the nestin labeled areas. In areas where the microgrooves were identifiable, fine nestin fibers and tuj-1 labeled fibers were seen elongated in the same direction as the grooves. This evidence points to the influence of oriented microgrooves in the alignment of axonal processes and neural progenitors *in vivo*.

The openness of both the Cylinder and the Orthogonal designs led to similar astrocytic migration into those scaffolds and indicate that there is probably a threshold of pore size, when compared to the Channel design, for astrocytic or glial cell migration from brain tissue. Glial cells are often associated with the formation of a glial scar or glia limitans which acts as a physical barrier to axonal regeneration in the brain and spinal cord. This barrier was seen in previous literature to form along the perimeter

of a porous polyester membrane 100-150 μm thick with 5 μm pores after 8 weeks. However, the glia limitans was breached at the entrance to many pores and glial cells were seen without any basal lamina to push into the membrane slightly, accompanied by axonal processes (Kristt, 1987). Glial processes also serve to guide neuroblasts during migration and extension of processes (Rakic, 1971), thus it is plausible that astrocytic migration could provide the pathway for neuronal and progenitor cell migration and elongation within the scaffold. Also, the interconnected channels and grooves of the Orthogonal design compared to the Cylinder were likely responsible for the increase in the total cellular population and the organization of neuronal and progenitor cells within the scaffolds. Increased connectivity by the orthogonally intersecting channels and grooves along the channels would have provided a better environment for migration into the scaffold than the plain Cylinder group with its randomly connected pores and unorganized roughness. The size of the pores created by the salt crystals (180-250 μm) was fairly large compared to the size of individual cells, such that the pore size itself would not have posed a significant barrier to cell migration in the Cylinders, with cell sizes in the 5-30 μm range. Channels in the Orthogonal and Channel designs were about 300-430 μm in diameter, roughly twice the size of the salt generated pores. It is unlikely that the diameter of the channels was more influential than the interconnectivity they provided or the grooved surfaces they presented as compared to the Cylinder group.

In summary: (1) Scaffolds slightly decreased secondary cell death compared to controls as demonstrated by the trends in defect width measurements. (2) Scaffolds did not cause severe inflammation compared to controls, as evidenced by the intensities of GFAP labeling in primary and secondary edge regions. (3) The Orthogonal design had the highest total cellular infiltration at 8 weeks, attributable to

its larger lateral wall pore size than the Channel and its higher interconnectivity and inwardly oriented microgrooves compared to the Cylinder. (4) Tuj-1 and nestin labelled cells/fibers aligned within microgrooves in Channel and Orthogonal scaffolds, an aspect not found in Cylinder scaffolds which contained no microgrooves. (5) The Channel design caused a fibrous encapsulation response at 8 weeks, likely due to the orientation of its channels toward the dura and its smaller pore sizes in the lateral walls. (6) Cylinder and Orthogonal designs had roughly equal inward astrocytic migration, which may be explained by their similar pore sizes in the lateral walls.

It is possible that longer time points would reveal a difference in this type of cellular migration, but a difference in total cellular migration between the two designs is seen at 8 weeks, as is a difference in the quality of nestin and Tuj-1 labeling. These data suggest that cerebral cortex regeneration can be positively influenced by interconnectivity of channels and groove orientation in designed scaffolds.

4.6 Conclusions

The data presented here suggest that well chosen scaffold details can be beneficial to brain tissue regeneration in the following ways: 1) Pore sizes oriented toward the parenchyma which are in the range of 100s of microns promote more robust inward astrocytic migration compared to smaller pore sizes. 2) Microgrooves can help to align nestin and Tuj-1 positive progenitor and neuronal fibers and enhance total cellular ingrowth when oriented in the direction of migration. 3) Fully interconnecting channels can improve cellular migration and prevent fibrous tissue encapsulation. These aspects can play a large role in the effectiveness of biological treatments such as stem cells and growth factors.

Acknowledgments

Thanks to Dr. Chris Nosrat for help with surgeries. Thanks to Jason Kutch for help with Matlab coding.

CHAPTER V

Open-path architectures promote nerve fiber regeneration and decrease secondary damage in spinal cord injury

5.1 Overview

Biomaterial scaffold architecture has not been investigated as a tunable source of influence on spinal cord regeneration. This study compared regeneration in a transected spinal cord within various designed macro-architectured scaffolds to determine if these architectures alone could enhance regeneration. 3-D designs were created and molds were built on a 3-D printer. Salt-leached porous poly(ϵ-caprolactone) was cast in five different macro-architectures: cylinder, tube, channel, open-path with core, and open-path without core. The two open-path designs were created in this experiment to compare different supportive aspects of architecture provided by scaffolds and their influence on regeneration. Rats received T8 transections and implanted empty scaffolds for 1 and 3 months. Overall morphology and orientation of sections were characterized by H&E, luxol fast blue, and cresyl violet staining. Borders between in-tact gray matter and non-regenerated defect were observed from GFAP immunolabeling. Nerve fibers and regenerating axons were identified with Tuj-1 immunolabeling.

The open-path designs allowed extension of myelinated fibers along the length of the defect exterior to and inside the scaffolds and maintained their defect length

over 3 months. In contrast, the cylinder, tube, and channel implants had a doubling of defect length from secondary damage and large scar and cyst formation with no neural tissue bridging. The benefits of the open-path designs are likely due to differences in macro-architecture, as material and microarchitecture were the same in all implants and no biological factors were used.

5.2 Introduction

The purpose of this study was to investigate the effects of varied implant architectures on spinal cord (SC) regeneration. Most studies of chronic spinal cord injury (SCI) repair have employed tubes or channels and combined their material implant with bio-active factors (Hadlock and Sundback, 2006; Nomura et al., 2006; Zhang et al., 2005). There have been no explicit comparisons of architectures or studies of designs which take into account how scaffold material is distributed with respect to white and gray matter distribution, though their physical organization is integral to the functions carried out by the spinal cord (see section 2.3.3).

Treatments for SCI under investigation include use of trophic factors, antibodies, enzymes, stem cells, schwann cells, or olfactory ensheathing cells (Barnett and Riddell, 2007) to help rebuild the tissue through re-myelination, axonal guidance, or prevention of secondary damage (Hadlock and Sundback, 2006; Nomura et al., 2006; Zhang et al., 2005). Cell transplantation and injected factor therapies under investigation may be limited to small injuries, as survival of injected cells and residence time of injected factors is often quite low (Friedman et al., 2002). If the injury is too large, or in a chronic stage with a large area of secondary damage, a material scaffold is useful for increasing cell survival and localizing cells or biologic factors to the target area (Friedman et al., 2002; Tate et al., 2002).

As discussed in section 2.3.2, several biomaterials have been investigated with varying architectures and mechanical properties, aimed at delivering cells or trophic factors to the injured spinal cord and guiding regeneration in a longitudinal direction (Bakshi et al., 2004; Carone and Hasenwinkel, 2006; Flynn et al., 2003; Gelain et al., 2007; Horn et al., 2007; Houle and Ziegler, 1994; Huang et al., 2005; Li et al., 2006; Nomura et al., 2006; Stokols and Tuszynski, 2006; Teng et al., 2002). Various injury models have been used to study different aspects of injury and regenerative capacity. Contusion, hemisection, and complete transection are the most common models (Hadlock and Sundback, 2006; Nomura et al., 2006; Zhang et al., 2005). While each of the models has reproducible effects it is more difficult in the contusion and hemisection models to determine if recovery is due to sparing and compensatory sprouting or new regeneration. Though contusions and hemisection models can be more clinically relevant, in cases where proof of concept and proof of regeneration is needed, the complete transection model is often useful, and is employed in this study.

The organization and reconnection of different tracts in the spinal cord are important to functional recovery (Figure 2.2). For example, lateral and ventral corticospinal tracts are most important to recovery of locomotor function, while dorsal tracts provide less improvement if spared (Kaegi et al., 2002; Mori, 1992; Noga et al., 1991; Schucht et al., 2002). When evaluating SCI in patients and their potential treatments, these types of anatomical distinctions have a great effect on the degree of functional recovery.

Newly severed axons have regenerative capacity in the first few days but meet with restrictive environments such as myelin inhibitory factors and a quickly growing glial scar, which prevent axonal extension and complete regeneration to their original tar-

gets (Busch and Silver, 2007; Maier and Schwab, 2006; Schwab et al., 2006; Schwab, 2002). Different neurotrophic factors (Thoenen, 1991) are being investigated to make the injured environment more permissive to axonal regeneration (Barritt et al., 2006; El Maarouf et al., 2006; Novikova et al., 2003). The local balance of permissive and inhibitory factors should be tipped toward permissive (Jones et al., 2003). While bio-active factors will indeed play a strong role in SC regeneration, the architecture of implant material may play an important, and more easily controlled, role as well.

This study has developed a method of manufacturing SC implants with very specific and varied designs which take into account white matter tracts. These new spinal cord implant designs were compared to conventional tube and channel architectures.

The novel designs were conceived to provide more surface area in key locations with grooves to direct growth while decreasing the barriers which might be presented by conventional designs like multi-channeled scaffolds, tubes with gels, or sponges (Nomura et al., 2006). Intended to take advantage of the circumferential location of the white matter and the early secondary death of the grey matter, the new designs in this study have an open path for the lateral funiculi where the corticospinal tracts descend, while one contains a central core to provide an added surface for guidance of nerve fibers from that region. Because the center of the cord dies first whenever the spinal cord is injured, leaving the exterior white matter tracts to cave in, resulting in a narrowing at the defect site (Maier and Schwab, 2006; Schwab et al., 2006), a scaffold was designed to support the white matter tracts from the center, in contrast to entubulation methods which provide surface contact guidance from the outside of the cord. The cylindrical core present in one open-path design is suspended by top and bottom fins from the shells anchored on the bottom of the spinal canal and at

the top with sutures to the two cut ends of the cord (Figure 5.1).

This study looked only at architectural effects in spinal cord transection, but future applications of these designs would include cell seeding or trophic factor impregnation or composite implants with infused hydrogels in the core and or other areas of the scaffold to enhance regeneration of the grey matter along with guided regeneration and support of the white matter. The designs could also be modified with the same basic principles to be applied to hemisection or contusion models of injury.

5.3 Methods

Scaffold design and fabrication:

Implants were made of PCL (50,000 kDa MW, Solvay Chemicals Inc., Houston, TX) dissolved in acetone, (13% wt.) and 180-250 μm sieved salt crystals were used for porogen leaching. The general shape and size of the implants was a 4mm long cylinder with 2.8 mm diameter. Five designs were used; cylinder, hollow tube, 5-channel, open-path with core, and open-path with no core (Figure 5.1a). Within the walls of each macro-design (gray areas in Figure 5.1a), the implants were given a porous structure by salt leaching. To achieve more intricate architectures, other implants were designed in Rhinoceros software (McNeel North America, Seattle, WA) and wax molds were built as described in section 4.2 on a 3D Solidscape printer (Solidscape Inc. Merrimack, NH) (Figure 5.1b, c, d). To impart longitudinal microgrooves, molds were built sideways with a funnel on top for pouring in salt and the polymer (Figure 5.1b). Cylinder design implants were made in teflon molds packed with salt and had no microgrooves (Figure 5.1e). Microgrooves are an artifact of the layer-by-layer mold printing process. The programmed layer thickness was set to 38.1 μm. A groove is generated in the z-direction between each layer in the mold. The grooves

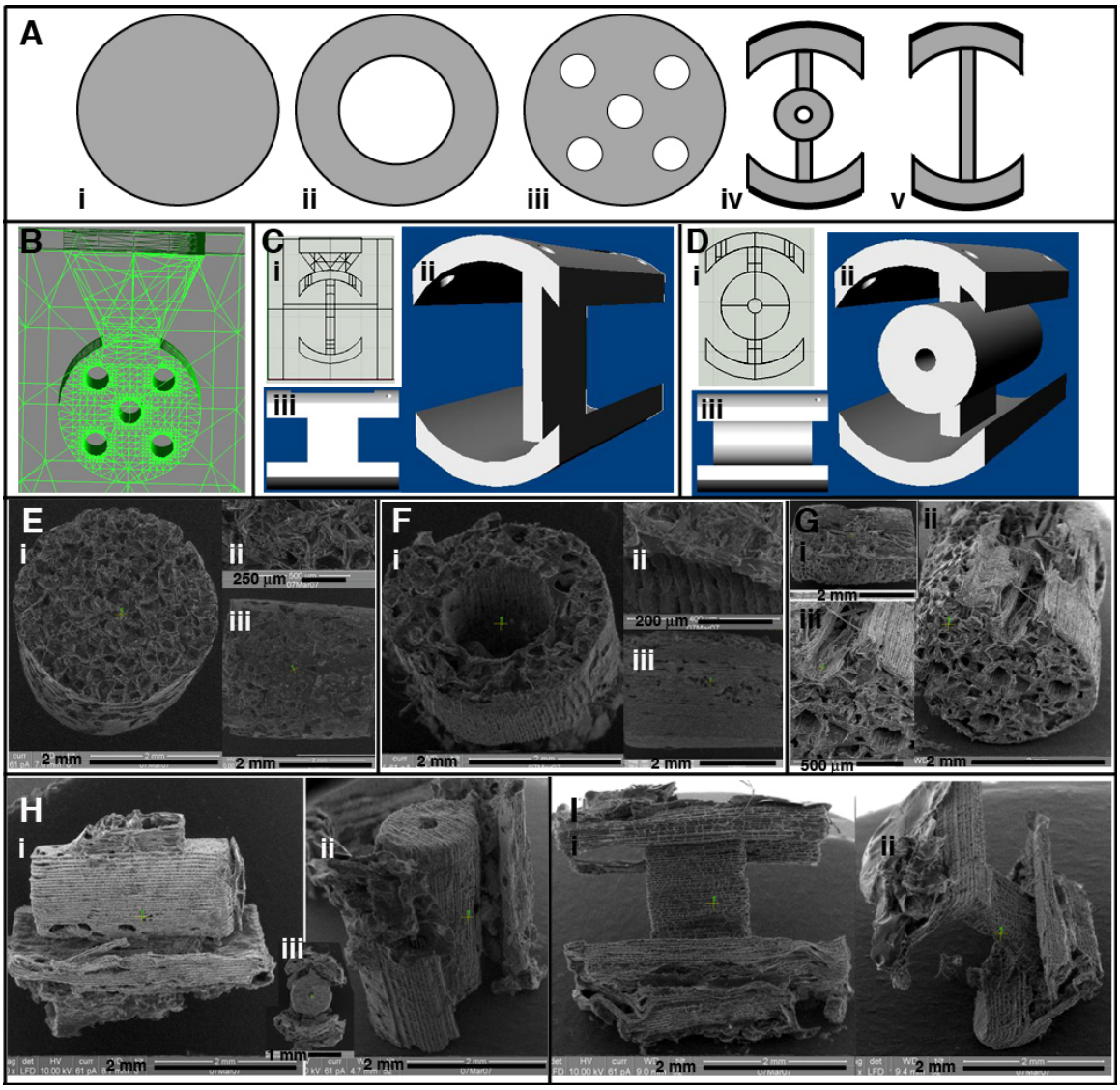

Figure 5.1: Design and fabrication of macro-architectures for spinal cord implants. a) Axial view of designs for cylinder (a.i), tube (a.ii), channel (a.iii), open-path with core (a.iv), and open-path without core (a.v). b) Wireframe view of a mold for the channel design, a funnel is built into the top through which salt and polymer are poured to fill the mold. c) The open-path without core mold design with polymer and salt inlet (c.i), oblique view (c.ii) and side view (c.iii). d) The open-path with core design (d.i), oblique view (d.ii) and side view (d.iii). SEM micrographs for cylinder (e), tube (f), channel (g), open-path with core (h), and open-path without core (i) scaffolds after fabrication.

are then transferred in the casting process to the actual polymer scaffold (Figure 5.1f, g, h, i). The excess polymer was trimmed from each implant and wax was dissolved in BioAct (Solidscape Inc. Merrimack, NH). The BioAct and salt particles were cleaned out with several washes of 70% ethanol and agitation, and implants were stored sterilized in fresh 70% ethanol. Prior to surgery, implants were transferred to sterile saline.

Surgical Implantation:

Female Sprague Dawley rats (200-250 g) were anesthetized and SC's completely transected at T8 with a 3mm long transection. Control groups received no implant. Implants were sutured to proximal and distal stumps and then covered with Durepair (Medtronic, Minneapolis, MN). Daily bladder expression, medications, and husbandry attention were administered as needed. Each time point and group contained replicate (n= 3) animals. Deaths reduced the number of rats in the Channel group to 1 rat at 1 month, and 2 rats at 3 months. Rats were sacrificed at 1 and 3 months by transcardial perfusion. SC's were cryosectioned longitudinally for immunohistochemistry and staining and placed onto gelatin coated slides. All surgery, post-surgical recovery and euthanasia were performed according to a protocol approved by the University of Michigan Committee on the Use and Care of Animals.

Histology and Immunohistochemistry:

Stains and antibodies used were hematoxylin and alcoholc eosin, Luxol Fast Blue (LFB) (myelin stain) and Cresyl Violet (Nissl substance, neuron stain), rabbit anti-GFAP for astrocytes (G9269 Sigma), mouse anti-Tuj-1 for axons (MMS-435P Covance, Berkeley, CA) with a Vecta-stain ABC kit (Vector Labs, Burlingame, CA) and biotinylated Alexa-488 (Invitrogen/Molecular Probes, Carlsbad, CA) for fluorescent

visualization. Images were taken using a Spot camera and Spot Advanced software (Diagnostic Instruments, Sterling Heights, MI).

Quantification and statistics:

Defect lengths were measured from serial sections labeled with GFAP to identify the extent of degeneration of the central core of grey matter. Because of the poor connectivity between some stumps of the control group and easy disruption during tissue handling, defect lengths for the control group were not measured (Figure 5.2). 2-way ANOVA was carried out on defect length measurements with time and group as independent variables. Tukeys Least Significant Difference post-hoc analysis was used for multiple comparison between groups if significance levels were below $P = 0.05$.

5.4 Results

From H&E staining and gross images, connectivity between the stumps was obtained in all implants to varying degrees. Much of the growth for the cylinder (Figure 5.3), and tube and channel groups (Figure 5.4) occurred along the outside of these implants. Much of the porous interior walls were filled with cellular debris, macrophages, and fibroblast-like cells as observed from H&E staining at 1 month (Figure 5.3a, Figure 5.4a, Figure 5.4h). By the 3 month time point several of these implants showed necrotic death within and around them (Figure 5.3b, Figure 5.4b, Figure 5.4i). A high degree of secondary death was evident in these three groups at both ends of the injury. In particular, fibrous capsules formed around the cylinder design scaffolds after 3 months (Figure 5.3b). GFAP antibodies labeled reactive astrocytes in intact spinal cord and became diffuse and non-existant closer to and within the scaffold as tissue was degenerating and fibrous tissue ingrowth occurred.

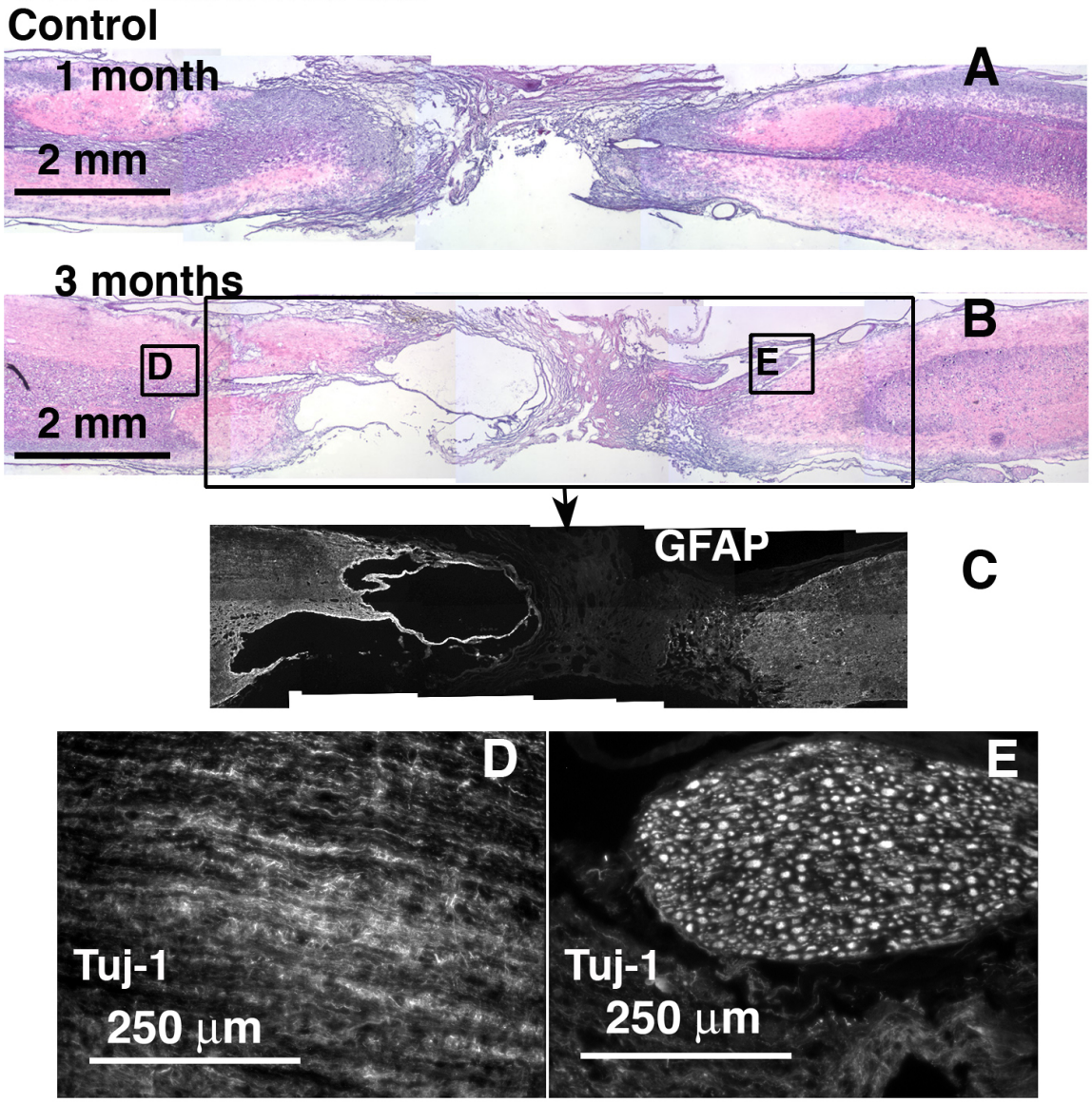

Figure 5.2: Control defect, no scaffold implant, at 1 and 3 months, H&E stained and immunolabeled. Caudal end is always to the right. a) 1 month H&E stained. b) 3 months H&E stained section with corresponding regions (boxed) immunolabeled for GFAP (c), and Tuj-1 (d and e).

(Figure 5.4c, g, j, n). Tuj-1 labeled axons were found only in the remaining spinal cord stumps (Figure 5.4d, k, l). Oriented tissue within the tube and channels contained no axons (Figure 5.4e, f, m).

In contrast, tissue grew interiorly along the entire length of both open-path implants and appeared well connected (Figure 5.5). Because of the uncommon architecture of these scaffolds, diagrams of orientation and approximate planes of sectioning have been provided for each of the open-path designs along with images of neighboring sections (Figure 5.5a, b, d, e). Histological results were consistent in replicate animals. An additional specimen is shown for each open-path design at the 3 month time point for comparison (Figure 5.5c, f). The gross shape and size of the spinal cord at the implant site was similar to uninjured areas of the cord, unlike the other three implant groups where large cysts and fibrotic tissue formed around the implants and their ends. There was less necrosis and scar tissue at both ends of the open-path implants and neural tissue entered from both proximal and distal stumps, and grew around the implants. Considerable tissue tracts along the periphery of the defect and the outside edges of the scaffolds contained intact Tuj-1 positive myelinated axonal fibers, though they never appeared to connect on the distal stump. Some of the thicker growths around the edges of the open-path designs could have been spinal nerves from either dorsal or ventral nerve roots, but instead of exiting the spinal canal may have merged with the scaffolds along the length of the defect before leaving the spinal cord (Figure 5.5). There were also Tuj-1 labeled axons within the open-path with core scaffolds, and fibers were observed straddling the edge of the bottom shell on both of its surfaces (Figure 5.5 f.3). The shell thickness was 200 μm.

Defect lengths measured from GFAP labeled serial sections after 3 months *in vivo* showed that defects with open-path designs maintained their original lengths from

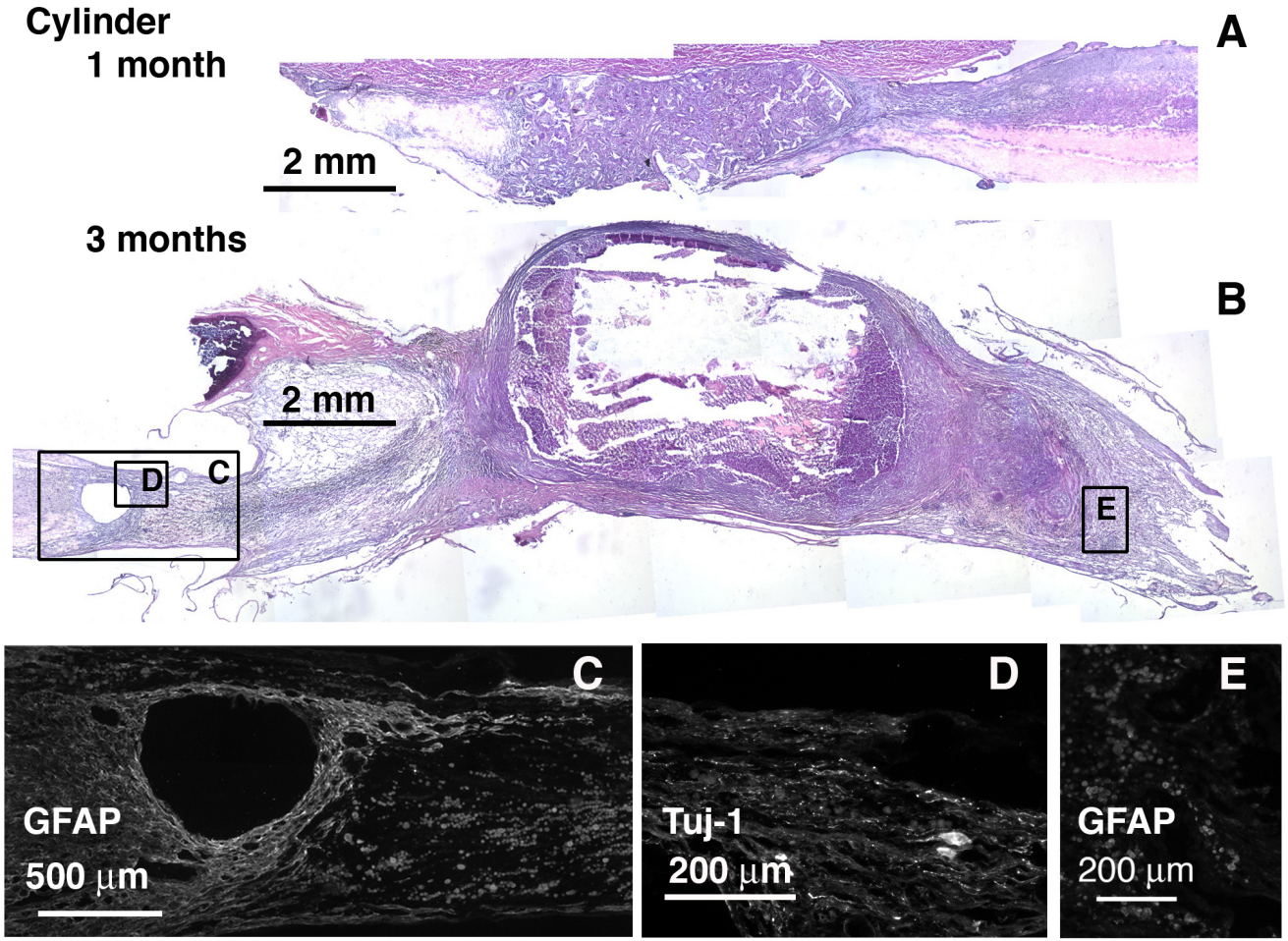

Figure 5.3: Cylinder implant at 1 and 3 months, sagital sections H&E stained and immunolabeled for GFAP and Tuj-1. Caudal end is always to the right. a) 1 month H&E stained. b) 3 months H&E stained with corresponding regions (boxed) immunolabeled for GFAP (c and e), and Tuj-1 (d).

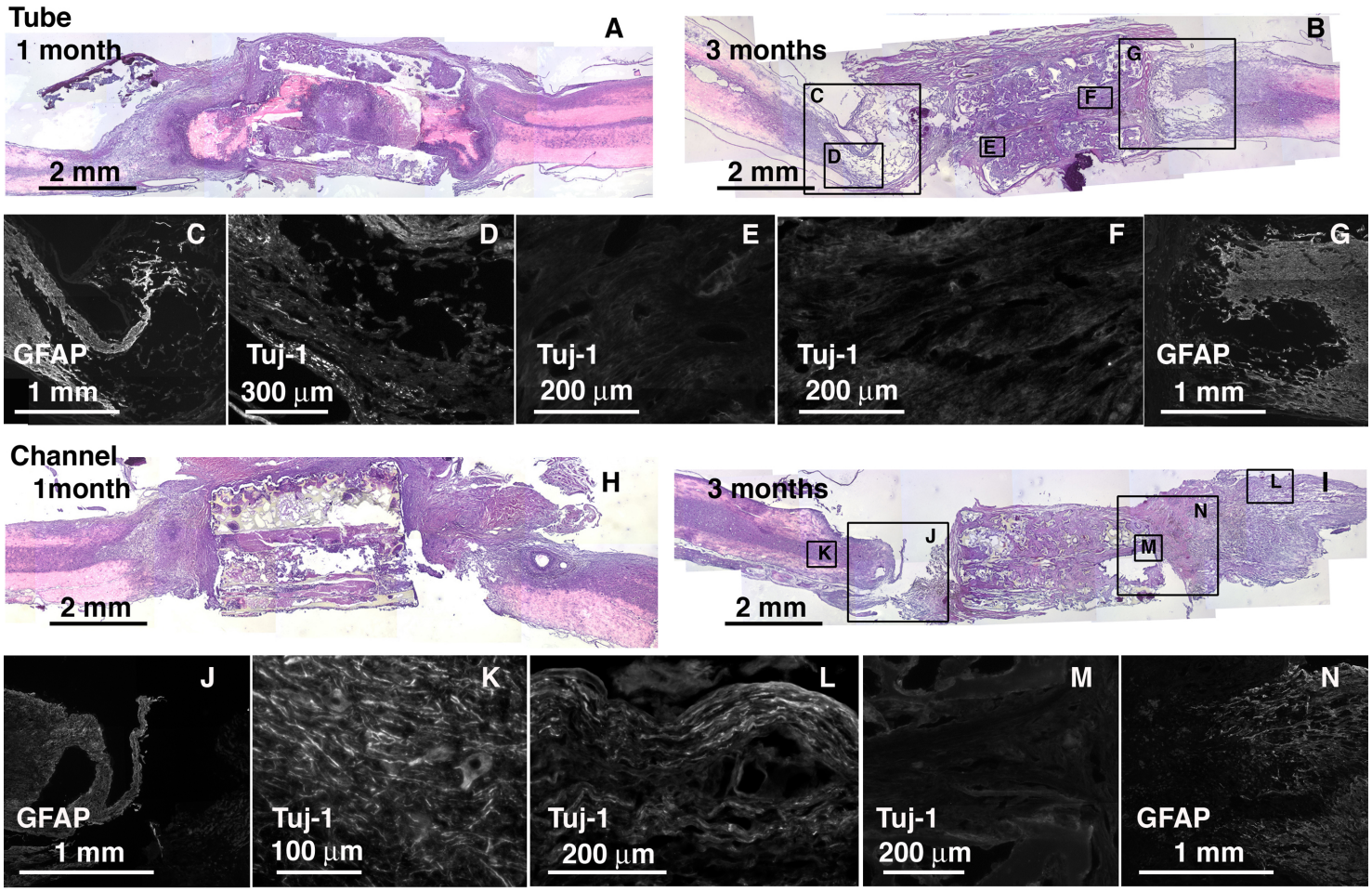

Figure 5.4: Tube and channel implants at 1 and 3 months, sagital sections H&E stained and immunolabeled for GFAP and Tuj-1. Caudal end is always to the right. a) Tube section at 1 month H&E stained. b) Tube section at 3 months H&E stained with correspondeing regions (boxed) immunolabeled for GFAP (c and g) and Tuj-1 (d, e, and f). c) Channel section at 1 month H&E stained. d) Channel section at 3 months H&E stained with corresponding regions (boxed) immunolabeled for GFAP (j and n) and Tuj-1 (k, l, and m).

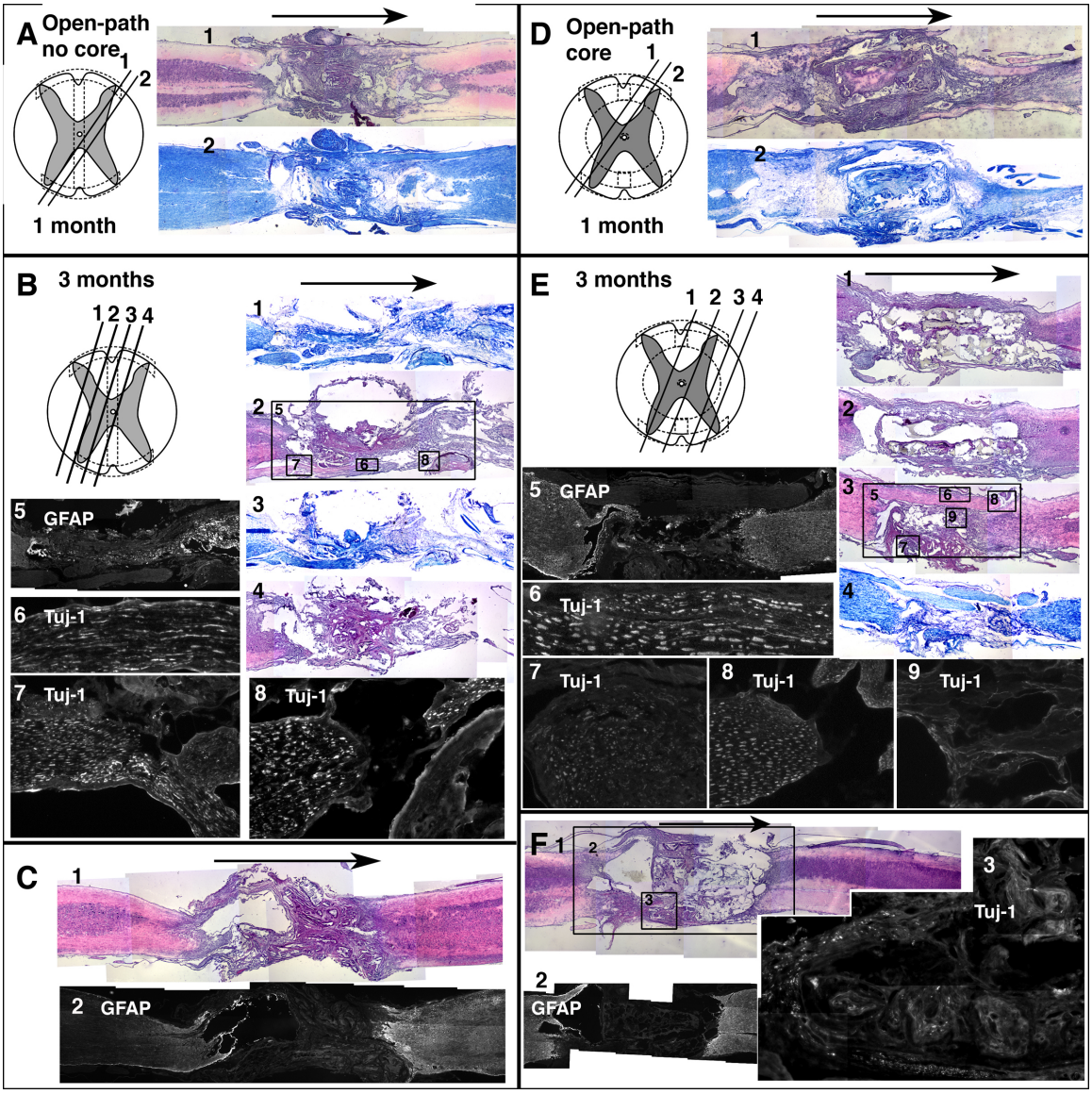

Figure 5.5: Open-path designs with and without core, sagittal sections stained and immunolabeled. Arrows indicate rostral to caudal direction. a) Two neighboring sections (orientation diagramed) from open-path without core at 1 month, H&E (a.1) and LFB (a.2) stained. b) Four neighboring sections (orientation diagramed) from open-path without core at 3 months, H&E (b.2 and b.4) and LFB (b.1 and b.3) stained. Section shown in b.2 has corresponding regions (boxed) immunolabeled for GFAP (b.5) and Tuj-1 (b.6, b.7, and b.8). c) Two sections from a different animal from open-path without core 3 month group H&E (c.1) and LFB (c.2) stained. d) Two neighboring sections (orientation diagramed) from open-path with core at 1 month, H&E (d.1) and LFB (d.2) stained. e) Four neighboring sections (orientation diagramed) from open-path without core at 3 months, H&E (e.1, e.2 and e.3) and LFB (e.4) stained. Section shown in e.3 has corresponding regions (boxed) immunolabeled for GFAP (e.5) and Tuj-1 (e.6, e.7, e.8, and e.9). f) Section from a different animal from open-path with core 3 month group H&E (f.1) stained with corresponding regions (boxed) immunolabeled for GFAP (f.2) and Tuj-1 (f.3).

the implant size of 4 mm (Figure 5.6), while defects with the three closed designs had nearly a doubling of defect length from the original implant size ($P = 0.002$). As most secondary cell death occurs in the first few weeks, there was no significant difference in defect lengths over the two time points 1 and 3 months ($P = 0.54$), thus only 3 month data is reported.

5.5 Discussion

The open-path implant designs both with and without core had a beneficial effect on the secondary injury progression by measure of the defect length. Overall morphological appearance of the cord specimens with these implants was more connected and less fibrotic. Axonal regeneration was seen within and around these implants, and particularly robust fibers were observed crossing the defects around the implants. These promising regenerative results were in complete contrast to the results in the conventional designs, whose defect lengths grew to 7 mm and had no neural tissue regeneration across the defect site.

To further differentiate the two open-path designs, the implant with a central core had more robust nerve fiber extension across the defect site both around the outside of the implant and within the scaffold itself. The design without a core showed only bundles of fibers along the outside. Though not statistically significant, the open-path with core implant even showed a decrease in defect length, indicating some regeneration of the central region of the spinal cord.

Though many nerve fibers were seen crossing the open-path scaffolds, it is possible that they were not newly regenerated fibers. Because the open-path designs were open rather than closed like the other three, there was space for nerve roots to potentially merge into the defect site prior to their exit (Figure 5.6b). It is possible that

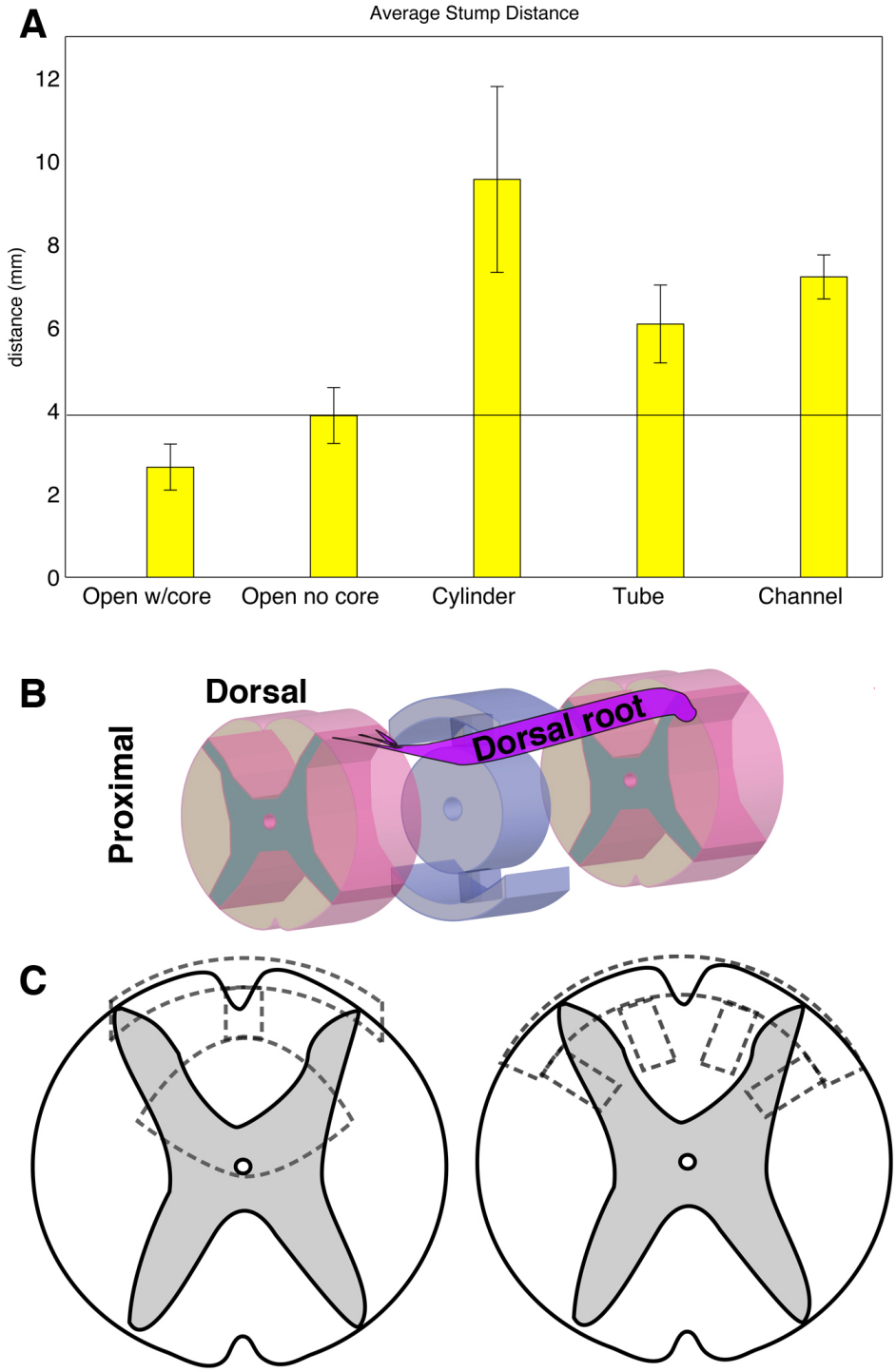

Figure 5.6: Defect lengths and illustrations of possible interactions. a) Average shortest distance between GFAP labeled intact cord stumps at 3 months. b) Illustration of open-path with core scaffold and its orientation within the defect. Nerve roots or regenerating white matter tracts from the lateral funiculus could possibly crawl along the inner core of the scaffold to bridge the defect. c) Modified designs (dotted lines) could accomodate contusion (left) or hemisection (right) injury models wile maintaining the same principles of complete transection designs.

these nerve roots served a protective role for the remaining cord, which could have prevented enlargment of the defect length. One of the most promising treatments for SCI currently is transplantation of peripheral nerve grafts (Houle et al., 2006; Kuo et al., 2007; Levi et al., 2002). Specifically after a preconditioning injury, the Schwann cells of these grafts have been shown to migrate from the graft and myelinate the axons of injured spinal cord (Dinh et al., 2007; Fukunaga et al., 2004). If those substantial nerve fibers seen crossing the defect of the open-path designs were indeed uninjured spinal roots which became physically engaged in the defect along the scaffolds, their proximity and activation due to the injury could have promoted some neuroprotection. This type of interaction between the native peripheral nervous system and the injured spinal cord would be impossible with entubulation methods which aim to enclose and protect the spinal cord from exterior perturbations. Still the spared spinal nerve root theory cannot account for the unbundled and disorganized axonal growth found within the open-path with core scaffolds (Figure 5.5 e.7, e.9, Figure 5.5 f.3).

The open-path with core design slightly out-performed the open-path without a core. The difference would be the additional cylindrical material. The core could have provided an additional surface for guiding white matter tracts from a convenient position in the inside of the cord, as intended.

The three conventional designs were unscuccessful in terms of providing an environment conducive to regeneration. The cylinder implant resulted in extreme defect enlargement and fibrous tissue encapsulation, likely worse than doing nothing at all. The tube and channel designs did allow oriented tissue to grow within, but it was fibrous and not neural. The tube walls essentially abutted the white matter tracts, in a similar fashion as the shells of the open-path designs. However, the tube walls

were thicker than the open-path shells, 650 μm compared to 200 μm. In addition, the tube walls went all the way around and were not open. The thickness of the walls may have played a part in the switching of roles from barrier, in the tube, to guiding surface, in the open-paths. It should be noted that the tube was not a true comparison for entubulation methods which push cord ends into the tubes. Those entubulation methods either necessitate extraction of the cord from the spinal canal or excessive destruction of the surrounding bone because the implant is too large to fit inside. Otherwise the tube walls must be so thin that they often collapse. The problem of collapse was addressed with reinforced tubes (Nomura et al., 2006) in one example of entubulation. However the added thickness caused the ends of the cord to be pinched, resulting a blocked cerebro-spinal fluid (CSF) flow and ultimately syringomyelia. For this reason, none of the designs used in the current study attempted to constrain the ends of the stumps, only abut. While multi-channeled scaffolds aim to increase surface areas to enhance guidance and carry trophic factors, the 5 channels, 450 μm diameters, presented in this study were not effectively integrated with the host tissue. Channels spaced closer and with greater density may be an improvement on that design, and have shown promise when used in conjunction with cells or trophic factors (Stokols and Tuszynski, 2006).

If simply modifying the architecture of a seemingly non-permissive material, a PCL salt-leached sponge, can provide enough guidance to allow robust nerve fiber bridging and inhibition of secondary damage, the effects of biologic factors could be greatly enhanced. Applying similar principles of architecture choice based on white and grey matter delineations to other injury models like contusion or hemisections might produce designs such as those displayed in Figure 5.6c. Porosity could be generated by alternate methods, and different materials could be employed using the

same mold. Open spaces could be filled with hydrogels loaded with neurotrophic factors, and neural stem cells could be seeded within the porous interstices. Now that the biological advancements in spinal cord regeneration are within reach and topographical guidance on the cellular level has been studied, the architectures of their material housing should receive as much creative thought.

5.6 Conclusions

The novel open-path designs allowed greater penetration of GFAP labeled neural tissue from both stumps and caused less scarring than the conventional implant designs. The open-path designs provided contact guidance using less material and allowed nerve fibers to extend across the entire defect length. These data suggest that implant architecture can be designed in more diverse ways to influence the growth of spinal cord tissue.

Acknowledgments

Thanks to J.C. Leveque, Hunter Brumblay, and Alex Garnepudi for all their assistance.

CHAPTER VI

Summary and future work

6.1 Summary

The influence of macro-architectures in CNS regeneration was investigated in brain and spinal cord by creating different macro-architectures for each site based on anatomical organization of the tissues. Solid free-form fabrication techniques were employed to fabricate these designs with a suitable porous degradable polymer. The architectural features, designed to coordinate anatomically directed regeneration in rats, enhanced regeneration of CNS without any use of biological factors or cells.

Cerebral cortex defects were implanted with porous degradable polymer scaffolds of PCL and PLGA. Through investigation of parenchymal inflammation and circulating inflammatory cell infiltration, as well as astrocytic and overall cellular infiltration and defect growth, the following findings allowed us to conclude that PCL would be a suitable polymer for investigating macro-architectural influences on CNS regeneration.

(1) PCL and PLGA are both biocompatible polymers in porous scaffold form in the cerebral cortex of rat.

(2) PCL and PLGA degradable scaffolds deterred growth of the defect cavity up to 4 weeks, in contrast to control defects with no implant whose cavities grew

significantly from the original size.

(3) PCL generated a lower inflammatory macrophage and astrocyte response and a higher neuroprotective microglial response than PLGA.

Through architectural variations based on the lamelar and columnar organization of neurons in the cerebral cortex, designed scaffolds implanted for up to 8 weeks showed differences in cellular migration and infiltration, and neural cell organization. The findings allowed us to conclude that in the cerebral cortex lateral migration of host cells is increased by lateral interconnecting channels but vertical migration, perpendicular to the surface of the cerebral cortex, is not enhanced by vertical channels alone. The white matter below the cerebral cortex is not a source of migrating cells, but the neighboring parenchyma, tissue comprising the laminae extending lateral to the defect, does provide more robust cell immigration. Vertical organization of axonal transmission is eclipsed by the need to first repopulate the defect cavity. However, microgrooves and vertical channels could improve vertical organization of axonal projections in the cavity once it is repopulated.

The next architectural pairing in the brain would be vertical microgrooves with vertical and lateral interconnected channels. In rats the cerebral cortex is quite smooth, making the singular orientation within a cylinder suitable for implantation in rats, but not a likely match for primates or humans whose cerebral cortex is similarly a few millimeters thick, but highly wrinkled. To address this difference, sheets of scaffolds could be created with the same interconnected pore structure and folded or wrinkled as needed. Other regions of the brain such as the stroma or hypothalamus might also benefit from oriented channels of different diameters and with different orientation.

Different architectures were created for spinal cord based on the locations of white

and gray matter and the progression of regenerative and degenerative phases. Open-path designs were fabricated to determine if support of circumferential white matter tracts medially would enhance their regeneration.

In a thoracic spinal cord transection, entubulation is not necessary when the spine still partially provides a natural enclosure. Though this may not be the case always in real injuries where the vertebral bodies are crushed, a simple wrap of the cord within the re-set bone fragments would protect the area, while a macro-architectural scaffold placed within could enhance the regeneration of the cord. Medial support of regenerating white matter tracts from the central core and outer shells prevents secondary damage in the centralized gray matter, possibly because of neuroprotective effects of regenerating nerve fibers and rostral nerve roots which are able to enter and bridge the open defect site. More clinically applicable injury models in the spinal cord, such as contusion or hemisection, could be accomodated with variations that omit the bottom shell of the open-path core design, or even the entire bottom half.

6.2 Related research for future work

These are the first *in vivo* experiments using scaffolds made by SFF techniques to have designed architectures in CNS regeneration. They show that different macro-scale architectures can affect tissue regeneration in the CNS, while micro-scale topography is confirmed to affect cellular behavior *in vivo*. The contribution of this work is to bring attention to the wide range of architectural possibilities for biomaterials in CNS regeneration. Aside from the delivery of neurotrophic factors and cells, appropriately designed biomaterials can enhance the regenerative potential of a defect site. Variation on these designed architectures can be extensive. Each of the designs for these CNS injury models can and should be combined with other tools

for regeneration: neurotrophic factors, cells, or extracellular matrix molecules.

6.2.1 Modifications to fabrication process

Because these architectures are created from a mold process, the material and the method of generating micro-pores could be changed. For instance, instead of using salt to generate pores, a freeze-drying technique (Patist et al., 2004; Stokols and Tuszynski, 2004) was used to generate longitudinal pores. PCL was dissolved

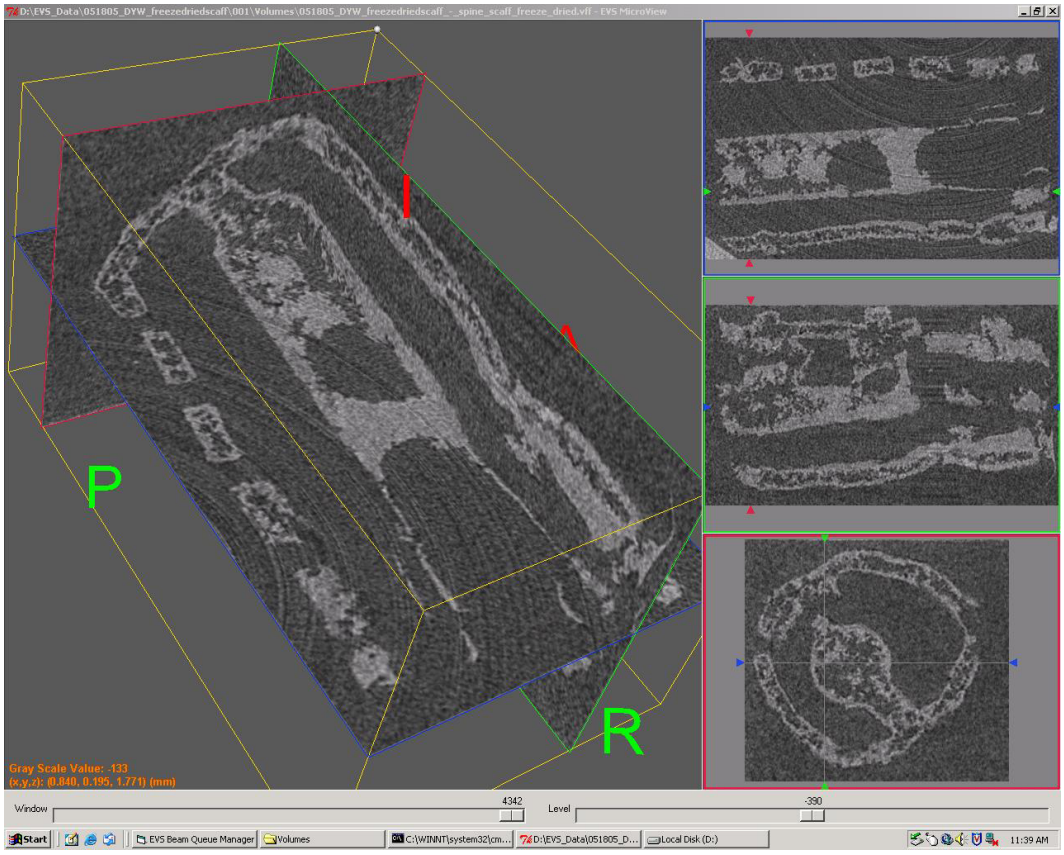

Figure 6.1: Micro-CT scan of a PCL scaffold made by a freeze-drying method in a wax mold. (left) And oblique view with three intersecting planes demonstrates the porous structure through different parts of the scaffold. The porosity was slightly unbalanced in the central core. (right, top to bottom) Two longitudinal views and one axial cross section of different planes show the structure of the scaffold to have a cenral cylinerical core within an outer cylinder that also has periodic holes spaced 1 mm apart. The outer and inner cylinders are held together by three separate fins lined along the top and three more lined along the opposite side. The breakage of the fins, which is visible in the bottom right image, belies the brittle nature of a scaffold produced by this method.

at 20% (wt:v) in acetone and poured directly into a mold with a general cylindrical shape 3 mm by 6 mm. In this case the mold was for a tube with a concentric cylinder

within held in place by three fins each on two sides. One end of the cylindrical shape was contacted with a metal plate atop dried ice in a styrofoam box to freeze the mold from only one face. After freezing, the mold was lyophylized to remove the acetone via sublimation and the wax mold removed by dissolution. The scaffold was scanned with a micro-computed tomography machine to examine the porosity (Figure 6.1). Though the resulting scaffold was too brittle for practical use, the method could be modified with a different solvent to polymer ratio, a different polymer, or a co-polymer of PCL with another polymer to change the mechanical properties.

Hydrogels might be cast in molds indirectly using another mold material which can be removed without degrading the hydrogel. Conducting polymers such as polypyrrole could be cast in these molds for added functionality of the scaffold (Schmidt and Leach, 2003).

6.2.2 Modifications to design

The brain implant scaffolds contained only two channel diameters and all channels were round. It might also be beneficial to design lateral channels with varying diameter or shape, eliptical or rectangular, and varied with the general sizes of each layer of the cortex. Different channels for different layers might be seeded with a specific cell type or growth factor to promote pyramidal neuron differentiation. A superficial layer with lateral microgrooves might also be added to coincide with the top layer of the cortex which contains horizontally organized dendrites but no neuronal cell bodies, to perhaps guide those dendrites to cover the defect.

The spinal cord designed architectures contained only longitudinally oriented microgrooves. While longitudinally oriented collagen filaments enhanced spinal cord regeneration much greater than transversely oriented filaments (Yoshii et al., 2004), the orientation of the fibers was also naturally the orientation of the available space

for cellular migration, the micro-architecture. It would be interesting to see if this orientation dependent growth holds for microgrooves on surfaces of a scaffold. The cylinder design described in V (Figure 5.1 does not have microgrooves at all. Compared to the tube and channel designs, which have longitudinally oriented fibrous tissue growing through the macro-channels (Figure 5.3), one cannot differentiate their morphological differences based on microgroove orientation or macro-architectural orientations. The designs for this dissertation could be built in the opposing orientation to align the grooves transversely. Comparing the same macro-architecture but oppositely oriented microgrooves on its surface could demonstrate the relative importance of topographical guidance cues for tissue regeneration *in vivo*. The microgroove size can also be changed based on the layer thickness of the 3-D printer. Also, one could potentially "erase" the microgrooves from the mold by rinsing the mold in a solution which gently degrades or melts the material. The grooves might be susceptible to this chemical or thermal smoothing, or the molds might be sonicated in a solution of fine sand particles to physically wear away the grooves.

To further investigate the macro-architectures, the diameter of the core for the open-path design could be varied, as well as wall thicknesses and size of the channel for the central canal. It might also be possible to create a scaffold with a short protruding tube on each end of the central channel small enough to fit into the host's central canal. This connection, similar to a Luer lock mechanism might be able to protect the CSF flow from disruption and help to keep the overall orientation of the scaffold aligned with the spinal cord anatomy. The shape of the core could also be changed to mimic the butterfly shape of the gray matter more closely. Scaffolds exactly matched to damaged regions could be generated from data gathered from MRI.

6.2.3 Surface modifications and delivered components

The scaffolds can be designed using the techniques outlined in this dissertation specifically with both supportive functions and delivery functions. Because this dissertation has shown that effective supportive designs can improve regeneration, the delivery of different biological components will be the next step in the overall goal of this work. The following describes preliminary work and directions for these next important advancements.

Surface modifications: PCL is not as amenable to cell attachment as tissue culture plastic. Often in these cases the surface may be modified with molecules discussed in section 2.2.2, extracellular matrix proteins or their identifying peptide sequences. One method of surface treatment includes aminolysis (Santiago et al., 2006; Zhu et al., 2002) of the PCL surface and further functionalization with an RGD peptide. Aside from that method, simple adsorption of molecules can also work.

PCL itself can be coated with fibornectin (FN) or laminin (LN) by simple adsorption. Dissolved in acetone at 13% (wt./v), PCL was cast into a 48-well plate, each well using 150μL in a surface area of 0.785 cm^2 per well. Each protein, including a bovine serum albumin (BSA) as a protein control standard, was diluted to different concentrations, 0, 2.5, 5, and 10 μg/mL, in Hanks Balanced Salt Solution (HBSS). A standard curve for each protein was generated (Figure 6.2).

Each PCL-coated well then received 200 μL of HBSS containing each concentration of protein and incubated overnight at 4 degrees. Wells were rinsed gently three times with fresh HBSS and a bicinchoninic acid (BCA) assay kit (Pierce Biotechnology, Rockford, IL)was used to quantify the amount of protein adsorbed to the PCL films and corrected to a standard curve and control film without any protein. With

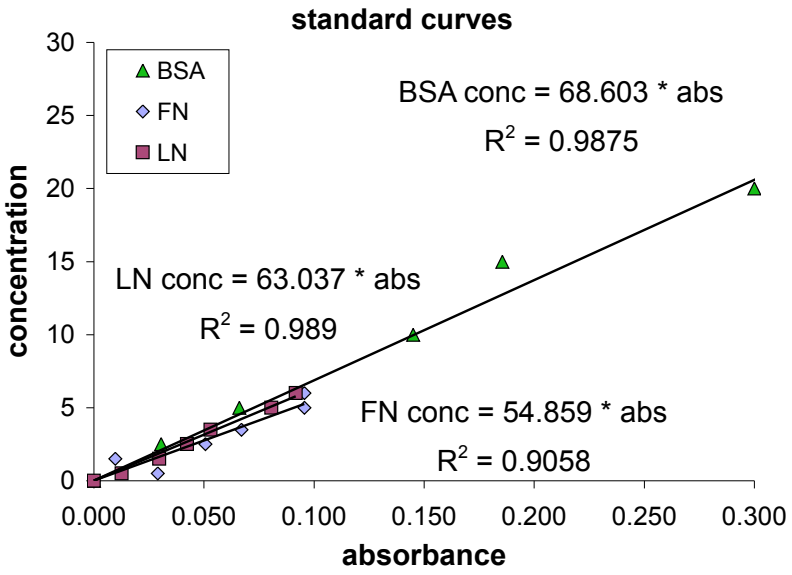

Figure 6.2: Standard curves for bovine serum albumin (BSA), fibronectin (FN), and laminin (LN) adsorption onto PCL films. Linear regression fits for data are provided for each protein.

the highest concentration protein the adsorption was lower than the total amount of protein present in the well (Figure 6.3a), indicating that the maximum adsorption density was roughly 1.5 μg/cm^2 (Figure 6.3b). There was no difference in adsorption between the proteins.

Partitioned biological components: With a porous base material, different cell types can be preferentially seeded into different regions of a designed scaffold. Micro-porous regions can be seeded with one cell type by gravity seeding, then the hollow regions filled in with a hydrogel containing a second cell type or a growth factor. Preliminary experiments show that this is possible. BMSC were gravity seeded into a porous PCL scaffold with interconnected 500μm diameter macro-channels for one day. After one day scaffolds were gently rinsed in fresh medium to remove unattached cells. Then a second population of BMSC's, pre-labeled with green fluorescent Vybrant DiI (Invitrogen, Molecular Probes, Carlsbad, CA), were suspended in fibrinogen containing serum free medium and pipetted into the scaffold which was

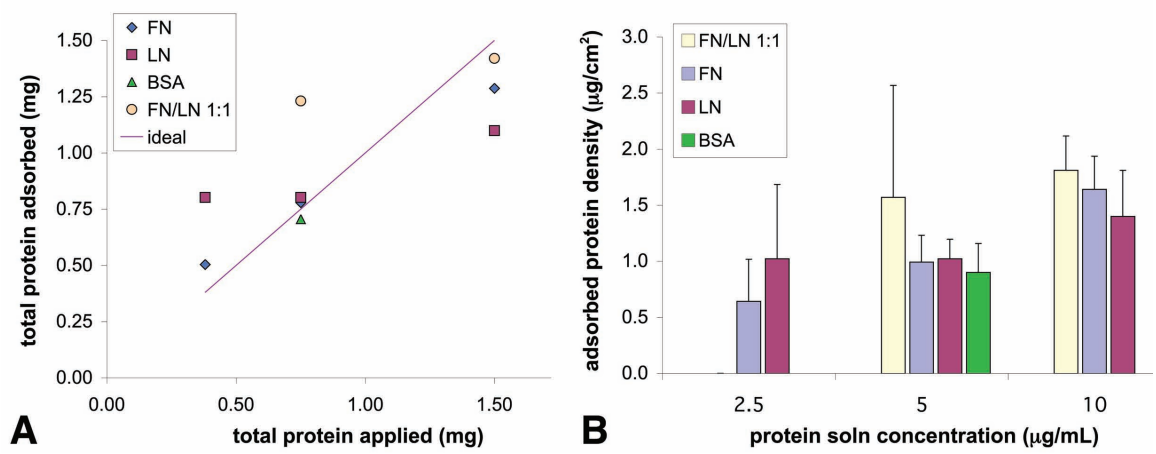

Figure 6.3: (a) Total protein adsorption and (b) concentration per surface area onto PCL films for bovine serum albumin (BSA), fibronectin (FN), and laminin (LN). (a) Concentrations from spectrum absorption data were combined with the fixed volume and known concentrations of proteins applied to each film to calculated total protein amounts applied and adsorbed to the films. Complete adsorption of all protein applied would coincide with the ideal line on the graph, which is well matched with the intermediate concentration. At the highest concentration the adsorbed protein amounts are less than applied. (b) Standard deviations shown in error bars. Concentrations calculated from spectrum absorption data and standard curve linear regressions for each protein. Based on the combined data from (a) and (b) the maximum adsorption capacity of PCL for these proteins is roughly 1.5 μg/cm^2.

then placed into a fitted untreated polystrene well. A small amount of thrombin solution was then added to form a fibrin gel within the scaffold containing the second, green labeled population of BMSC's.

These scaffolds were cultured again for one day, then cryosectioned at 20 μm thickness, labeled with DAPI and cover-slipped. Cells with only blue nuclei would indicate the first gravity seeded population of BMSC while cells which had green cytoplasm would indicate the second fibrin gel seeded population. One would expect to see simple blue nucleated cells only in the porous interstices of the scaffold or along the channel walls, while green cells should be located within the open channel regions, as well as perhaps the porous material. This was found to be the case (Figure 6.4), though survival of the second gel seeded population was low, and retention of the fibrin gel was low. The method of gravity seeding could be changed to a rotating or spinner flask seeding method to increase the penetration of the cells through the

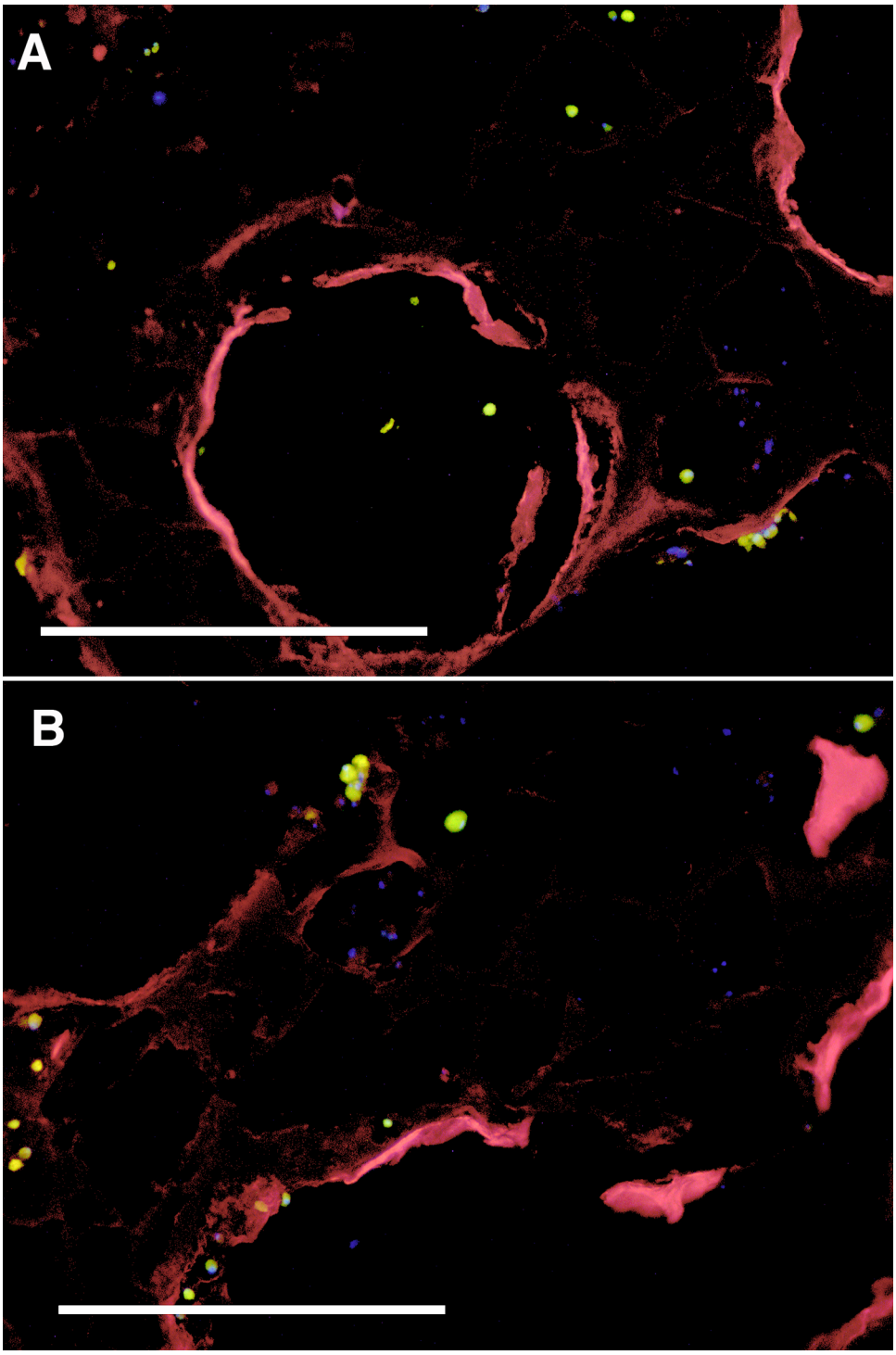

Figure 6.4: Two separate populations of BMSC seeded selectively into separate locations in a macro-designed PCL scaffold. Scale bars 500 μm. PCL is autofluorescent, red. Gravity seeded BMSC seeded first into the porous interstices of the walls are blue nucleated (DAPI) and found primarily within the walls or on the surfaces of the channels. Green cells (Vybrant DiI) were seeded with a fibrin gel after the first population was allowed to attach and then rinsed. Green cells are found in the channels (A), but also able to enter the porous walls with the blue cells (B). The majority of cells in the the walls were blue cells.

porous regions. Also the hydrogel could be changed to collagen or hyaluronic acid, or some other more slowly degrading material.

Adult stem cell delivery: Because of the relative ease of isolation, SchC, OEC, and BMSC may be the most practical cell sources when compared to NSC or ESC. While studies of BMSC induction to neural differentiation have been performed in monolayer culture, none have looked at the effects of 3-D culture even though all cell types in their natural environment depend on 3-D cell-cell interactions. Chondrocytes maintain their phenotype only when cultured in 3-D. Monolayer culture of BMSC does, however, show most recently through microarray analysis that chemical induction decreases the mesechymal lineage mRNA expression and expands the neural differentiation related mRNA and neurotrophic factor mRNA expression. The cells become weighted toward neural lineage differentiation, though they do not differentiate fully (Yamaguchi et al., 2006). Additionally BMSC cultured in monolayer with chemical induction can improve functional recovery in traumatic brain injury in rodent models, though it was not a significant improvement over BMSCs injected without chemical induction (Lu et al., 2006). This might indicate that the 3-D *in vivo* environment of the brain has an impact on the BMSCs' neural phenotype potential.

Preliminary data shows that BMSC cultured in a 3-D *in vitro* environment with a serum replacement (SR) medium designed for neural progenitor differentiation of mouse embryonic stem cells (Barberi et al., 2003) increases neural-related gene expression. The SR medium contained DMEM-F12, 15% Knockout Serum Replacement, 1% penicillin and streptomycin, 2mM L-glutamine, and 10μM β-mercaptoethanol (all from Invitrogen, Carlsbad, CA). A control medium for BMSC maintenance was formulated as follows: DMEM, 10% Fetal Bovine Serum (FBS), 1% penicillin and streptomycin. Rat long-bone BMSC were cultured in monolayer on tissue culture

polystyrene or in 3-D cylindrical scaffolds of PCL 3 mm height and 5 mm in diameter. These scaffolds were of the same salt-leached porosity as the studies described in Chapter 3. The seeding density of cells in scaffolds was 500,000 cells/scaffold seeded with a fibrin gel. Cells cultured in monolayer were switched to SR medium just prior to complete confluency. Cells seeded in scaffolds were switched to SR medium 1 day after seeding to allow attachment of cells. RNA was harvested from scaffolds and cell culture wells with Trizol at times points up to 1 week. Other specimens were fixed for immunocytochemistry. The following primers were used for RT-PCR with 30 cycles.

Nestin: F: 5' ggaggaccagaggattgtgaacc 3', R: 5' actgccatctgctcattccctac 3'

Musashi: F: 5' aggtgaaagagtgtctggtga 3', R: 5' ctaacatgccaataccagca 3'

Primary antibodies used were for nestin(Chemicon), musashi (Chemicon), and Tuj-1(Covance).

Nestin is an intermediate filament protein commonly found in neural progenitors and other multi-lineage progenitor cells. It is strongly expressed in BMSC control groups because of their progenitor state. Musashi is a transcription factor expressed in neuronal progenitors, but is also found in BMSC control groups. They are both found in neural progenitors and astroclia in adult rat brain (Komitova and Eriksson, 2004). Both nestin and musashi mRNA expression were affected by culture in SR medium (Figure 6.5). GAPDH house keeping gene was comparable in all samples (data not shown). When cultured in monolayer with SR medium, BMSC decreased their expression of nestin, a sign of differentiation. This same phenomenon occurred when cultured in 3-D in a scaffold even without SR, indicating that 3-D culture increases differentiation of BMSC. Musashi expression in monolayer, however, was not affected by SR medium, at most being maintained in monolayer culture with

SR medium, while in 3-D musashi mRNA expression was increased after 1 week of culture with and without the SR medium. The mRNA expression was also confirmed by protein localization through immunocytochemistry. Cells cultured in monolayer were labeled in the cytoskeleton with nestin (Figure 6.6) and within the nucleus with musashi (Figure 6.7).

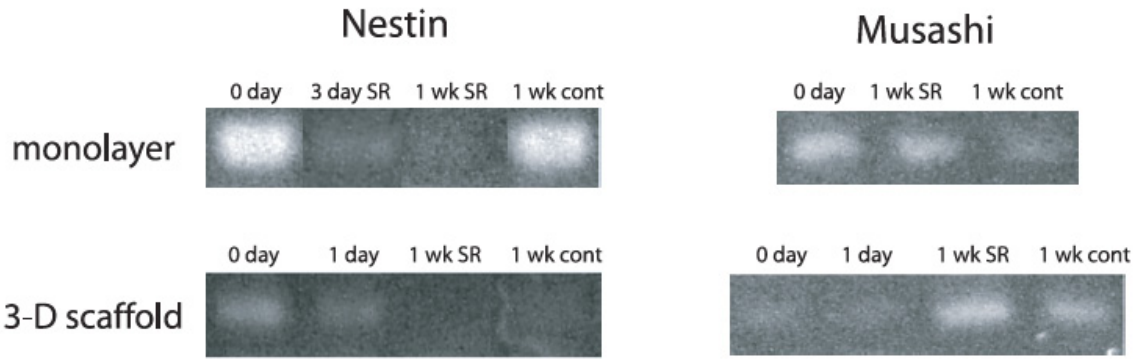

Figure 6.5: RT-PCR bands for nestin and musashi mRNA expression in BMSC cultured in monolayer and in 3-D scaffolds with and without serum replacement medium. Serum Replacement (SR) medium was effective in decreasing nestin expression and maintaining musashi expression in monolayer (top). In 3-D scaffold culture (bottom) cells took on a more neuronally differentiated state with or without the SR medium.

The 1 day scaffold groups showed no immediate change in musashi or nestin from the 0 day groups, suggesting that these changes are not an artifact in the PCR process caused by the presence of polymer, but rather gradual changes over the course of the experiment in 3-D.

Tuj-1 antibodies for class III β-tubulin, microtubule associated proteins, found in axons of mature neurons were also localized to the cytoskeleton of some (less than 10%) of the cells after monolayer culture in SR medium (Figure 6.8). Because of the many commonalities between different classes of tubulin molecules, no good RT-PCR primer exists for the neuronal class III β-tubulin, and while confocal microscopy makes it possible to view cells cultured in 3-D scaffolds, the search for fewer than 10% of cells which might be expressing the antibody matched protein is difficult

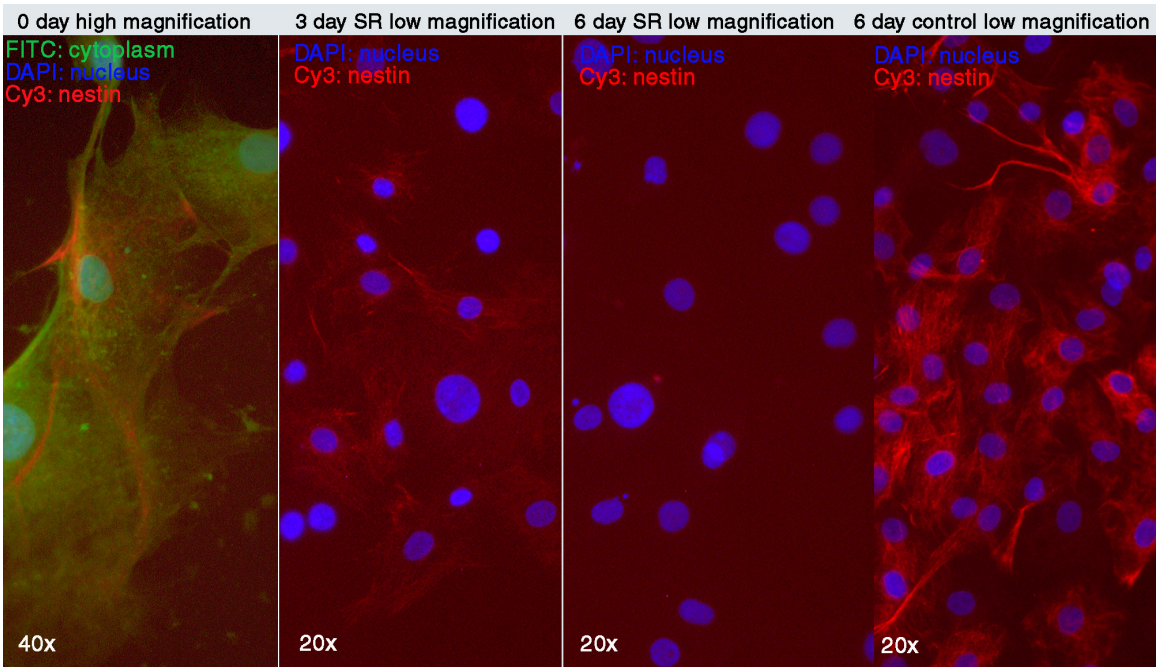

Figure 6.6: Expression of nestin protein by BMSC in monolayer was confirmed by immunocytochemistry. Intermediate filament proteins are found in the cytoskeleton. The presence of nestin in 0 day and control groups along with its disappearance in the SR groups over time mirror the mRNA expression pattern found in RT-PCR.

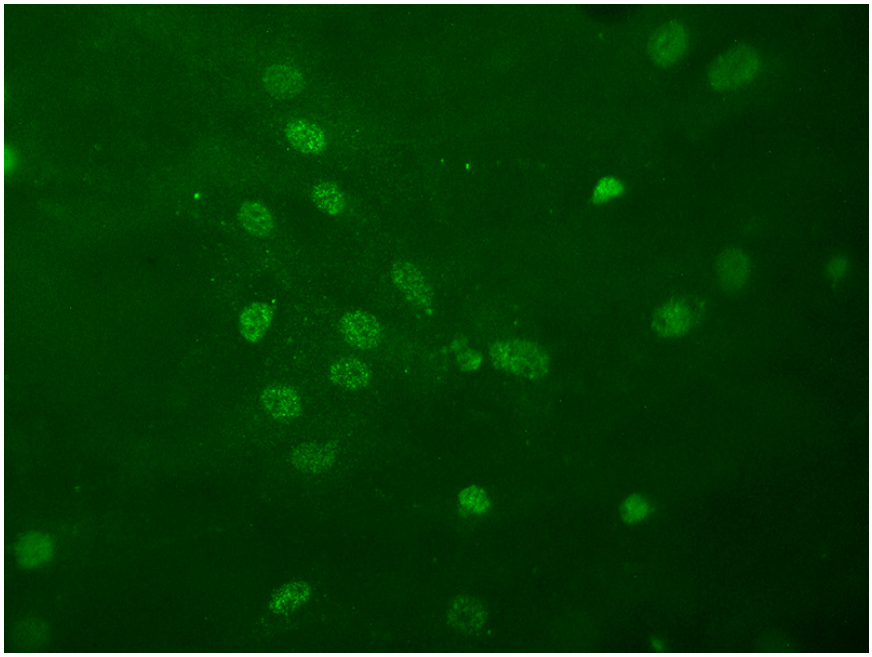

Figure 6.7: Expression of musashi protein in monolayer was confirmed by immunocytochemistry. Transcription factors are localized to the nucleus.

and in practice was not successful. A Western Blot analysis revealed presence of this protein only after running the entire concentrated protein sample in one lane, making semi-quantitative comparisons impossible, yet suggesting again the low percentage of cells with a mature neuronal phenotype in 3-D culture (data not shown).

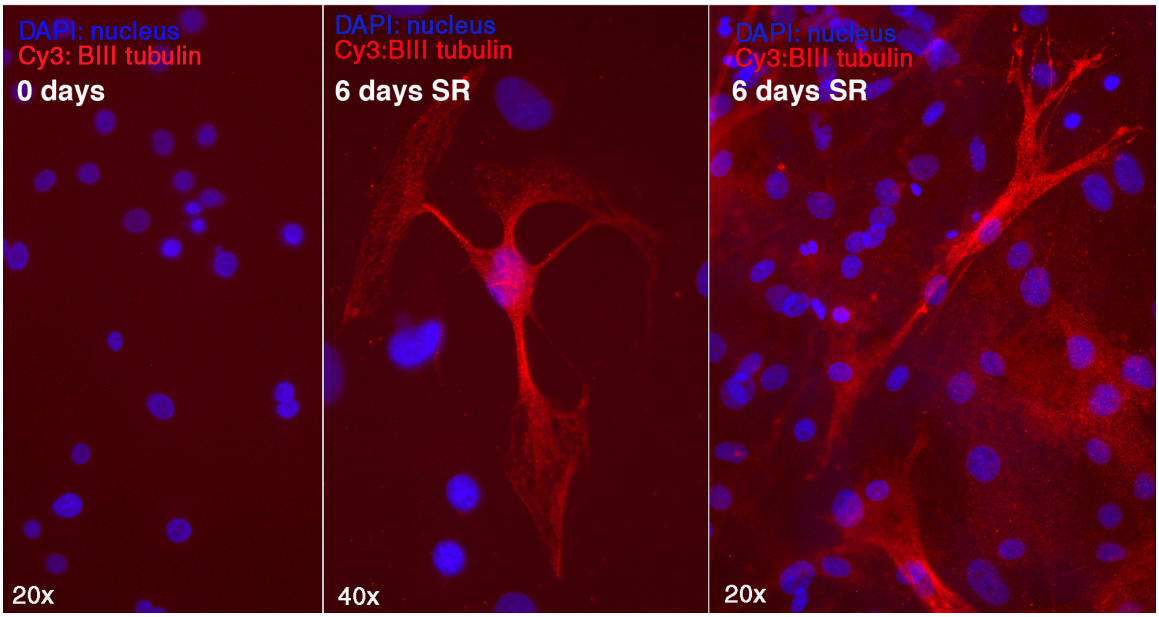

Figure 6.8: Expression of Tuj-1 protein after SR medium treatment in monolayer was found in small proportions by immunocytochemistry. Fewer than 10% of cells after 1 week of culture in SR medium exhibited Tuj-1 antibody reactivity in the cytoskeleton.

In the future it may be possible to take autologous BMSC from a patient, perform minimal expansion, and culture them in 3-D scaffold for implantation. Because they can be influenced by the 3-D culture, fewer additives would be needed in the culture medium, decreasing the barriers to FDA approval. Their impregnation within a specific region of the scaffold, for instance the core of the open-path design, could provide cues for migration of resident progenitor cells in the spinal cord, shown to be present after injury (nestin positive), into the central region where gray matter should be located. The surfaces of the scaffold could be coated with laminin to improve axonal guidance. In the hollow regions, a hydrogel could be set containing

schwann cells or OEC to aid in the remyelination of regenerating fibers.

6.3 Prospectus for future work

Within the field of CNS regeneration this work forges a new piece of the puzzle which previously was not recognized. The use of macro-architectural designs in both brain and spinal cord scaffolds to enhance regeneration complements existing literature which emphasizes the impact of biological factors on cell behavior and regeneration. In predicting future work stemming from this dissertation, the interaction between the biomaterial scaffold architecture and multiple biological components will critical.

Because the field of tissue regeneration in the brain is less advanced than in the spinal cord with regard to scaffold use, the next step would be to further investigate the effects and possible benefits of microgroove orientation and channel spacing. Because so much of the *in vitro* data on topographical guidance is collected from monolayer culture, an *in vitro* experiment where neurons or neural stem cells were cultured in a 3-D scaffold with microgroove topography could facilitate the study of neural cell alignment and organization influenced by topography in an environment more easily transferable to the ultimate implantation procedure. The influence of cerebral cortex organization can now become more prominent in the design of the macro-architecture, possibly increasing the density of vertical channels and placing transverse channels in more than just two orthogonally intersecting directions. Instead, these transverse channels can span three or four directions to increase the openness of the tissue/scaffold interface. The measurements of success could include fMRI studies of brain activity in the same animal over time to better track the temporal progress. Stimulating the regenerating region with electrical or chemical

depolarization could be a way to identify any networks being formed with undamaged regions of the nervous system. This line of work would further develop the macro-architectural library available to researchers whose biological treatments are still lacking in their full effectiveness. To address recovery of function as a result of the architectural influences on organization of regenerated tissue, the location of implant should be moved to the motor cortex or barrel cortex in rat for a more accessible measurement of success. If the recovery of function in these regions is improved by macro-architectural organization a more clinically relevant injury model such as middle cerebral artery occlusion should be used, and architectures re-tailored to the tissue damage.

With the goal of CNS repair for recovery of function it would be most direct in the case of spinal cord injury to investigate the effectiveness of the most successful biological components in combination with the marco-architectured scaffolds. Peripheral nerve grafts used in combination with growth factors have been, to date, most successful in spinal cord injury research. However, a successful clinical treatment is still unavailable. The hurdle of translating animal model research to human benefit lies in a confluence of difficulties. However, the factors which researchers have direct control over is the true effectiveness of their strategy, which can still be improved. If the scaffold architecture gives the overall strategy an additional boost, it may be the key to unlocking the rest of the doors to a clinically applicable cure for spinal cord injury. The open-path core design could readily accomodate stem cells seeded within the porous regions to help regenerate the grey matter, while a growth factor is coated on the surfaces of the material or incorporated into the polymer for release upon degredation to enhance host cell migration inward. In addition, peripheral nerve grafts can be placed within the open lateral regions around the core, effectively fixing them

in the regions of white matter tract regeneration. Aside from observable recovery of motor function, retrograde and anterograde axonal tracing can provide a more complete understanding of regeneration and the intrinsic reorganization of neural networks through these implants.

One of the greatest obstacles researchers face in regenerating the CNS is the appropriate functional recovery. Because of the complex nature of the CNS in both its morphological organization and its fundamental functions, repopulating the area with the right cell types may be the easiest step. Controlling or influencing the precise and original networks of communication may be the most difficult step. However, the absolute necessity for science and medicine to influence that networking after injury is unknown. It is plausible that if given the right regenerative environment and ample encouragement through topographical and chemical guidance, axons will selectively reach the necessary targets in similar or different pathways from the original organization. If function is recovered by compensatory mechanisms of neuroplasticity possibly the cure to CNS injury is closer than expected.

APPENDIX

Threshold Image.m : Matlab program files for pixel area calculations based on threshold intensity

The following code is from a .m file for Matlab which takes as inputs two grayscale .tif files, 1) a raw composite image file and 2) a mask file of the same pixel dimensions with a black region of interest and white background corresponding to the raw image file. The mask is usually generated using Adobe Photoshop with the path tool. The interactive selection of a threshold value allows the user to view the thresholded region of interest and confirm the value selected before it calculates the pixel numbers for thresholded areas and the total masked region. Data is generated and saved to a .txt file one row at a time, which can be converted to a .xls file after all the images have been processed.

```
function [PTotal,PMask,PThreshold] = ThresholdImage

% an image threshold
% data is written (appendend) to a text file in the format
% datafile maskfile PTotal Pmask PThreshold Threshold PThresh/Pmask
% PTotal = total number of image pixels
% PMask = number of pixels blocked by the mask
% PThreshold = number of pixels visible through the mask and above threshold
% Threshold = value between 0 and 255

clear all;
close all;

[DataFile,DataPath] = uigetfile('*.*','Data Image File');
[MaskFile,MaskPath] = uigetfile('*.*','Mask Image File');

D = imread([DataPath '\' DataFile]);                    % import files
M = imread([MaskPath '\' MaskFile]);

D = double(D);                                  % convert to double for processing
M = double(M);

D = D/255;

M = M/255;                                      % rescale M into 0 to 1
M = 1-M;

PTotal = size(D,1)*size(D,2);

PMask = length(find(M == 0));

C = D.*M;                                       % apply the mask

figure,colormap gray                                % display the masked image

Satisfied = 0;
                                        % select the threshol value
while Satisfied == 0
   figure(1),imagesc(C,[0 1]),colorbar
   Threshold = input('Enter a desired threshold: ');
   X = C;
   X(find(C < Threshold)) = 0;
   X(find(C > Threshold)) = 1;
   figure(1),imagesc(X,[0 1]),colorbar
   Satisfied = input('Are you satisfied (0 for no, 1 for yes)? ');
end

PThreshold = length(find(X == 1));              % Threshold is selected and used to calculated the pixel area

[SaveFile,SavePath] = uiputfile('*.xls','Save File');

fid = fopen([SavePath '\' SaveFile],'a');                   % open file for appending
fprintf(fid,[DataFile '\t' MaskFile]);                  % append the pixel counts and ratios to the appropriate columns
fprintf(fid,['\t' num2str(PTotal) '\t' num2str(PTotal-PMask) '\t' num2str(PThreshold) '\t' num2str(Threshold) '\t'
num2str(PThreshold/(PTotal-PMask))]);
fprintf(fid,'\n');
fclose(fid);
```

ThresholdBoxes.m : Matlab program files for intensity calculations with background intensity correction

The following code is from a .m file for Matlab which allows the user to select rectangular regions of interest with any rotation within a grayscale image and calculates the average intensity of those regions. It also allows selection of three different small background regions to calculate and subtract the background intensity. It takes as input one grayscale .tif file and allows the user to define 2 sets of 2 points, or two line segments within the image. After each selection the line segment is displayed and can be confirmed or re-selected by the user. These two line segments define the linear portions of the bordering parenchyma of the defect cavity in the brain from Chapters 3 and 4. The right hand side of the defect must be defined before the left hand side. Two immediately adjacent rectangular regions perpendicular to each line segment are defined for intensity calculations. Those regions of interest can be extracted for display as the user chooses, rotated to a normal axis. The code is currently such that the width of the rectangles corresponds to 250 μm in the original image taken at 10x magnification, but the line segment length alone determines the length of the rectangle. Three additional line segments can be selected to define background regions for background intensity calculation. These line segments can not be perfectly vertical, or the application will quit. These background defining line segments can also be confirmed or re-selected and all selected regions are displayed as colored layers on the original image for verification. Their rectangular width from the line segment is set at 100 μm. The main .m file uses two other files, InsideIndex.m and IndexSetMex.c to rotate the rectangular selections and generate perpendicular selections to the line segments.

```
%ThresholdBoxes

clear;
close all;

[DataFile,DataPath] = uigetfile('*.*','Data Image File');

I = imread([DataPath '\' DataFile]);                    % import master image

J = histeq(I);                                          % equalize the histogram for display only

figure(1);                                              % display J in figure 1
set(1,'doublebuffer','on');
imshow(J);

% define the size and color of the rectangles from the selected line segments to display
set(1,'pos',[215        100        1123        865]);
L1 = line(rand(1,2),rand(1,2),'vis','off','color','yellow','linewidth',2);
L2 = line(rand(1,2),rand(1,2),'vis','off','color','yellow','linewidth',2);
L3 = line(rand(1,2),rand(1,2),'vis','off','color','green','linewidth',2);
L4 = line(rand(1,2),rand(1,2),'vis','off','color','green','linewidth',2);
L5 = line(rand(1,2),rand(1,2),'vis','off','color','green','linewidth',2);

% get first set of points for right-hand side rectangles extending right
% each line segement is displayed for confirmation, press any button
% otherwise press space bar to re-select lines segment.
set(1,'currentcharacter','n');
while strcmp(get(1,'currentcharacter'),'n') == 1            % p1-5 are 2x2 matrices
   set(L1,'vis','off');                                     % first row of p is first point clicked
   p1 = ginput(2);                                              % second row is second point clicked
   set(L1,'xdata',p1(:,1),'ydata',p1(:,2),'vis','on');
   waitforbuttonpress;
end

% get second set of points for left-hand side rectangles extending left
set(1,'currentcharacter','n');
while strcmp(get(1,'currentcharacter'),'n') == 1            %generate p2 matrix
   set(L2,'vis','off');
   p2 = ginput(2);
   set(L2,'xdata',p2(:,1),'ydata',p2(:,2),'vis','on');
   waitforbuttonpress;
end

%get background points from three separate line segments
set(1,'currentcharacter','n');
while strcmp(get(1,'currentcharacter'),'n') == 1            %generate p3 matrix
   set(L3,'vis','off');
   p3 = ginput(2);
   set(L3,'xdata',p3(:,1),'ydata',p3(:,2),'vis','on');
   waitforbuttonpress;
end

set(1,'currentcharacter','n');
while strcmp(get(1,'currentcharacter'),'n') == 1            %p4 matrix
   set(L4,'vis','off');
   p4 = ginput(2);
   set(L4,'xdata',p4(:,1),'ydata',p4(:,2),'vis','on');
   waitforbuttonpress;
end

set(1,'currentcharacter','n');
while strcmp(get(1,'currentcharacter'),'n') == 1            %p5 matrix
```

```
   set(L5,'vis','off');
   p5 = ginput(2);
   set(L5,'xdata',p5(:,1),'ydata',p5(:,2),'vis','on');
   waitforbuttonpress;
end

% define the rectangular regions extending perpendicular to line segments.
% pixel dimensions of rectangles can be modified here
% depending on resolution of images and desired area of measurement
[R1,r1lenx,r1leny] = InsideIndex(p1,1,275);        % selected rectangles are rotated
[R2,r2lenx,r2leny] = InsideIndex(p1,276,276+275);  %to a normal axis and re-indexed
[R3,r3lenx,r3leny] = InsideIndex(p2,-1,-275);
[R4,r4lenx,r4leny] = InsideIndex(p2,-276,-(276+275));
[back1,b1lenx,b1leny] = InsideIndex(p3,1,150);   %background rectangles
[back2,b2lenx,b2leny] = InsideIndex(p4,1,150);
[back3,b3lenx,b3leny] = InsideIndex(p5,1,150);

hold on    %displaying the location of selected rotated rectangles over the raw image
plot(R1(1,:),R1(2,:),'.');       %the user can confirm the selection visually here
plot(R2(1,:),R2(2,:),'r.');      % and decide whether the data is fairly chosen
plot(R3(1,:),R3(2,:),'.');       % if not, restart the program.
plot(R4(1,:),R4(2,:),'r.');
plot(back1(1,:),back1(2,:),'g.');
plot(back2(1,:),back2(2,:),'g.');
plot(back3(1,:),back3(2,:),'g.');

%defining the indices of each pixel in order after the appropriate rotations
r1 = (R1(1,:)-1)*size(I,1)+R1(2,:);
r2 = (R2(1,:)-1)*size(I,1)+R2(2,:);
r3 = (R3(1,:)-1)*size(I,1)+R3(2,:);
r4 = (R4(1,:)-1)*size(I,1)+R4(2,:);
b1 = (back1(1,:)-1)*size(I,1)+back1(2,:);
b2 = (back2(1,:)-1)*size(I,1)+back2(2,:);
b3 = (back3(1,:)-1)*size(I,1)+back3(2,:);

%re-assign the line-indexed pixels in original image vector I to separate vectors for
% performing calculations on the pixel intensity values
K1 = I(r1);
K2 = I(r2);
K3 = I(r3);
K4 = I(r4);
K5 = I(b1);
K6 = I(b2);
K7 = I(b3);
%matrices are re-generated with the pixels properly rotated
L1 = reshape(K1,r1leny,r1lenx);
L2 = reshape(K2,r2leny,r2lenx);
L3 = reshape(K3,r3leny,r3lenx);
L4 = reshape(K4,r4leny,r4lenx);
L5 = reshape(K5,b1leny,b1lenx);
L6 = reshape(K6,b2leny,b2lenx);
L7 = reshape(K7,b3leny,b3lenx);

% calculate the mean background intensity value
backmean(1,1) = mean2(L5);
backmean(2,1) = mean2(L6);
backmean(3,1) = mean2(L7);
bmean = mean(backmean);

L1M = mean2(L1);       % take the mean intensity of images
L2M = mean2(L2);       %L1-4, the rectangular selections
L3M = mean2(L3);
```

```
L4M = mean2(L4);
%display the selected rectangular images
figure,subplot(1,4,1)
image(L4),colormap gray
subplot(1,4,2)
image(L3),colormap gray
subplot(1,4,3)
image(L1),colormap gray
subplot(1,4,4)
image(L2),colormap gray
%generate a histogram of the intensity values for each rectangle
% 1 bin for every two integral increments in intensity
[L1counts, L1bins] = imhist(L1,128);
[L2counts, L2bins] = imhist(L2,128);
[L3counts, L3bins] = imhist(L3,128);
[L4counts, L4bins] = imhist(L4,128);
figure,subplot(2,2,1)
bar(L1bins,L1counts)
subplot(2,2,2)
bar(L2bins,L2counts)
subplot(2,2,3)
bar(L3bins,L3counts)
subplot(2,2,4)
bar(L4bins,L4counts)
L1countslength = length(L1counts');
L1countscell = num2cell(L1counts');
L2countscell = num2cell(L2counts');
L3countscell = num2cell(L3counts');
L4countscell = num2cell(L4counts');
L1binscell = num2cell(L1bins');

D{1,2} = {'bins'};
D(2,1:2) = {[DataFile], 'L1'};
D(3,1:2) = {[DataFile], 'L2'};
D(4,1:2) = {[DataFile], 'L3'};
D(5,1:2) = {[DataFile], 'L4'};
D(1,3:L1countslength+2) = L1binscell;
D(2,3:L1countslength+2) = L1countscell;
D(3,3:L1countslength+2) = L2countscell;
D(4,3:L1countslength+2) = L3countscell;
D(5,3:L1countslength+2) = L4countscell;


[SaveFile,SavePath] = uiputfile('*.xls','Save File');
fid = fopen([SavePath '\' SaveFile],'a');         % open file for appending means, can designate a new file on first run
fprintf(fid,[DataFile]);    % write mean value data to a new row in an excel/txt file
fprintf(fid,['\t' num2str(bmean) '\t' num2str(length(K5)+length(K6)+length(K7))]);
fprintf(fid,['\t' num2str(length(K1)) '\t' num2str(L1M) '\t' num2str(length(K2)) '\t' num2str(L2M) '\t' num2str(length(K3))
'\t' num2str(L3M) '\t' num2str(length(K4)) '\t' num2str(L4M)]);
fprintf(fid,'\n');
fclose(fid);
% values for each bin in each histogram are printed to a row in an excel/txt file
% this file must already exist, and to begin, have a 1 value in the A1 cell.
[SaveFile2,SavePath2] = uiputfile('*.xls','Save File');
increment = xlsread([SavePath2 '\' SaveFile2],'Sheet1','A1');
increment = 1 + increment;
xlswrite([SavePath2 '\' SaveFile2],D,'Sheet1',['A' num2str(increment)]);
increment = increment + 5;
xlswrite([SavePath2 '\' SaveFile2],increment,'Sheet1','A1');
```

InsideIndex.m

This code rotates the pixels for the rectangular selection so that the indices and rows are in the same coordinate system as the new axes generate by the line segment.

```
function I = InsideIndex(p,startx,endx)

v = p(2,:)-p(1,:);
LenV = round(norm(v));

Y = 1:LenV;

if endx > 0
   X = startx:endx;
else X = endx:startx;
end

I1 = IndexSetMex(X,Y);

angle = acos(v/LenV*[0 1]');

if v(1) > 0
   angle = -angle;
end

R = [cos(angle) -sin(angle)
   sin(angle) cos(angle)];

I = R*I1;
I(1,:) = I(1,:) + p(1,1);
I(2,:) = I(2,:) + p(1,2);
```

IndexSetMex.c

This code is a C file and converts the x,y coordinate numbering system of the pixels in matlab into a single line indexed numbering system.

```
#include "mex.h"
#include "math.h"

void mexFunction(int nlhs, mxArray *plhs[], int nrhs, const mxArray *prhs[])
{

    double *X;
    double *Y;

    int M;
    int N;
    int i;
    int j;
    int c;
    double *I;

    X = mxGetPr(prhs[0]);
    Y = mxGetPr(prhs[1]);

    M = mxGetN(prhs[0]);
    N = mxGetN(prhs[1]);

    plhs[0] = mxCreateDoubleMatrix(2,M*N,mxREAL);

    I = mxGetPr(plhs[0]);


    c = 0;

    for (i = 0; i < M; i++) {
        for (j = 0; j < N; j++) {
  /*          I[c*2+0] = X[i];
            I[c*2+1] = Y[j];
            c++;  */
    /*        mexPrintf("%.6f %.6f\n",X[i],Y[j]);   */
            I[c*2+0] = X[i];
            I[c*2+1] = Y[j];
            c++;
        }
    }
}
```

BIBLIOGRAPHY

Aebischer P, Guenard V, Valentini RF (1990) The morphology of regenerating peripheral-nerves is modulated by the surface microgeometry of polymeric guidance channels. *Brain Research* 531:211–218.

Ahmed Z, Brown RA (1999) Adhesion, alignment, and migration of cultured schwann cells on ultrathin fibronectin fibres. *Cell Motility and the Cytoskeleton* 42:331–343.

Aihara N, Hall JJ, Pitts LH, Fukuda K, Noble LJ (1995) Altered immunoexpression of microglia and macrophages after mild head injury. *Journal of Neurotrauma* 12:53–63.

Aimedieu P, Grebe R (2004) Tensile strength of cranial pia mater: preliminary results. *Journal of Neurosurgery* 100:111–4.

Attiah DG, Kopher RA, Desai TA (2003) Characterization of pc12 cell proliferation and differentiation-stimulated by ecm adhesion proteins and neurotrophic factors. *Journal of Materials Science-Materials in Medicine* 14:1005–1009.

Bakshi A, Fisher O, Daggi T, Himes BT, Fischer I, Lowman A (2004) Mechanically engineered hydrogel scaffolds for axonal growth and angiogenesis after transplantation in spinal cord injury. *Journal of Neurosurgery-Spine* 1:322–329.

Barberi T, Klivenyi P, Calingasan NY, Lee H, Kawamata H, Loonam K, Perrier AL, Bruses J, Rubio ME, Topf N, Tabar V, Harrison NL, Beal MF, Moore MAS, Studer L (2003) Neural subtype specification of fertilization and nuclear transfer embryonic stem cells and application in parkinsonian mice. *Nature Biotechnology* 21:1200–1207.

Barnett SC, Alexander CL, Iwashita Y, Gilson JM, Crowther J, Clark L, Dunn LT, Papanastassiou V, Kennedy PGE, Franklin RJM (2000) Identification of a human olfactory ensheathing cell that can effect transplant-mediated remyelination of demyelinated cns axons. *Brain* 123:1581–1588.

Barnett SC, Riddell JS (2007) Olfactory ensheathing cell transplantation as a strategy for spinal cord repair - what can it achieve? *Nature Clinical Practice Neurology* 3:152–161.

Barritt AW, Davies M, Marchand F, Hartley R, Grist J, Yip P, McMahon SB, Bradbury EJ (2006) Chondroitinase abc promotes sprouting of intact and injured spinal systems after spinal cord injury. *Journal of Neuroscience* 26:10856–10867.

Batchelor PE, Howells DW (2003) Cns regeneration: clinical possibility or basic science fantasy? *Journal of Clinical Neuroscience* 10:523–534.

Ben-Hur T, Idelson M, Khaner H, Pera M, Reinhartz E, Itzik A, Reubinoff BE (2004) Transplantation of human embryonic stem cell-derived neural progenitors improves behavioral deficit in parkinsonian rats. *Stem Cells* 22:1246–1255.

Bianco F, Pravettoni E, Colombo A, Schenk U, Moller T, Matteoli M, Verderio C (2005) Astrocyte-derived atp induces vesicle shedding and il-1 beta release from microglia. *Journal of Immunology* 174:7268–77.

Bracken MB, Collins WF, Freeman DF, Shepard MJ, Wagner FW, Silten RM, Hellenbrand KG, Ransohoff J, Hunt WE, Perot PL, Grossman RG, Green BA, Eisenberg HM, Rifkinson N, Goodman JH, Meagher JN, Fischer B, Clifton GL, Flamm ES, Rawe SE (1984) Efficacy of methylprednisolone in acute spinal-cord injury. *Jama-Journal of the American Medical Association* 251:45–52.

Bracken MB, Shepard MJ, Collins WF, Holford TR, Young W, Piepmeier J, Leosummers L, Baskin DS, Eisenberg HM, Flamm E, Marshall LF, Maroon J, Wilberger J, Perot PL, Sonntag VKH, Wagner FC, Winn HR (1990) A randomized, controlled trial of methylprednisolone or naloxone in the treatment of acute spinal-cord injury. *New England Journal of Medicine* 323:1209–1209.

Brook GA, Lawence JM, Raisman G (2001) Columns of schwann cells extruded into the cns induce in-growth of astrocytes to form organized new glial pathways. *Glia* 33:118–130.

Bullock MR, Chesnut R, Ghajar J, Gordon D, Hartl R, Newell DW, Servadei F, Walters BC, Wilberger J (2006) Surgical management of traumatic parenchymal lesions. *Neurosurgery* 58:S25–46; discussion Si–iv.

Busch SA, Silver J (2007) The role of extracellular matrix in cns regeneration. *Current Opinion in Neurobiology* 17:120–127.

Carone TW, Hasenwinkel JM (2006) Mechanical and morphological characterization of homogeneous and bilayered poly(2-hydroxyethyl methacrylate) scaffolds for use in cns nerve regeneration. *Journal of Biomedical Materials Research Part B-Applied Biomaterials* 78B:274–282.

Chen AQ, Xu XM, Kleitman N, Bunge MB (1996) Methylprednisolone administration improves axonal regeneration into schwann cell grafts in transected adult rat thoracic spinal cord. *Experimental Neurology* 138:261–276.

Chen S, Pickard JD, Harris NG (2003) Time course of cellular pathology after controlled cortical impact injury. *Experimental Neurology* 182:87–102.

Chen XG, Katakowski M, Li Y, Lu DY, Wang L, Zhang LJ, Chen JL, Xu YX, Gautam S, Mahmood A, Chopp M (2002) Human bone marrow stromal cell cultures conditioned by traumatic brain tissue extracts: Growth factor production. *Journal of Neuroscience Research* 69:687–691.

Clark P, Connolly P, Curtis ASG, Dow JAT, Wilkinson CDW (1990) Topographical control of cell behavior .2. multiple grooved substrata. *Development* 108:635–644.

Clark P, Connolly P, Curtis ASG, Dow JAT, Wilkinson CDW (1991) Cell guidance by ultrafine topography invitro. *Journal of Cell Science* 99:73–77.

Coats B, Margulies SS (2006) Material properties of porcine parietal cortex. *Journal of Biomechanics* 39:2521–2525.

Coleman WP, Benzel E, Cahill DW, Ducker T, Geisler F, Green B, Gropper MR, Goffin J, Madsen PW, Maiman DJ, Ondra SL, Rosner M, Sasso RC, Trost GR, Zeidman S (2000) A critical appraisal of the reporting of the national acute spinal cord injury studies (ii and iii) of methylprednisolone in acute spinal cord injury. *Journal of Spinal Disorders* 13:185–199.

Coyne TM, Marcus AJ, Woodbury D, Black IB (2006) Marrow stromal cells transplanted to the adult brain are rejected by an inflammatory response and transfer donor labels to host neurons and glia. *Stem Cells* 24:2483–2492.

Cui FZ, Tian WM, Fan YW, Hou SP, Xu QY, Lee IS (2003) Cerebrum repair with phpma hydrogel immobilized with neurite-promoting peptides in traumatic brain injury of adult rat model. *Journal of Bioactive and Compatible Polymers* 18:413–432.

Curtis A, Wilkinson C (1997) Topographical control of cells. *Biomaterials* 18:1573–1583.

Darvish KK, Crandall JR (2001) Nonlinear viscoelastic effects in oscillatory shear deformation of brain tissue. *Med Eng Phys* 23:633–45.

De Carvalho M, Costa J, Swash M (2005) Clinical trials in als: A review of the role of clinical and neurophysiological measurements. *Amyotrophic Lateral Sclerosis and Other Motor Neuron Disorders* 6:202–212.

Dinh P, Bhatia N, Rasouli A, Suryadevara S, Cahill K, Gupta R (2007) Transplantation of preconditioned schwann cells following hemisection spinal cord injury. *Spine* 32:943–949.

Doetsch F, Caille I, Lim DA, Garcia-Verdugo JM, Alvarez-Buylla A (1999) Subventricular zone astrocytes are neural stem cells in the adult mammalian brain. *Cell* 97:703–716.

Douen AG, Dong L, Vanance S, Munger R, Hogan MJ, Thompson CS, Hakim AM (2004) Regulation of nestin expression after cortical ablation in adult rat brain. *Brain Research* 1008:139–46.

El Maarouf A, Petridis AK, Rutishauser U (2006) Use of polysialic acid in repair of the central nervous system. *Proceedings of the National Academy of Sciences of the United States of America* 103:16989–16994.

Ellis-Behnke RG, Liang YX, You SW, Tay DKC, Zhang SG, So KF, Schneider GE (2006) Nano neuro knitting: Peptide nanofiber scaffold for brain repair and axon regeneration with functional return of vision. *Proceedings of the National Academy of Sciences of the United States of America* 103:5054–5059.

Evans GRD, Brandt K, Katz S, Chauvin P, Otto L, Bogle M, Wang B, Meszlenyi RK, Lu LC, Mikos AG, Patrick CW (2002) Bioactive poly(l-lactic acid) conduits seeded with schwann cells for peripheral nerve regeneration. *Biomaterials* 23:841–848.

Fallenstein G, Hulce VD, Melvin JW (1969) Dynamic mechanical properties of human brain tissue. *Journal of Biomechanics* 2:217.

Feron F, Perry C, Cochrane J, Licina P, Nowitzke A, Urquhart S, Geraghty T, Mackay-Sim A (2005) Autologous olfactory ensheathing cell transplantation in human spinal cord injury. *Brain* 128:2951–2960.

Fiford RJ, Bilston LE (2005) The mechanical properties of rat spinal cord in vitro. *Journal of Biomechanics* 38:1509–15.

Flynn L, Dalton PD, Shoichet MS (2003) Fiber ternplating of poly(2-hydroxyethyl methacrylate) for neural tissue engineering. *Biomaterials* 24:4265–4272.

Fournier E, Passirani C, Montero-Menei CN, Benoit JP (2003) Biocompatibility of implantable synthetic polymeric drug carriers: focus on brain biocompatibility. *Biomaterials* 24:3311–3331.

Friedman JA, Windebank AJ, Moore MJ, Spinner RJ, Currier BL, Yaszemski MJ (2002) Biodegradable polymer grafts for surgical repair of the injured spinal cord. *Neurosurgery* 51:742–751.

Frostick SP, Yin Q, Kemp GJ (1998) Schwann cells, neurotrophic factors, and peripheral nerve regeneration. *Microsurgery* 18:397–405.

Fukunaga S, Sasaki S, Fu T, Yokoyama H, Lee I, Nakagaki I, Hori S, Tateishi H, Maruo S (2004) Experimental study of neural repair of the transected spinal cord using peripheral nerve graft. *Journal of Orthopaedic Science* 9:605–612.

Gelain F, Lomander A, Vescovi AL, Zhang SG (2007) Systematic studies of a self-assembling peptide nanofiber scaffold with other scaffolds. *Journal of Nanoscience and Nanotechnology* 7:424–434.

Georges PC, Miller WJ, Meaney DF, Sawyer ES, Janmey PA (2006) Matrices with compliance comparable to that of brain tissue select neuronal over glial growth in mixed cortical cultures. *Biophysical Journal* 90:3012–3018.

Goldner JS, Bruder JM, Li G, Gazzola D, Hoffman-Kim D (2006) Neurite bridging across micropatterned grooves. *Biomaterials* 27:460–72.

Hadlock T, Sundback C (2006) Biologically inspired approaches to drug delivery for nerve regeneration. *Expert Opinion on Biological Therapy* 6:1105–1111.

Hall ED, Braughler JM (1982) Effects of intravenous methylprednisolone on spinal-cord lipid-peroxidation and (na+ + k+)-atpase activity - dose-response analysis during 1st hour after contusion injury in the cat. *Journal of Neurosurgery* 57:247–253.

Heath JW (1982) Double myelination of axons in the sympathetic nervous-system. *Journal of Neurocytology* 11:249–262.

Hermanns S, Klapka N, Muller HW (2001) The collagenous lesion scar - an obstacle for axonal regeneration in brain and spinal cord injury. *Restorative Neurology and Neuroscience* 19:139–148.

Hersel U, Dahmen C, Kessler H (2003) Rgd modified polymers: biomaterials for stimulated cell adhesion and beyond. *Biomaterials* 24:4385–4415.

Hollister SJ (2005) Porous scaffold design for tissue engineering. *Nature Materials* 4:518–524.

Holmin S, Almqvist P, Lendahl U, Mathiesen T (1997) Adult nestin-expressing subependymal cells differentiate to astrocytes in response to brain injury. *European Journal of Neuroscience* 9:65–75.

Holmin S, Mathiesen T (1995) Biphasic edema development after experimental brain contusion in rat. *Neuroscience Letters* 194:97–100.

Horn EM, Beaumont M, Shu XZ, Harvey A, Prestwich GD, Horn KM, Gibson AR, Preul MC, Panitch A (2007) Influence of cross-linked hyaluronic acid hydrogels on neurite outgrowth and recovery from spinal cord injury. *Journal of Neurosurgery-Spine* 6:133–140.

Hou SP, Xu QY, Tian WM, Cui FZ, Cai Q, Ma J, Lee IS (2005) The repair of brain lesion by implantation of hyaluronic acid hydrogels modified with laminin. *Journal of Neuroscience Methods* 148:60–70.

Houle JD, Tom VJ, Mayes D, Wagoner G, Phillips N, Silver J (2006) Combining an autologous peripheral nervous system "bridge" and matrix modification by chondroitinase allows robust, functional regeneration beyond a hemisection lesion of the adult rat spinal cord. *Journal of Neuroscience* 26:7405–7415.

Houle JD, Ziegler MK (1994) Bridging a complete transection lesion of adult-rat spinal-cord with growth factor-treated nitrocellulose implants. *Journal of Neural Transplantation & Plasticity* 5:115–124.

Huang YC, Huang YY, Huang CC, Liu HC (2005) Manufacture of porous polymer nerve conduits through a lyophilizing and wire-heating process. *Journal of Biomedical Materials Research Part B-Applied Biomaterials* 74B:659–664.

Hughes PM, Wells GMA, Perry VH, Brown MC, Miller KM (2002) Comparison of matrix metalloproteinase expression during wallerian degeneration in the central and peripheral nervous systems. *Neuroscience* 113:273–287.

Hurlbert RJ (2000) Methylprednisolone for acute spinal cord injury: an inappropriate standard of care. *Journal of Neurosurgery* 93:1–7.

Hurtado A, Moon LDF, Maquet V, Blits B, Jerome R, Oudega M (2006) Poly (d,l-lactic acid) macroporous guidance scaffolds seeded with schwann cells genetically modified to secrete a bifunctional neurotrophin implanted in the completely transected adult rat thoracic spinal cord. *Biomaterials* 27:430–442.

Hutmacher DW, Sittinger M, Risbud MV (2004) Scaffold-based tissue engineering: rationale for computer-aided design and solid free-form fabrication systems. *Trends in Biotechnology* 22:354–362.

Hyman C, Hofer M, Barde YA, Juhasz M, Yancopoulos GD, Squinto SP, Lindsay RM (1991) Bdnf is a neurotrophic factor for dopaminergic-neurons of the substantia-nigra. *Nature* 350:230–232.

Ibrahim A, Li Y, Li DQ, Raisman G, El Masry WS (2006) Olfactory ensheathing cells: ripples of an incoming tide? *Lancet Neurology* 5:453–457.

Imaizumi T, Lankford KL, Waxman SG, Greer CA, Kocsis JD (1998) Transplanted olfactory ensheathing cells remyelinate and enhance axonal conduction in the demyelinated dorsal columns of the rat spinal cord. *Journal of Neuroscience* 18:6176–6185.

Ito Y (1999) Surface micropatterning to regulate cell functions. *Biomaterials* 20:2333–2342.

Iuliano DJ, Saavedra SS, Truskey GA (1993) Effect of the conformation and orientation of adsorbed fibronectin on endothelial-cell spreading and the strength of adhesion. *Journal of Biomedical Materials Research* 27:1103–1113.

Jellinger KA (2006) Alzheimer 100 - highlights in the history of alzheimer research. *Journal of Neural Transmission* 113:1603–1623.

Jones LL, Sajed D, Tuszynski MH (2003) Axonal regeneration through regions of chondroitin sulfate proteoglycan deposition after spinal cord injury: A balance of permissiveness and inhibition. *Journal of Neuroscience* 23:9276–9288.

Kaegi S, Schwab ME, Dietz V, Fouad K (2002) Electromyographic activity associated with spontaneous functional recovery after spinal cord injury in rats. *European Journal of Neuroscience* 16:249–258.

Kandel ER, Schwartz JH, Jessell TM (2000) *Principles of neural science* McGraw-Hill, Health Professions Division, New York, 4th edition 99044479 edited by Eric R. Kandel, James H. Schwartz, Thomas M. Jessell ; art direction by Sarah Mack and Jane Dodd. ill. (some col.) ; 29 cm. Includes bibliographical references and index.

Karp JM, Dalton PD, Shoichet MS (2003) Scaffolds for tissue engineering. *Mrs Bulletin* 28:301–306.

Keilhoff G, Stang F, Goihl A, Wolf G, Fansa H (2006) Transdifferentiated mesenchymal stem cells as alternative therapy in supporting nerve regeneration and myelination. *Cellular and Molecular Neurobiology* 26:1235–1252.

Kerschensteiner M (2007) Strategies for axonal repair in central nervous system diseases. *Journal of Neurology* 254:29–32.

Kerschensteiner M, Schwab ME, Lichtman JW, Misgeld T (2005) In vivo imaging of axonal degeneration and regeneration in the injured spinal cord. *Nature Medicine* 11:572–577.

Kerwin BA, Chang BS, Gegg CV, Gonnelli M, Li T, Strambini GB (2002) Interactions between peg and type i soluble tumor necrosis factor receptor: modulation by ph and by pegylation at the n terminus. *Protein Science* 11:1825–33.

Keselowsky BG, Collard DM, Garcia AJ (2003) Surface chemistry modulates fibronectin conformation and directs integrin binding and specificity to control cell adhesion. *Journal of Biomedical Materials Research Part A* 66A:247–259.

Khan T, Dauzvardis M, Sayers S (1991) Carbon-filament implants promote axonal growth across the transected rat spinal-cord. *Brain Research* 541:139–145.

Kidd GJ, Heath JW (1988a) Double myelination of axons in the sympathetic nervous-system of the mouse .1. ultrastructural features and distribution. *Journal of Neurocytology* 17:245–261.

Kidd GJ, Heath JW (1988b) Double myelination of axons in the sympathetic nervous-system of the mouse .2. mechanisms of formation. *Journal of Neurocytology* 17:263–276.

Kidd GJ, Heath JW (1991) Myelin sheath survival following axonal degeneration in doubly myelinated nerve-fibers. *Journal of Neuroscience* 11:4003–4014.

Komitova M, Eriksson PS (2004) Sox-2 is expressed by neural progenitors and astroglia in the adult rat brain. *Neuroscience Letters* 369:24–27.

Kou JH, Emmett C, Shen P, Aswani S, Iwamoto T, Vaghefi F, Cain G, Sanders L (1997) Bioerosion and biocompatibility of poly(d,l-lactic-co-glycolic acid) implants in brain. *Journal of Controlled Release* 43:123–130.

Krebsbach PH, Kuznetsov SA, Bianco P, Robey PG (1999) Bone marrow stromal cells: Characterization and clinical application. *Critical Reviews in Oral Biology & Medicine* 10:165–181.

Kristt DA (1987) Morphological responses to local cns trauma: sprouting and synaptogenesis within membranes implanted into mature cerebral cortex of the rat. *Journal of Neuropathology and Experimental Neurology* 46:668–81.

Kuhn TB, Williams CV, Dou P, Kater SB (1998) Laminin directs growth cone navigation via two temporally and functionally distinct calcium signals. *Journal of Neuroscience* 18:184–194.

Kuo HS, Tsai MJ, Huang MC, Huang WC, Lee MJ, Kuo WC, You LH, Szeto KC, Tsai IL, Chang WC, Chiu CW, Ma H, Chak KF, Cheng H (2007) The combination of peripheral nerve grafts and acidic fibroblast growth factor enhances arginase i and polyamine spermine expression in transected rat spinal cords. *Biochemical and Biophysical Research Communications* 357:1–7.

Langer R, Vacanti JP (1993) Tissue engineering. *Science* 260:920–926.

Larsen M, Artym VV, Green JA, Yamada KM (2006) The matrix reorganized: extracellular matrix remodeling and integrin signaling. *Current Opinion in Cell Biology* 18:463–471.

Lee HJ, Kim KS, Kim EJ, Choi HB, Lee KH, Park IH, Ko Y, Jeong SW, Kim SU (2007) Brain transplantation of immortalized human neural stem cells promotes functional recovery in mouse intracerebral hemorrhage stroke model. *Stem Cells* 25:1204–1212.

Levi ADO, Dancausse H, Li XM, Duncan S, Horkey L, Oliviera M (2002) Peripheral nerve grafts promoting central nervous system regeneration after spinal cord injury in the primate. *Journal of Neurosurgery* 96:197–205.

Leypold BG, Flanders AE, Schwartz ED, Burns AS (2007) The impact of methylprednisolone on lesion severity following spinal cord injury. *Spine* 32:373–378.

Lhoest JB, Detrait E, van den Bosch de Aguilar P, Bertrand P (1998) Fibronectin adsorption, conformation, and orientation on polystyrene substrates studied by radiolabeling, xps, and tof sims. *Journal of Biomedical Materials Research* 41:95–103.

Li J, Habibovic P, Doel Mvd, Wilson C, Wijn Jd, Blitterswijk Cv, Groot Kd (2007) Bone ingrowth in titanium implants produced by 3d fiber deposition. *Biomaterials* 28:2810–2820.

Li XG, Yang ZY, Yang Y (2006) Studies on repairing of hemisected thoracic spinal cord of adult rats by using a chitosan tube filled with alginate fibers. *Progress in Natural Science* 16:1051–1055.

Li Y, Chopp M (1999) Temporal profile of nestin expression after focal cerebral ischemia in adult rat. *Brain Research* 838:1–10.

Linninger AA, Xenos M, Zhu DC, Somayaji MR, Kondapalli S, Penn RD (2007) Cerebrospinal fluid flow in the normal and hydrocephalic human brain. *IEEE Trans Biomed Eng* 54:291–302.

Lu D, Li Y, Mahmood A, Wang L, Rafiq T, Chopp M (2002) Neural and marrow-derived stromal cell sphere transplantation in a rat model of traumatic brain injury. *Journal of Neurosurgery* 97:935–40.

Lu D, Mahmood A, Wang L, Li Y, Lu M, Chopp M (2001) Adult bone marrow stromal cells administered intravenously to rats after traumatic brain injury migrate into brain and improve neurological outcome. *Neuroreport* 12:559–563.

Lu J, Moochhala S, Moore XL, Ng KC, Tan MH, Lee LKH, He BP, Wong MC, Ling EA (2006) Adult bone marrow cells differentiate into neural phenotypes and improve functional recovery in rats following traumatic brain injury. *Neuroscience Letters* 398:12–17.

Lu P, Jones LL, Tuszynski MH (2007) Axon regeneration through scars and into sites of chronic spinal cord injury. *Experimental Neurology* 203:8–21.

LuckenbillEdds L (1997) Laminin and the mechanism of neuronal outgrowth. *Brain Research Reviews* 23:1–27.

Luo J, Borgens R, Shi R (2004) Polyethylene glycol improves function and reduces oxidative stress in synaptosomal preparations following spinal cord injury. *Journal of Neurotrauma* 21:994–1007.

Mahmood A (2002) Intravenous administration of marrow stromal cells after traumatic brain injury induces proliferation of intrinsic neural stem cells in the ventricular zone and subventricular zone in rat brain. *Neurosurgery* 51:555–556.

Mahmood A, Lu D, Chopp M (2004a) Marrow stromal cell transplantation after traumatic brain injury promotes cellular proliferation within the brain. *Neurosurgery* 55:1185–1192.

Mahmood A, Lu DY, Chopp M (2004b) Intravenous administration of marrow stromal cells (mscs) increases the expression of growth factors in rat brain after traumatic brain injury. *Journal of Neurotrauma* 21:33–39.

Mahmood A, Lu DY, Li Y, Chen JL, Chopp M (2001) Intracranial bone marrow transplantation after traumatic brain injury improving functional outcome in adult rats. *Journal of Neurosurgery* 94:589–595.

Mahmood A, Lu DY, Lu M, Chopp M (2003) Treatment of traumatic brain injury in adult rats with intravenous administration of human bone marrow stromal cells. *Neurosurgery* 53:697–702.

Mahmood A, Lu DY, Qu CS, Chopp M (2006) Collagen scaffolds populated with human marrow stromal cells reduce lesion volume and improve functional outcome after traumatic brain injury. *Neurosurgery* 59:469–469.

Mahmood A, Lu DY, Qu CS, Goussev A, Chopp M (2005) Human marrow stromal cell treatment provides long-lasting benefit after traumatic brain injury in rats. *Neurosurgery* 57:1026–1030.

Mahmood A, Lu DY, Qu CS, Goussev A, Chopp M (2006a) Long-term recovery after bone marrow stromal cell treatment of traumatic brain injury in rats. *Journal of Neurosurgery* 104:272–277.

Mahmood A, Lu DY, Qu CS, Goussev A, Chopp M (2006b) Treatment of traumatic brain injury in rats with a combination therapy of marrow stromal cells and atorvastatin. *Journal of Neurosurgery* 104:A646–A647.

Mahmood A, Lu DY, Wang L, Chopp M (2002) Intracerebral transplantation of marrow stromal cells cultured with neurotrophic factors promotes functional recovery in adult rats subjected to traumatic brain injury. *Journal of Neurotrauma* 19:1609–1617.

Maier IC, Schwab ME (2006) Sprouting, regeneration and circuit formation in the injured spinal cord: factors and activity. *Philosophical Transactions of the Royal Society B-Biological Sciences* 361:1611–1634.

Malda J, Woodfield T, Vloodt Fvd, Wilson C, Martens D, Tramper J, Blitterswijk Cv, Riesle J (2005) The effect of pegt/pbt scaffold architecture on the composition of tissue engineered cartilage. *Biomaterials* 26:63–72.

Manwaring ME, Walsh JF, Tresco PA (2004) Contact guidance induced organization of extracellular matrix. *Biomaterials* 25:3631–3638.

Martin D, Robe P, Franzen R, Delree P, Schoenen J, Stevenaert A, Moonen G (1996) Effects of schwann cell transplantation in a contusion model of rat spinal cord injury. *Journal of Neuroscience Research* 45:588–597.

McDonald JW, Becker D, Holekamp TF, Howard M, Liu S, Lu AW, Lu J, Platik MM, Qu Y, Stewart T, Vadivelu S (2004) Repair of the injured spinal cord and the potential of embryonic stem cell transplantation. *Journal of Neurotrauma* 21:383–393.

McKeon RJ, Schreiber RC, Rudge JS, Silver J (1991) Reduction of neurite outgrowth in a model of glial scarring following cns injury is correlated with the expression of inhibitory molecules on reactive astrocytes. *Journal of Neuroscience* 11:3398–3411.

Menei P, Croue A, Daniel V, Pouplardbarthelaix A, Benoit JP (1994) Fate and biocompatibility of 3 types of microspheres implanted into the brain. *Journal of Biomedical Materials Research* 28:1079–1085.

Mikos AG, Thorsen AJ, Czerwonka LA, Bao Y, Langer R, Winslow DN, Vacanti JP (1994) Preparation and characterization of poly(l-lactic acid) foams. *Polymer* 35:1068–1077.

Miller C, Jeftinija S, Mallapragada S (2001) Micropatterned schwann cell-seeded biodegradable polymer substrates significantly enhance neurite alignment and outgrowth. *Tissue Engineering* 7:705–715.

Miller C, Jeftinija S, Mallapragada S (2002) Synergistic effects of physical and chemical guidance cues on neurite alignment and outgrowth on biodegradable polymer substrates. *Tissue Engineering* 8:367–378.

Miller K, Chinzei K (1997) Constitutive modelling of brain tissue: experiment and theory. *Journal of Biomechanics* 30:1115–21.

Miller K, Chinzei K (2002) Mechanical properties of brain tissue in tension. *Journal of Biomechanics* 35:483–90.

Miller RG (2001) Examining the evidence about treatment in als/mnd. *Amyotrophic Lateral Sclerosis and Other Motor Neuron Disorders* 2:3–7.

Miller T, Boettiger D (2003) Control of intracellular signaling by modulation of fibronectin conformation at the cell-materials interface. *Langmuir* 19:1723–1729.

Molcanyi M, Riess P, Bentz K, Maegele M, Hescheler J, Schafke B, Trapp T, Neugebauer E, Klug N, Schafer U (2007) Trauma-associated inflammatory response impairs embryonic stem cell survival and integration after implantation into injured rat brain. *Journal of Neurotrauma* 24:625–37.

Moore MJ, Friedman JA, Lewellyn EB, Mantila SM, Krych AJ, Ameenuddin S, Knight AM, Lu L, Currier BL, Spinner RJ, Marsh RW, Windebank AJ, Yaszemski MJ (2006) Multiple-channel scaffolds to promote spinal cord axon regeneration. *Biomaterials* 27:419–429.

Mori S (1992) Neuronal constituents of postural and locomotor control-systems and their interactions in cats. *Brain & Development* 14:S109–S120.

Morrissey TK, Kleitman N, Bunge RP (1991) Isolation and functional-characterization of schwann-cells derived from adult peripheral-nerve. *Journal of Neuroscience* 11:2433–2442.

Mountcastle VB (1997) The columnar organization of the neocortex. *Brain* 120:701–722.

Munoz-Elias G, Woodbury D, Black IB (2003) Marrow stromal cells, mitosis, and neuronal differentiation: Stem cell and precursor functions. *Stem Cells* 21:437–448.

Nandoe RDS, Hurtado A, Levi ADO, Grotenhuis A, Oudega M (2006) Bone marrow stromal cells for repair of the spinal cord: Towards clinical application. *Cell Transplantation* 15:563–577.

Noga BR, Kriellaars DJ, Jordan LM (1991) The effect of selective brain-stem or spinal-cord lesions on treadmill locomotion evoked by stimulation of the mesencephalic or pontomedullary locomotor regions. *Journal of Neuroscience* 11:1691–1700.

Nomizu M, Kuratomi Y, Ponce ML, Song SY, Miyoshi K, Otaka A, Powell SK, Hoffman MP, Kleinman HK, Yamada Y (2000) Cell adhesive sequences in mouse laminin beta 1 chain. *Archives of Biochemistry and Biophysics* 378:311–320.

Nomura H, Katayama Y, Shoichet MS, Tator CH (2006) Complete spinal cord transection treated by implantation of a reinforced synthetic hydrogel channel results in syringomyelia and caudal migration of the rostral stump. *Neurosurgery* 59:183–192.

Nomura H, Tator CH, Shoichet MS (2006) Bioengineered strategies for spinal cord repair. *Journal of Neurotrauma* 23:496–507.

Novikova LN, Novikov LN, Kellerth JO (2003) Biopolymers and biodegradable smart implants for tissue regeneration after spinal cord injury. *Current Opinion in Neurology* 16:711–715.

Ochs S (1977) The early history of nerve regeneration beginning with cruikshank's observations in 1776. *Med Hist* 21:261–74.

Olah L, Filipczak K, Jaegermann Z, Czigany T, Borbas L, Sosnowski S, Ulanski P, Rosiak JM (2006) Synthesis, structural and mechanical properties of porous polymeric scaffolds for bone tissue regeneration based on neat poly(epsilon-caprolactone) calcium carbonate. *Polymers for Advanced Technologies* 17:889–897.

Otsuki B, Takemoto M, Fujibayashi S, Neo M, Kokubo T, Nakamura T (2006) Pore throat size and connectivity determine bone and tissue ingrowth into porous implants: three-dimensional micro-ct based structural analyses of porous bioactive titanium implants. *Biomaterials* 27:5892–5900.

Oudega M, Gautier SE, Chapon P, Fragoso M, Bates ML, Parel JM, Bunge MB (2001) Axonal regeneration into schwann cell grafts within resorbable poly(alpha-hydroxyacid) guidance channels in the adult rat spinal cord. *Biomaterials* 22:1125–1136.

Park KI, Teng YD, Snyder EY (2002) The injured brain interacts reciprocally with neural stem cells supported by scaffolds to reconstitute lost tissue. *Nature Biotechnology* 20:1111–7.

Patist CM, Mulder MB, Gautier SE, Maquet V, Jerome R, Oudega M (2004) Freeze-dried poly(d,l-lactic acid) macroporous guidance scaffolds impregnated with brain-derived neurotrophic factor in the transected adult rat thoracic spinal cord. *Biomaterials* 25:1569–1582.

Pauwelyn KA, Verfaillie CM (2006) Transplantation of undifferentiated, bone marrow-derived stem cells In *Current Topics in Developmental Biology, Vol 74*, Vol. 74 of *Current Topics in Developmental Biology*, pp. 201–+ Times Cited: 2 Review.

Pearse DD, Pereira FC, Marcillo AE, Bates ML, Berrocal YA, Filbin MT, Bunge MB (2004) camp and schwann cells promote axonal growth and functional recovery after spinal cord injury. *Nature Medicine* 10:610–616.

Piantino J, Burdick JA, Goldberg D, Langer R, Benowitz LI (2006) An injectable, biodegradable hydrogel for trophic factor delivery enhances axonal rewiring and improves performance after spinal cord injury. *Experimental Neurology* 201:359–367.

Pierschbacher MD, Ruoslahti E (1984) Cell attachment activity of fibronectin can be duplicated by small synthetic fragments of the molecule. *Nature* 309:30–33.

Pinzon A, Calancie B, Oudega M, Noga BR (2001) Conduction of impulses by axons regenerated in a schwann cell graft in the transected adult rat thoracic spinal cord. *Journal of Neuroscience Research* 64:533–541.

Polikov VS, Tresco PA, Reichert WM (2005) Response of brain tissue to chronically implanted neural electrodes. *Journal of Neuroscience Methods* 148:1–18.

Popovic N, Brundin P (2006) Therapeutic potential of controlled drug delivery systems in neurodegenerative diseases. *International Journal of Pharmacology* 314:120–6.

Prange MT, Margulies SS (2002) Regional, directional, and age-dependent properties of the brain undergoing large deformation. *Journal of Biomechanical Engineering-Transactions of the Asme* 124:244–252.

Raghupathi R (2004) Cell death mechanisms following traumatic brain injury. *Brain Pathol* 14:215–22.

Raisman G (2006) Repair of spinal cord injury: ripples of an incoming tide, or how i spent my first 40 years in research. *Spinal Cord* 44:406–413.

Rakic P (1971) Guidance of neurons migrating to the fetal monkey neocortex. *Brain Research* 33:471–6.

Ramón y Cajal S, DeFelipe J, Jones EG (1991) *Cajal's degeneration and regeneration of the nervous system* History of neuroscience. Oxford University Press, New York 91003890 translated by Raoul M. May ; edited, with an introduction and additional translations, by Javier DeFelipe and Edward G. Jones. ill. ; 24 cm. Translation of: Estudios sobre la degeneración y regeneración del sistema nervioso. Includes bibliographical references and indexes.

Recknor JB, Recknor JC, Sakaguchi DS, Mallapragadaa SK (2004) Oriented astroglial cell growth on micropatterned polystyrene substrates. *Biomaterials* 25:2753–2767.

Rosenblueth A, Dempsey EW (1939) A study of wallerian degeneration. *American Journal of Physiology* 128:0019–0030.

Saha K, Irwin EF, Kozhukh J, Schaffer DV, Healy KE (2007) Biomimetic interfacial interpenetrating polymer networks control neural stem cell behavior. *Journal of Biomedical Materials Research Part A* 81A:240–249.

Sahin Kaya S, Mahmood A, Li Y, Yavuz E, Chopp M (1999) Expression of nestin after traumatic brain injury in rat brain. *Brain Research* 840:153–7.

Salzer JL, Bunge RP (1980) Studies of schwann-cell proliferation .1. analysis in tissue-culture of proliferation during development, wallerian degeneration, and direct injury. *Journal of Cell Biology* 84:739–752.

Santiago LY, Nowak RW, Rubin JP, Marra KG (2006) Peptide-surface modification of poly(caprolactone) with laminin-derived sequences for adipose-derived stem cell applications. *Biomaterials* 27:2962–2969.

Schmidt CE, Leach JB (2003) Neural tissue engineering: Strategies for repair and regeneration. *Annual Review of Biomedical Engineering* 5:293–347.

Schouten JW, Fulp CT, Royo NC, Saatman KE, Watson DJ, Snyder EY, Trojanowski JQ, Prockop DJ, Maas AI, McIntosh TK (2004) A review and rationale for the use of cellular transplantation as a therapeutic strategy for traumatic brain injury. *Journal of Neurotrauma* 21:1501–38.

Schucht P, Raineteau O, Schwab ME, Fouad K (2002) Anatomical correlates of locomotor recovery following dorsal and ventral lesions of the rat spinal cord. *Experimental Neurology* 176:143–153.

Schwab JM, Bernard F, Moreau-Fauvarque C, Chedotal A (2005) Injury reactive myelin/oligodendrocyte-derived axon growth inhibition in the adult mammalian central nervous system. *Brain Research Reviews* 49:295–299.

Schwab JM, Brechtel K, Mueller CA, Failli V, Kaps HP, Tuli SK, Schluesener HJ (2006) Experimental strategies to promote spinal cord regeneration - an integrative perspective. *Progress in Neurobiology* 78:91–116.

Schwab ME (2002) Repairing the injured spinal cord. *Science* 295:1029–1031.

Shear DA, Tate MC, Archer DR, Hoffman SW, Hulce VD, LaPlaca MC, Stein DG (2004) Neural progenitor cell transplants promote long-term functional recovery after traumatic brain injury. *Brain Research* 1026:11–22.

Short DJ, El Masry WS, Jones PW (2000) High dose methylprednisolone in the management of acute spinal cord injury - a systematic review from a clinical perspective. *Spinal Cord* 38:273–286.

Singh N, Pillay V, Choonara YE (2007) Advances in the treatment of parkinson's disease. *Progress in Neurobiology* 81:29–44.

Singhvi R, Stephanopoulos G, Wang DIC (1994) Effects of substratum morphology on cell physiology - review. *Biotechnology and Bioengineering* 43:764–771.

Spyridonidis A, Tomann T, Zeiser R, Follo M, Metaxas Y, Finke J (2005) Stem cell plasticity - the debate begins to clarify. *Stem Cell Reviews* 1:37–43.

Stabenfeldt SE, Garcia AJ, LaPlaca MC (2006) Thermoreversible laminin-functionalized hydrogel for neural tissue engineering. *Journal of Biomedical Materials Research Part A* 77A:718–725.

Stokols S, Sakamoto J, Breckon C, Holt T, Weiss J, Tuszynski MH (2006) Templated agarose scaffolds support linear axonal regeneration. *Tissue Engineering* 12:2777–2787.

Stokols S, Tuszynski MH (2004) The fabrication and characterization of linearly oriented nerve guidance scaffolds for spinal cord injury. *Biomaterials* 25:5839–5846.

Stokols S, Tuszynski MH (2006) Freeze-dried agarose scaffolds with uniaxial channels stimulate and guide linear axonal growth following spinal cord injury. *Biomaterials* 27:443–451.

Streit WJ (2002) Microglia as neuroprotective, immunocompetent cells of the cns. *Glia* 40:133–9.

Sugar O, Gerard RW (1940) Spinal cord regeneration in the rat. *Journal of Neurophysiology* 3:1–19.

Sun HF, Mei L, Song CX, Cui XM, Wang PY (2006) The in vivo degradation, absorption and excretion of pcl-based implant. *Biomaterials* 27:1735–1740.

Sung HJ, Meredith C, Johnson C, Galis ZS (2004) The effect of scaffold degradation rate on three-dimensional cell growth and angiogenesis. *Biomaterials* 25:5735–5742.

Sykova E, Homola A, Mazanec R, Lachmann H, Konradova SL, Kobylka P, Padr R, Neuwirth J, Komrska V, Vavra V, Stulik J, Bojar M (2006a) Autologous bone marrow transplantation in patients with subacute and chronic spinal cord injury. *Cell Transplantation* 15:675–687.

Sykova E, Jendelova P, Urdzikova L, Lesny P, Hejcl A (2006b) Bone marrow stem cells and polymer hydrogels-two strategies for spinal cord injury repair. *Cellular and Molecular Neurobiology* 26:1113–1129.

Tabar V, Studer L (2002) Novel sources of stem cells for brain repair. *Clinical Neuroscience Research* 2:2–10.

Takagi Y, Nishimura M, Morizane A, Takahashi J, Nozaki K, Hayashi J, Hashimoto N (2005) Survival and differentiation of neural progenitor cells derived from embryonic stem cells and transplanted into ischemic brain. *Journal of Neurosurgery* 103:304–310.

Tang ZG, Black RA, Curran JM, Hunt JA, Rhodes NP, Williams DF (2004) Surface properties and biocompatibility of solvent-cast poly[epsilon-caprolactone] films. *Biomaterials* 25:4741–4748.

Tashiro K, Sephel GC, Weeks B, Sasaki M, Martin GR, Kleinman HK, Yamada Y (1989) A synthetic peptide containing the ikvav sequence from the a-chain of laminin mediates cell attachment, migration, and neurite outgrowth. *Journal of Biological Chemistry* 264:16174–16182.

Tate MC, Shear DA, Hoffman SW, Stein DG, Archer DR, LaPlaca MC (2002) Fibronectin promotes survival and migration of primary neural stem cells transplanted into the traumatically injured mouse brain. *Cell Transplantation* 11:283–295.

Tate MC, Shear DA, Hoffman SW, Stein DG, LaPlaca MC (2001) Biocompatibility of methylcellulose-based constructs designed for intracerebral gelation following experimental traumatic brain injury. *Biomaterials* 22:1113–1123.

Tator CH (2006) Review of treatment trials in human spinal cord injury: Issues, difficulties, and recommendations. *Neurosurgery* 59:957–982.

Taylor MS, Daniels AU, Andriano KP, Heller J (1994) 6 bioabsorbable polymers - in-vitro acute toxicity of accumulated degradation products. *Journal of Applied Biomaterials* 5:151–157.

Temple S, Alvarez-Buylla A (1999) Stem cells in the adult mammalian central nervous system. *Current Opinion in Neurobiology* 9:135–141.

Teng YD, Lavik EB, Qu XL, Park KI, Ourednik J, Zurakowski D, Langer R, Snyder EY (2002) Functional recovery following traumatic spinal cord injury mediated by a unique polymer scaffold seeded with neural stem cells. *Proceedings of the National Academy of Sciences of the United States of America* 99:3024–3029.

Thoenen H (1991) The changing scene of neurotrophic factors. *Trends in Neurosciences* 14:165–170.

Thompson DM, Buettner HM (2001) Schwann cell response to micropatterned laminin surfaces. *Tissue Engineering* 7:247–265.

Thompson TP, Lunsford LD, Kondziolka D (1999) Restorative neurosurgery: Opportunities for restoration of function in acquired, degenerative, and idiopathic neurological diseases. *Neurosurgery* 45:741–752.

Tian WM, Hou SP, Ma J, Zhang CL, Xu QY, Lee IS, Li HD, Spector M, Cui FZ (2005a) Hyaluronic acid-poly-d-lysine-based three-dimensional hydrogel for traumatic brain injury. *Tissue Engineering* 11:513–525.

Tian WM, Zhang CL, Hou SP, Yu X, Cui FZ, Xu QY, Sheng SL, Cui H, Li HD (2005b) Hyaluronic acid hydrogel as nogo-66 receptor antibody delivery system for the repairing of injured rat brain: in vitro. *Journal of Controlled Release* 102:13–22.

Tom VJ, Doller CM, Malouf AT, Silver J (2004) Astrocyte-associated fibronectin is critical for axonal regeneration in adult white matter. *Journal of Neuroscience* 24:9282–9290.

Trivedi A, Olivas AD, Noble-Haeusslein LJ (2006) Inflammation and spinal cord injury: Infiltrating leukocytes as determinants of injury and repair processes. *Clinical Neuroscience Research* 6:283–292.

Tsai EC, Dalton PD, Shoichet MS, Tator CH (2004) Synthetic hydrogel guidance channels facilitate regeneration of adult rat brainstem motor axons after complete spinal cord transection. *Journal of Neurotrauma* 21:789–804.

Tsai EC, Dalton PD, Shoichet MS, Tator CH (2006) Matrix inclusion within synthetic hydrogel guidance channels improves specific supraspinal and local axonal regeneration after complete spinal cord transection. *Biomaterials* 27:519–533.

Tsuruma A, Tanaka M, Yamamoto S, Fukushima N, Yabu H, Shimomura M (2006) Topographical control of neurite extension on stripe-patterned polymer films. *Colloids and Surfaces a-Physicochemical and Engineering Aspects* 284:470–474.

Tsutsumi S, Ueta T, Shiba K, Yamamoto S, Takagishi K (2006) Effects of the second national acute spinal cord injury study of high-dose methylprednisolone therapy on acute cervical spinal cord injury - results in spinal injuries center. *Spine* 31:2992–2996.

Vance RJ, Miller DC, Thapa A, Haberstroh KM, Webster TJ (2004) Decreased fibroblast cell density on chemically degraded poly-lactic-co-glycolic acid, polyurethane, and polycaprolactone. *Biomaterials* 25:2095–2103.

Wen XJ, Tresco PA (2006) Effect of filament diameter and extracellular matrix molecule precoating on neurite outgrowth and schwann cell behavior on multifilament entubulation bridging device in vitro. *Journal of Biomedical Materials Research Part A* 76A:626–637.

Williams AJ, Hartings JA, Lu XC, Rolli ML, Tortella FC (2006) Penetrating ballistic-like brain injury in the rat: differential time courses of hemorrhage, cell death, inflammation, and remote degeneration. *Journal of Neurotrauma* 23:1828–46.

Willits RK, Skornia SL (2004) Effect of collagen gel stiffness on neurite extension. *Journal of Biomaterials Science-Polymer Edition* 15:1521–1531.

Windle WF (1981) Recollections of research in spinal-cord regeneration. *Experimental Neurology* 71:1–5.

Windle WF, Chambers WW (1951) Regeneration in the spinal cord of the cat and dog. *Ama Archives of Neurology and Psychiatry* 65:261–262.

Wong D, Hollister SJ, Krebsbach P, Nosrat C (2007) Pcl and plga degradable polymer sponges attenuate astrocyte response and lesion growth in acute traumatic brain injury. *Tissue Engineering* 13.

Woodbury D, Reynolds K, Black IB (2002) Adult bone marrow stromal stem cells express germline, ectodermal, endodermal, and mesodermal genes prior to neurogenesis. *Journal of Neuroscience Research* 69:908–917.

Woodbury D, Schwarz EJ, Prockop DJ, Black IB (2000) Adult rat and human bone marrow stromal cells differentiate into neurons. *Journal of Neuroscience Research* 61:364–370.

Xu XM, Chen A, Guenard V, Kleitman N, Bunge MB (1997) Bridging schwann cell transplants promote axonal regeneration from both the rostral and caudal stumps of transected adult rat spinal cord. *Journal of Neurocytology* 26:1–16.

Xu XM, Guenard V, Kleitman N, Aebischer P, Bunge MB (1995a) Combination of bdnf and nt-3 promotes supraspinal axonal regeneration into schwann-cell grafts in adult-rat thoracic spinal-cord. *Experimental Neurology* 134:261–272.

Xu XM, Guenard V, Kleitman N, Bunge MB (1995b) Axonal regeneration into schwann cell-seeded guidance channels grafted into transected adult-rat spinal-cord. *Journal of Comparative Neurology* 351:145–160.

Xu XM, Zhang SX, Li HY, Aebischer P, Bunge MB (1999) Regrowth of axons into the distal spinal cord through a schwann-cell-seeded mini-channel implanted into hemisected adult rat spinal cord. *European Journal of Neuroscience* 11:1723–1740.

Yamaguchi S, Kuroda S, Kobayashi H, Shichinohe H, Yano S, Hida K, Shinpo K, Kikuchi S, Iwasaki Y (2006) The effects of neuronal induction on gene expression profile in bone marrow stromal cells (bmsc) - a preliminary study using microarray analysis. *Brain Research* 1087:15–27.

Yoshii S, Oka M, Shima M, Akagi M, Taniguchi A (2003) Bridging a spinal cord defect using collagen filament. *Spine* 28:2346–2351.

Yoshii S, Oka M, Shima M, Taniguchi A, Taki Y, Akagi M (2004) Restoration of function after spinal cord transection using a collagen bridge. *Journal of Biomedical Materials Research Part A* 70A:569–575.

Zhang N, Yan HH, Wen XJ (2005) Tissue-engineering approaches for axonal guidance. *Brain Research Reviews* 49:48–64.

Zhang Z, Artelt M, Burnet M, Trautmann K, Schluesener HJ (2006) Early infiltration of cd8+ macrophages/microglia to lesions of rat traumatic brain injury. *Neuroscience* 141:637–44.

Zhu YB, Gao CY, Liu XY, Shen JC (2002) Surface modification of polycaprolactone membrane via aminolysis and biomacromolecule immobilization for promoting cytocompatibility of human endothelial cells. *Biomacromolecules* 3:1312–1319.